

Forks on a dusty road - Studies in Classical and Quantum Gravity

by

Masooma Ali

Master of Science, University of Bonn, 2011

A DISSERTATION SUBMITTED IN PARTIAL FULFILLMENT
OF THE REQUIREMENTS FOR THE DEGREE OF

Doctor of Philosophy

In the Graduate Academic Unit of Physics

Supervisor(s): Viqar Husain, Ph.D., Dept. of Mathematics & Statistics

Examining Board: Abdelhaq Hamza, Ph.D., Dept. of Physics
Ben Newling, Ph.D., Dept. of Physics
Edward Wilson-Ewing, Ph.D., Dept. of Mathematics & Statistics

External Examiner: Luca Bombelli, Ph.D., Dept of Physics & Astronomy,
University of Mississippi

This dissertation is accepted

Dean of Graduate Studies

THE UNIVERSITY OF NEW BRUNSWICK

July, 2019

©Masooma Ali, 2019

Abstract

This thesis explores the classical and quantum aspects of dust + gravity systems with the dust field playing the role of time.

In the classical setting we explored the linearized theory of dust + General Relativity around a Minkowski background. The resulting theory has three physical degrees of freedom at each spacetime point. At the linearized level we recovered two graviton modes and an ultralocal scalar mode. Remarkably the graviton modes remain Lorentz covariant despite the time gauge fixing. The other classical models we studied were the homogeneous and anisotropic Bianchi I and IX spacetimes. The dust time gauge analysis of Bianchi IX spacetime gives a new physical picture where dust Bianchi IX dynamics is characterized by transitions between dust-Kasner solutions rather than vacuum-Kasner solutions. We derived a generalized transition law between these solutions which includes a matter component. Sufficiently close to the singularity this law reduces to the usual Belinski-Khalatnikov-Lifshitz map.

In the quantum setting we explored two homogeneous models with dust. We

de-parameterized the theory using the dust time gauge before quantization. For homogeneous models this is the reduced phase space approach to quantization. The first model we studied was spatially flat Friedmann-Lemaître-Robertson-Walker model with dust and a cosmological constant (Λ). We showed that after gauge fixing and a canonical transformation the model reduces to a simple harmonic oscillator with frequency $\sqrt{\Lambda}$. The (Lorentzian) quantum theory of this model is then immediate. The model provides a simple demonstration of non-perturbative singularity avoidance. The other model we investigated was the Bianchi I model with dust. We formulated the path integral for the model using the physical Hamiltonian obtained after gauge fixing the theory using dust as time. The quantum theory of this model is not solvable analytically. We studied the quantum dynamics using Markov Chain Monte Carlo techniques by considering the Euclidean path integral. Numerical semiclassical analysis shows that quantum fluctuations in the spatial volume and anisotropies are larger for smaller universes. We also evaluated the no-boundary wavefunction for this model. The no-boundary wavefunction implies a suppression of large universes while large anisotropies appear to dominate.

Acknowledgements

I am greatly indebted to my supervisor, Viqar Husain, who has not only taught me a great deal about quantum gravity but has been a wonderful mentor to me, offering patient guidance, invaluable advice and encouragement. I am thankful to him for always being generous with his time when answering my questions and discussing ideas. His work provided much of the background and essential ideas in this thesis and his confidence in my research has been a great source of inspiration.

I would like to thank my collaborators Sanjeev Seahra, Jonathan Ziprick, Syed Moez Hassan and Shohreh Rahmati for everything they have taught me and for the illuminating discussions we have had.

I am grateful to Edward Wilson-Ewing for always being willing to peruse drafts of papers and providing insightful comments. His comments helped notably improve not only my papers but also this manuscript.

My time as a graduate student was greatly enriched by the company of my office mates in P204 and my fellow graduate students in the gravity group. I would like to thank Alex Adair, Razieh Enjilela, Amy-Rae Gauthier,

Moez Hassan and Christopher Vail for providing a dynamic environment with stimulating tea and conversations. I am indebted to them for all their help and support during my time at UNB.

The completion of this thesis would not have been possible without the continued support of my loving family. I feel deep gratitude towards my father for ensuring that I always had the freedom to pursue my dreams. I am extremely lucky to have been able to share all the ups and downs of graduate life with my husband Saquib and I thank him for his unfaltering love, support and understanding.

Table of Contents

Abstract	ii
Acknowledgments	iv
Table of Contents	vi
List of Tables	ix
List of Figures	x
1 Gravity and Time	1
1.1 Approaches to Quantum Gravity	2
1.2 ADM Formalism	5
1.3 Time in Quantum Gravity	8
2 Quantization with an Ideal Clock	12
2.1 General Relativity + Dust	13
2.2 Dust time gauge	15
2.3 The Path Integral approach	19
2.3.1 Symmetry reduced Path Integrals	22

2.4	Path Integral Monte Carlo	24
2.4.1	Importance Sampling and Markov Chains	25
2.4.2	Metropolis - Hastings algorithm	28
2.4.3	Evaluating Path Integrals	30
3	Linearized theory with dust	40
3.1	The Linearized Theory	41
3.1.1	Linearized equations of motion	45
3.1.2	Diffeomorphism constraint	47
3.2	Dust potential	50
3.3	Deformation of the Hamiltonian	51
3.4	Discussion	53
4	Mixmaster dynamics in the dust time gauge	55
4.1	The spatially homogeneous sector	59
4.2	Dust-Bianchi I spacetime	61
4.2.1	Kasner solution: $H_K = 0$	62
4.2.2	Dust-Kasner solution: $H_K > 0$	63
4.2.3	Dust-Kasner solution for $H_K < 0$	65
4.2.4	Dust-Bianchi I spacetime with scalar field	66
4.3	Dust-Bianchi IX spacetime	68
4.3.1	Method of Consistent Potentials	71
4.4	Transitions between dust-Bianchi I epochs	75
4.4.1	Transition Law: $H_p = 0$	77

4.4.2	Transition Law: $H_p \neq 0$	78
4.5	Bianchi IX dynamics with dust and scalar field	84
4.6	Discussion	87
5	The Universe as an Oscillator	89
5.1	The Homogeneous and Isotropic Sector	90
5.2	Quantization and wave functions of the Universe	92
5.2.1	Quantization on the half-line	92
5.2.2	Quantization on \mathbb{R}	97
5.3	Discussion	99
6	Quantum dynamics of Bianchi I spacetimes	103
6.1	Bianchi I Path Integral	105
6.1.1	Classical Euclidean solutions	107
6.2	Semiclassical PIMC Analysis	109
6.3	Wavefunction of the universe	114
6.3.1	$L_E > 0$	116
6.3.2	$S_E \geq 0$	118
6.4	Discussion	120
7	Summary and Future Directions	125
	Bibliography	132
	Vita	

List of Tables

- 6.1 Values of the Kasner exponents extracted from fitting curves to the expectation values of the scale factors. The first Kasner sum rule is approximately satisfied by the quantum exponents but there is a discrepancy with the second sum rule. 114

List of Figures

1.1	A 3 + 1 foliation of spacetime.	6
2.1	Change in action during thermalization of Markov Chain	33
2.2	Semiclassical expectation values for $A(t)$	35
2.3	Semiclassical fluctuations in volume.	36
2.4	Ground state wavefunction for $\Lambda = -1$	36
2.5	Correlation functions for the case $\Lambda = -1$	37
2.6	No boundary wavefunction for $\Lambda = 1$	38
4.1	Potential for the Bianchi IX spacetime	69
4.2	Mixmaster dynamics	70
4.3	Inequalities obtained from the Method of Consistent Potentials	74
4.4	Inequalities obtained using the Method of Consistent Potentials in the presences of a scalar field	86
5.1	Snapshots of $ \psi(x, t) ^2$ with the initial data $f(x) = \frac{e^{-(x-3)^2}}{\sqrt[4]{\pi/2}}$, and parameters $\Lambda = -1$ and $\alpha = 1.0$	96
5.2	Snapshots of $ \psi(x, t) ^2$ with the initial data $f(x) = \frac{e^{-(x-3)^2}}{\sqrt[4]{\pi/2}}$, and parameters $\Lambda = 1$ and $\alpha = 1.0$	98

6.1	A plot of the action versus Monte Carlo sweeps($\times 100$) from a representative thermalization run.	110
6.2	Semiclassical expectation values for volume and anisotropies. .	111
6.3	Quantum fluctuations in the anisotropies with respect to time.	112
6.4	Quantum fluctuations in x and <i>volume</i> with respect to time. .	113
6.5	Semiclassical Kasner exponents.	115
6.6	No boundary wavefunction with initial values of the anisotropies held fixed.	118
6.7	No boundary wavefunction with free boundaries for the anisotropies.	119
6.8	No boundary wavefunction with the regularization $S_E \geq 0$. . .	120

Chapter 1

Gravity and Time

Modern theories of fundamental physics are formulated within the framework of quantum mechanics (and quantum field theory) and have enjoyed immense experimental success. A common feature of these theories is that at sufficiently low energies these theories reduce to their classical counterparts. The only exception are theories of gravity which are inherently classical and have resisted a quantum formulation for more than half a century. A theory of quantum gravity would provide a mathematically consistent way of incorporating gravity into the quantum framework which describes all other interactions in our universe. But the need for quantum gravity goes beyond the demands of consistency and elegance. Our most successful theory of gravity, Einstein's theory of General Relativity (GR), appears to break down in regimes with extremely high densities of matter where the curvature of spacetime diverges to infinity. Examples of such regimes are interiors of

black holes and the period of the Big Bang predicted by classical cosmology. These regimes are marked by the appearance of singularities (spacetime points with infinite curvature) where trajectories of free falling observers (geodesics) come to an abrupt end. Given the high energy densities in these regions we expect both geometry and matter to be described by a quantum theory. The hope is that these singularities in the classical theory will be resolved in the quantum theory. Understanding these singularities provides an urgent motivation for developing a quantum theory of gravity.

The next section provides a general overview of approaches to Quantum Gravity. Section 1.2 discusses the ADM formalism which is the starting point for canonical quantisation of GR and Section 1.3 elucidates the problem of time in the canonical approach to quantum gravity.

1.1 Approaches to Quantum Gravity

The most successful theory of gravity is Einstein's theory of General Relativity (GR)[91]. Predictions of GR have been verified by solar system experiments [43, 82, 28], galactic experiments [14, 2], in binary pulsar systems [89, 64, 90] and by the direct observation of gravitational waves [1].

However, in the roster of successful physical theories GR stands apart. Unlike other theories, GR is not formulated on a fixed background structure but intertwines the roles of matter and geometry. This implies that there is no preferred coordinate system in which the theory takes an especially

simple form. This lack of preferred markers of space and time has profound consequences for both the classical theory and any attempt to quantize it.

In the classical theory the lack of fixed background structure implies that what appear to be different configurations of matter and geometry may in fact be equivalent (under diffeomorphisms). That is, much like a gauge theory, there exist redundant (or non-physical) degrees of freedom in the theory and we must take great care in distinguishing between true physical effects and coordinate artefacts.¹ The central difference between gauge transformations in GR and gauge transformations in Yang-Mills type gauge theories is that the Yang-Mills gauge group acts at a fixed spacetime point whereas the diffeomorphism group transforms the spacetime points themselves.

For the quantum theory the lack of fixed background structure implies that standard quantization techniques when applied to GR either lead to inconsistencies or result in a non-renormalizable theory. Thus, several approaches are being investigated to formulate a theory of quantum gravity and each comes with its own set of challenges. These approaches can be classified into three broad categories (with considerable overlap)[59]:

- The most conservative set of approaches attempt to apply some quantization procedure to a formulation of GR and consist of the two branches of covariant quantization techniques, which aim to keep the general covariance of GR transparent during quantization, and canonical quanti-

¹This redundancy in the description of the theory is most easily seen in the ADM formalism which we will discuss in Section 1.2.

zation techniques, which start from a Hamiltonian formulation of the theory. Loop quantum gravity and its modern variants like spin foams as well as causal dynamical triangulations are examples of such approaches.

- The second category of approaches begin from a particle physics standpoint and attempt to incorporate gravity into quantum theories of matter by extending or generalizing these theories. Though the initial approaches in this category were stalled due to the perturbative non-renormalizability of gravity, String Theory and the asymptotic safety program are flourishing directions.
- The third category comprises approaches that attempt to formulate a theory of quantum gravity ab initio and recover either full GR or connect with more conservative approaches in some appropriate limit. Programs like Causal Set Theory, modern formulations of Spin Foams and Group Field Theory are examples from this category.

In this thesis we will consider an approach that belongs to the first category. In particular, we start from a Hamiltonian formulation of GR and attempt to quantize the theory after a partial gauge fixing. This allows us to circumvent the well known problem of time in canonical quantum gravity.

1.2 ADM Formalism

The Arnowitt-Deser-Misner (ADM) formulation is a Hamiltonian formulation of GR which starts with the Einstein-Hilbert Lagrangian density

$$\mathcal{L} = \sqrt{-g}R, \tag{1.1}$$

where g is the determinant of the spacetime metric and R is its Ricci scalar. ADM performed a Legendre transform of this Lagrangian, by foliating the spacetime manifold into a series of spacelike hypersurfaces, to arrive at a Hamiltonian in terms of the spatial metric on these hypersurfaces (q_{ab}) and its momentum conjugate (π^{ab}), which contains information about the extrinsic curvature of the hypersurfaces, along with the lapse function (N) and the shift vector (N^a) which encode the foliation independence of the theory [13].

Consider a globally hyperbolic manifold \mathcal{M} foliated into a family of one parameter spacelike hypersurfaces Σ_t labelled by a parameter t which is constant over each hypersurface (see Figure 1.1). Let g_{ab} be the spacetime metric. If the manifold \mathcal{M} has the topological structure $\Sigma \times \mathbb{R}$ the spacetime metric can be decomposed as

$$g_{ab} = q_{ab} - n_a n_b, \tag{1.2}$$

where q_{ab} is a Riemannian metric on the spacelike hypersurface Σ and n^a is a timelike unit normal to Σ . Let t^a be a timelike vector field \mathcal{M} . We can

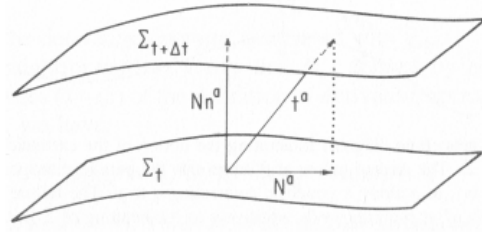


Figure 1.1: A 3 + 1 foliation of spacetime.

interpret t^a as the *flow of time* and decompose it as

$$t^a = Nn^a + N^a, \quad (1.3)$$

where N is the lapse function and N^a is the shift vector defined as

$$N = -g_{ab}t^an^b, \quad N^a = q_b^at^b. \quad (1.4)$$

Thus, the lapse function gives the rate of flow of proper time with respect to t and the shift vector gives the movement tangential to the hypersurface Σ_t .

The spacetime metric can be written as

$$g_{ab}dx^a dx^b = -(Ndt)^2 + q_{ab}(dx^a + N^a dt)(dx^b + N^b dt). \quad (1.5)$$

Thus the configuration variables q_{ab} , N and N^a are equivalent to g_{ab} . The canonical momenta conjugate to these variables are defined as

$$\pi^{ab} = \frac{\partial \mathcal{L}}{\partial \dot{q}_{ab}}, \quad \pi_N = \frac{\partial \mathcal{L}}{\partial \dot{N}}, \quad \pi_N^a = \frac{\partial \mathcal{L}}{\partial \dot{N}^a}, \quad (1.6)$$

where dot indicates a Lie derivative along t^a . The Hamiltonian of GR in

terms of these variables is

$$\begin{aligned}
\mathcal{H} &= N \left(\frac{1}{\sqrt{q}} \left(\pi_{ab} \pi^{ab} - \frac{1}{2} \pi^2 \right) - \sqrt{q} {}^{(3)}R \right) - 2N^a D_b(\pi_a^b) \\
&= N\mathcal{H}_G + N^a \mathcal{C}_a.
\end{aligned}
\tag{1.7}$$

The Hamiltonian does not contain any terms with π_N and π_N^a which are identically zero. This implies that the lapse and shift are not dynamical variables but act as Lagrange multipliers enforcing the Hamiltonian ($\mathcal{H}_G = 0$) and diffeomorphism $\mathcal{C}_a = 0$ constraints. These are first class constraints which impose the diffeomorphism invariance of GR. The Hamiltonian constraint results from the time reparameterization invariance of GR while the diffeomorphism constraints encode invariance under spatial diffeomorphisms.

The complexity as well as elegance of GR lies in the fact that the Hamiltonian of the theory is a combination of constraints. Since the constraints commute weakly with all observables, this implies that the Poisson bracket of all observables with the Hamiltonian (Hamilton's equations) is zero, implying that the dynamics of the theory is trivial. This does not mean that there is no dynamical content in the theory. Instead it means we should focus on relational dynamics, that is evolution with respect to an intrinsic time (which is some function of the phase space variables) as opposed to an external time parameter.

The other possibility is to construct gauge invariant observables. The simplest such observables that one can construct are integrals of scalar den-

sities, however these are extremely non-local and it is difficult to extract local physics from these observables. Within the framework of perturbation theory around a fixed background one can construct observables which are gauge invariant only up to a particular order in perturbations. This has proven to be a successful strategy in studying local phenomena like gravitational waves and in Cosmology. Another framework for constructing local observables that embraces the relational nature of dynamics in GR was introduced in [79, 80] and extended in [41]. However, going beyond the formal level within this framework has posed a formidable challenge.

A third approach is de-parameterization of the theory by using suitable matter fields for gauge fixing. Essentially the matter fields play the role of a dynamically coupled reference frame. De-paramaterized models with dust fields and scalar fields have been explored in literature [30]. A disadvantage of de-parameterization with matter fields is the complexity of the physical Hamiltonian obtained after gauge fixing. In this thesis we will focus on a partially de-parameterized model which uses a dust field to fix the time gauge. The main advantage of this approach is that the physical Hamiltonian obtained after this partial de-parameterization has a particularly simple form.

1.3 Time in Quantum Gravity

The role and consequences of diffeomorphism invariance in classical GR are well understood. However, such an understanding has proved elusive in the

quantum regime. Although the full diffeomorphism invariance of the theory poses significant challenges for any quantization program, here we will focus on the role of time reparameterization invariance.

Conventional formulations of quantum theory (quantum mechanics and quantum field theory) rely heavily on the assumption that a well defined notion of time external to the quantum system under consideration is available. Important aspects of the quantum theory like the definition of the vacuum and the invariance of the inner product under evolution are connected with a notion of time. Moreover, the construction of the Hilbert space requires a complete set of observables which commute at a fixed time or for spacelike points. If quantum gravity is to be interpreted as a theory of quantum geometry then notions such as spacelike separation become ambiguous since these are defined with respect to a fixed Lorentzian metric and not a fluctuating quantum entity.

Within the canonical formalism, following the procedure of Dirac quantization for constrained systems we can proceed by promoting the canonical variables (q_{ab}, π^{ab}) introduced in Section 1.2 as operators acting on a Hilbert space satisfying canonical commutation relations. The constraints are imposed as operators acting on the Hilbert space which annihilate all physical states. Thus the physical Hilbert space is a subspace of the kinematical Hilbert space and consists of states annihilated by the constraints. For the

Hamiltonian constraint this gives the famous Wheeler-DeWitt equation

$$\mathcal{H}_G |\psi\rangle = 0 \tag{1.8}$$

This equation lies at the heart of the ‘problem of time’ in canonical quantum gravity. Since the Hamiltonian \mathcal{H}_G is the generator of time translations, the WDW equation tells us that the state vectors $|\psi\rangle$ are ‘frozen’. The problem can also be stated for observables of the theory. Since physical observables in any gauge theory must commute with the constraints, observables in canonical quantum gravity commute with the Hamiltonian and are therefore non evolving. As in the classical theory this means that in order to talk about dynamics we need some intrinsic notion of time. At this point there are two ways to proceed. An internal time is identified and the theory is deparameterized before quantization or a timeless quantization is implemented and time is identified after quantization. A criticism of the first approach is that the degree of freedom chosen to play the role of time remains classical. If a matter degree of freedom is chosen as the internal time, this raises the question of applicability of this formalism in regions of high energy densities where we expect matter to behave quantum mechanically. The second approach faces several technical and interpretational challenges like identification of a suitable inner product and interpretation of the wavefunction. For details see [9, 62].

There are other approaches to quantum gravity which proceed without

any identification of time either before or after quantization. The most conservative of such approaches attempt to formulate dynamics in purely relational terms. The most well developed of these approaches is the formalism of complete and partial observables [78, 42, 41, 49, 85]. The main challenge with this approach is the complexity involved in pushing calculations beyond the formal level.

In this thesis we will focus on the first approach of indentifying a time and deparameterizing the theory before quantization. We focus on using a particular type of matter field (dust) to partially deparameterize the theory and investigate both the classical and quantum dynamics of this partially deparameterized theory.

This thesis is organized as follows: Chapter 2 outlines our model and deparameterization scheme. It also introduces the quantization scheme used to quantize the deparameterized theory and the Monte Carlo techniques we use for numerical computations. Chapter 3 explores the linearized theory in this matter time gauge. Chapter 4 investigates the mixmaster dynamics in the dust time gauge. Chapter 5 and 6 discuss the quantum dynamics of two symmetry reduced models. Chapter 7 provides a summary of the work detailed in this thesis and discusses future directions.

Chapter 2

Quantization with an Ideal Clock

Our everyday experience of time involves clocks made of matter. Modelling these clocks requires that we specify the internal dynamics of these clocks, which can be extremely complex. However, we can deal with this in the same way as we deal with other complex problems in physics - by means of an idealization. Instead of real matter clocks an ideal matter field may be used as a clock. As we'll show in this chapter, using a dust field as our ideal clock leads to a simple physical Hamiltonian [61].

It is well known that for full general relativity with matter content like dust fields [30] and scalar fields, the theory can be fully de-parameterized by treating the matter fields as a dynamically coupled physical reference frame. However, after a complete gauge fixing the physical Hamiltonian obtained

by solving the Hamiltonian constraint for the momentum conjugate to these matter fields is usually a square root Hamiltonian. The dust time gauge discussed in this chapter is a modification of the approach presented in [30]. It involves a partial gauge fixing by using the dust field as a time variable and solving the Hamiltonian constraint while leaving the spatial diffeomorphism constraints intact. This leads to a regular gauge theory with a physical Hamiltonian. Sections 2.1 and 2.2 detail the particulars of this partial gauge fixing. Section 2.3 presents the path integral approach to quantization for general relativity in the dust time gauge and Section 2.4 provides details of the Monte Carlo techniques we will use in this thesis to study the quantum dynamics of gravity + dust models.

2.1 General Relativity + Dust

The action for GR coupled to a dust field is given by

$$S = \frac{1}{2\pi} \int d^4x \sqrt{-g} R - \frac{1}{4\pi} \int d^4x \sqrt{-g} M (g^{\mu\nu} \partial_\mu \phi \partial_\nu \phi + 1). \quad (2.1)$$

The second term is the dust action. The parameter M enforces the constraint that the gradient of the dust field (ϕ) is timelike. The form of the stress energy tensor indicates that on-shell M is the energy density of the dust field.

The ADM canonical theory obtained from this action is

$$S = \frac{1}{2\pi} \int dt d^3x \left(\pi^{ab} \dot{q}_{ab} + p_\phi \dot{\phi} - N\mathcal{H} - N^a \mathcal{C}_a \right), \quad (2.2)$$

where the pairs (q_{ab}, π^{ab}) and (ϕ, p_ϕ) are respectively the phase space variables of gravity and dust. The lapse and shift functions, N and N^a are the coefficients of the Hamiltonian and diffeomorphism constraints

$$\mathcal{H} = \mathcal{H}^G + \mathcal{H}^D, \quad (2.3)$$

$$\begin{aligned} \mathcal{C}_a &= \mathcal{C}_a^G + \mathcal{C}_a^D \\ &= -2D_b \pi_a^b + p_\phi \partial_a \phi, \end{aligned} \quad (2.4)$$

where \mathcal{H}^G is the gravitational part of the Hamiltonian constraint and

$$\mathcal{H}^D = \frac{1}{2} \left(\frac{p_\phi^2}{M\sqrt{q}} + M\sqrt{q}(q^{ab}\partial_a\phi\partial_b\phi + 1) \right). \quad (2.5)$$

The momentum conjugate to the field M is zero since it appears as a Lagrange multiplier in the covariant action. At this point one could enlarge the phase space to treat M and its conjugate momentum as independent degrees of freedom, subsequently eliminating them by gauge fixing. However, it is more straightforward to vary the term \mathcal{H}^D in the canonical action with

respect to M , and use the resulting equation of motion:

$$M = \pm \frac{p_\phi}{\sqrt{q(q^{ab}\partial_a\phi\partial_b\phi + 1)}}. \quad (2.6)$$

This can then be substituted back into \mathcal{H}^D to give

$$\mathcal{H}^D = \text{sgn}(M) p_\phi \sqrt{q^{ab}\partial_a\phi\partial_b\phi + 1}, \quad (2.7)$$

leaving a canonical action for $(q_{ab}, \pi^{ab}), (\phi, p_\phi)$. It is readily verified that the constraints remain first class with this elimination of M . We will see in the gauge fixing below how the sign is selected.

2.2 Dust time gauge

We can now partially reduce the theory by fixing only a time gauge, and solving the Hamiltonian constraint to obtain a physical Hamiltonian. The spatial coordinates remain unfixed. We use the dust time gauge [61, 83] which equates the physical time with the dust field, i.e., the spatial hypersurfaces are level surfaces of the dust field,

$$\lambda \equiv \phi - \epsilon t \approx 0, \quad \epsilon = \pm 1. \quad (2.8)$$

This is a special case of the Brown-Kuchař matter reference frame that fixes all four coordinate gauges. The condition Eq. (2.8) has a nonzero Pois-

son bracket with the Hamiltonian constraint, so this pair of constraints together is second class. Furthermore, this condition implies that $q^{ab}\partial_a\phi\partial_b\phi = 0$, resulting in a dust Hamiltonian linear in the momentum i.e., $\mathcal{H}^D = \text{sgn}(M)p_\phi$.

A gauge condition is deemed good if the matrix of Poisson brackets of second class constraints is invertible and demanding that the gauge condition be preserved in time does not lead to new constraints. The first of these gives, using Eq. (2.7), the Dirac matrix of second class constraints

$$C = \begin{bmatrix} 0 & \{\lambda, \mathcal{H}\} \\ \{\mathcal{H}, \lambda\} & 0 \end{bmatrix} = \text{sgn}(M) \begin{bmatrix} 0 & 1 \\ -1 & 0 \end{bmatrix}. \quad (2.9)$$

This matrix is invertible everywhere on the manifold. Thus, the dust time gauge does not breakdown at any point and is therefore a robust choice. The second condition, requiring that the gauge condition be preserved in time, gives an equation for the lapse function:

$$\epsilon = \dot{\phi} = \left\{ \phi, \int d^3x (N\mathcal{H} + N^a\mathcal{C}_a) \right\} \Big|_{\phi=t} = \text{sgn}(M)N. \quad (2.10)$$

The corresponding physical Hamiltonian density is

$$\mathcal{H}_P = -\epsilon p_\phi = \text{sgn}(M) \epsilon \mathcal{H}^G = N\mathcal{H}^G, \quad (2.11)$$

where the third equality follows from solving the Hamiltonian constraint and

the last follows using (2.10). We also note that the definition of p_ϕ from the dust action, in this gauge, gives

$$p_\phi = \frac{M}{N} \sqrt{q} \dot{\phi} = \text{sgn}(M) \epsilon \frac{|M|}{N} \sqrt{q} = |M| \sqrt{q} \epsilon. \quad (2.12)$$

Thus, positive dust energy density corresponds to a positive Hamiltonian density if $N = -1$, implying $\epsilon = -1$. Substituting into Eq. (2.2) gives the gauge fixed action

$$S^{GF} = \frac{1}{2\pi} \int dt d^3x [\pi^{ab} \dot{q}_{ab} + \mathcal{H}^G - N^a \mathcal{C}_a^G], \quad (2.13)$$

up to surface terms, which do not concern us here. Thus we see that in the dust time gauge the diffeomorphism constraint reduces to that with only the gravity contributions, and the physical Hamiltonian is

$$H_p = -\frac{1}{2\pi} \int d^3x \mathcal{H}^G. \quad (2.14)$$

The corresponding spacetime metric is

$$ds^2 = -dt^2 + (dx^a + N^a dt)(dx^b + N^b dt) q_{ab}. \quad (2.15)$$

In the presence of other matter fields the gauge fixed action takes the simple

form

$$S^{GF} = \frac{1}{2\pi} \int dt d^3x [\pi^{ab} \dot{q}_{ab} + p_\chi \dot{\chi} + (\mathcal{H}^G + \mathcal{H}^M) - N^a (\mathcal{C}_a^G + \mathcal{C}_a^M)], \quad (2.16)$$

where the matter fields are symbolically denoted by (χ, p_χ) although the number of fields and their tensorial structures depend on the choice of matter Lagrangian. The matter Hamiltonian is denoted as \mathcal{H}^M and the matter part of the diffeomorphism constraint is denoted as \mathcal{C}_a^M .

By fixing the time gauge we have only partially reduced the theory. The gauge fixed action is still invariant under spatial diffeomorphisms. However, now the theory resembles a conventional gauge theory with a physical Hamiltonian providing dynamics.

It is curious that in the dust time gauge solutions that satisfy $H_p = 0$ correspond to vacuum solutions of GR. This leads to the apparent contradiction that vacuum solutions of GR are recovered in the presence of a dust field. At the level of the covariant Lagrangian for the GR + dust system no contradiction exists. Here, the parameter M plays the role of a Lagrange parameter that enforces the constraint that the four velocity of the dust is timelike. As it happens, the equations of motion allow for solutions for which the Lagrange parameter vanishes and the dust field is allowed to be arbitrary. These solutions correspond to vacuum solutions of GR. The dust time gauge then picks out some such solutions for which the $\dot{\phi} = 1$. At the canonical level, it is important to note that when $H_p = 0$, the energy density of the dust

field (M) also vanishes. An important aspect in which the dust time gauge solutions differ from vacuum GR solutions is that these systems still involve an additional physical degree of freedom which can be perturbed. This is evident when we study the linearized theory around Minkowski spacetime in the dust time gauge.

In the remainder of this thesis we will explore the classical and quantum aspects of this theory. In particular, we will discuss the quantum dynamics of the homogeneous sector of the theory. We will proceed by symmetry reducing the theory before quantization. Though it is unclear how this truncated model relates to the quantum theory of the full model, we hope that central features of the quantum dynamics of the symmetry reduced model survive in the full theory.

2.3 The Path Integral approach

The main considerations in setting up a path integral for gravity are the choice of the action for gravity, the choice of measure on the space of paths (here spacetime metrics) and the choice of discretization scheme for the gravitational action. Formally we can write the path integral as

$$Z[g] = \int \mathcal{D}[g] \exp\{i S_{GR}[g]\} \quad (2.17)$$

or in the canonical formalism as:

$$Z[\pi, q] = \int \mathcal{D}[q] \mathcal{D}[\pi] \mathcal{D}[N] \exp\{iS_{ADM}\}, \quad (2.18)$$

where the integrations ($\int \mathcal{D}[N]$) over the lapse function (N) and the shift vector (N^a) impose the hamiltonian and diffeomorphism constraints. The difficulty in defining the measure arises due to the diffeomorphism invariance of GR, which necessitates that in order to ensure the path integral converges the measure must be chosen such that all geometries related by diffeomorphisms are counted only once. In the language of gauge theories, we need to define a measure on the space of all metrics quotiented by the diffeomorphism group. Generally for gauge theories, such an overcounting is prevented by imposing a gauge condition in the path integral using a procedure like Faddeev-Popov or more generally by constructing the integral using BRST quantization. Such procedures have been investigated in the context of perturbation theory, quantum cosmology and lower dimensional gravity theories, but these analyses have resisted attempts towards generalization for full GR in $3 + 1$ dimensions [84, 86, 87, 12].

In the context of canonical quantization, saddle point (semiclassical) approximations of the Euclidean Path Integral approach have been studied extensively to find solutions of the Wheeler DeWitt equation (WDW) in the minisuperspace setting. Specifying solutions to the WDW equation involves selecting appropriate boundary conditions for the equation i.e., prescribing

initial conditions for the universe. For the path integral this corresponds to the choice of paths to be included in the integration. It was demonstrated by Hartle and Hawking that the amplitude for a 3-geometry to arise from “nothing” can be obtained by evaluating the sum over all 4-geometries it bounds. This is the no-boundary proposal. Several proposals have since been made for both the boundary conditions and the set of paths to be included in the sum to find solutions of the WDW. However these proposals are all restricted to semiclassical approximations of the path integral and no generalization to the full non-perturbative setting has been explored.

Another possibility of constructing the path integral and bypassing these difficulties is offered by the reduced phase space approach. Here, the quantization proceeds after classically fixing all gauges and solving all first class constraints. Using the dust time gauge detailed in the previous sections, we obtain a simple physical Hamiltonian and the path integral can be constructed as follows:

$$Z = \int \mathcal{D}[\pi] \mathcal{D}[q] \mathcal{D}N^a \exp\{iS^{GF}\} \quad (2.19)$$

where we have used the gauge fixed action S^{GF} given in Eq. (2.16). Since we have not done a complete gauge fixing, the spatial diffeomorphism constraint still needs to be imposed and thus the path integral involves an integration over the shift vector. This approach is exactly equivalent to the reduced phase space approach in the minisuperspace setting i.e., after symmetry reduction

to homogeneity.

2.3.1 Symmetry reduced Path Integrals

We are interested in constructing the minisuperspace path integral in the dust time gauge. Classically, the reduction to the homogeneous sector in the dust time gauge begins with the spacetime metric ansatz:

$$ds^2 = -dt^2 + q_{ij}(t)\omega^i\omega^j \quad (2.20)$$

where ω^i are invariant 1-forms corresponding to the isometry group of the spatial manifold and we set $N^i = 0$ without loss of generality.

Due to homogeneity the diffeomorphism constraint is trivially satisfied and the gauge fixed action is given by

$$S^{SR-GF} = \frac{1}{2\pi} \int dt d^3x [\pi^{ab}\dot{q}_{ab} - \mathcal{H}_p], \quad (2.21)$$

with

$$\mathcal{H}_p = -\mathcal{H}^G. \quad (2.22)$$

It is straightforward to construct the path integral for this symmetry reduced model. We first define the Lagrangian density for the degrees of freedom of the reduced phase space via a Legendre transform:

$$\mathcal{L}_p(q_{ab}, \dot{q}_{ab}) = \pi^{ab}\dot{q}_{ab} - \mathcal{H}_p \quad (2.23)$$

and construct the Feynman path integral as:

$$Z = \int \mathcal{D}[q] \exp \left\{ i \int dt d^3x \mathcal{L}_p([q], [\dot{q}]) \right\}. \quad (2.24)$$

The measure is defined as

$$\mathcal{D}[q] = \lim_{N \rightarrow \infty} \prod_{n=1}^N d[q_n] \quad (2.25)$$

where $[q_n]$ denotes the spatial metric for the n^{th} hypersurface i.e., each hypersurface is a 3-dimensional time slice and the square brackets denote that we have suppressed the indices of a tensor.

In this symmetry reduced sector the quantization of this gauge fixed theory is equivalent to reduced phase space quantization. It is important to note that a time gauge other than dust time would lead to an unitarily inequivalent theory. Furthermore, most other time gauges explored in literature (like York time, scalar field time etc.) lead to a square root Hamiltonian, resulting in further technical complications. It is also important to keep in mind that reduced phase space quantization is generally inequivalent to Dirac quantization [81]. In Chapter 5 we discuss a quantum gravity model for which the path integral is exactly solvable and quantization using the dust time gauge is equivalent to Dirac quantization with a particular operator ordering.

2.4 Path Integral Monte Carlo

Even though the dust time gauge results in a relatively simple Hamiltonian, in general the path integral in Eq. (2.25) is not exactly solvable and must be tackled numerically. Monte Carlo methods are a staple tool in many areas of physics (e.g. Lattice QCD [50], atomic and nuclear physics [31, 77]) for solving analytically intractable integrals. In the context of quantum cosmology these methods have been applied to cosmological models [24, 23, 20] where the Hamiltonian constraint is not solved classically but instead implemented as a constraint on the paths evaluated numerically. In [5] we applied the Path Integral Monte Carlo (PIMC) technique to study the reduced phase space quantization of a spatially closed Friedmann-Lematre-Robertson-Walker (FLRW) model with a non-zero cosmological constant and a dust field. This section introduces the central ideas behind Monte Carlo Integration, details the PIMC algorithm and discusses some results from [5]. In Chapter 6 we will discuss the application of Path Integral Monte Carlo (PIMC) to numerically evaluate the path integral for a Bianchi I model.

Monte Carlo integration is based on the observation that the integral of a function $f(x)$ can be interpreted as the expected value of $f(X)$ where X is a random variable uniformly distributed over the domain of integration. That is,

$$\int_a^b f(x)dx = (b - a) \int f(s)p_X(s)ds \quad (2.26)$$

where

$$p_X(s) = \begin{cases} \frac{1}{b-a}, & a \leq s \leq b \\ 0, & \text{otherwise} \end{cases} \quad (2.27)$$

A Monte Carlo algorithm generates samples of the random variable and approximates the function $f(x)$ with the average over N samples ($X_i, i = 1..N$).

We have

$$(b-a) \lim_{N \rightarrow \infty} \frac{1}{N} \sum_{i=1}^N f(X_i) = \int_a^b f(x) dx. \quad (2.28)$$

For finite N , we have

$$\int f(x) dx \approx \langle f \rangle \pm \sqrt{\frac{\langle f^2 \rangle - \langle f \rangle^2}{N}}. \quad (2.29)$$

The generalization to higher dimensions is straightforward. In the limit $N \rightarrow \infty$, the Monte Carlo estimate tends to a normal distribution whereas the error terms tends to a standard deviation. Given the form of the second term (error) in the equation above, the error in the integration is smaller for flatter $f(x)$. This observation leads us to notion of importance sampling for reducing the error.

2.4.1 Importance Sampling and Markov Chains

Suppose we can find a positive function $g(x)$ such that $\int g(x) dx = 1$ and $f(x) = h(x)g(x)$ with $h(x)$ nearly constant, then the integral in Eq. (2.29)

can be evaluated as

$$\int f(x)dx = \int h(x)g(x)dx \sim \frac{1}{N} \sum_{j=1}^N h(X_j), \quad (2.30)$$

where X_j is sampled from the distribution $\int g(x)dx$. The function $g(x)$ accomplishes the importance sampling allowing more points to be sampled near peaked regions i.e., where the function $f(x)$ takes its largest values. Since $h(x)$ is nearly flat the standard deviation of the sampled values is small and the error in the integration is controlled.

Sampling an arbitrary distribution $\int g(x)dx$ is not straightforward if the cumulative distribution for the probability density function (PDF) $g(x)$ is not analytically calculable and invertible. In such scenarios, the PDF can be sampled by a rejection method which involves choosing a random point with uniform probability in the area under the curve $g(x)$. Such a method is easy to implement for one-dimensional PDFs, but does not generalize well to higher dimensions. For multi-dimensional integrals importance sampling can be done using stationary stochastic processes.

A stochastic process is a sequence of events X_t for $t = 0, 1, 2, \dots$, that are governed by a probabilistic law $P(X_t|X_0, \dots, X_{t-1})$ such that the conditional probability of the event X_t occurring depends on any number of previous events and may also depend on t . The central idea of importance sampling using stochastic processes is to set up a stationary stochastic process whose probabilistic law is the target distribution to be sampled for the integration.

A stochastic process is said to be stationary when the conditional probabilities are unchanged by shifts in t . This implies that the mean $E(X_t) = \mu$ is independent of t and the variance $E((X_t - \mu)^2)$ is independent of t if $E(X_t^2)$ is finite. Monte Carlo integration as described above requires statistically independent random samples. However, the events in a stationary stochastic process are not statistically independent random variates. The degree of statistical dependence of the current sample on previous samples is quantified using the autocorrelation function. By collecting samples separated by several time steps from the stationary stochastic processes we can ensure the autocorrelation between consecutive samples is low¹. The number of time steps that must be skipped is determined by the particular stochastic process. Furthermore, it is possible to calculate the error introduced in the Monte Carlo estimate due to the autocorrelation between samples,

$$\int f(x)p(x)dx \sim \frac{1}{N} \sum_{i=1}^N f(X_i) \pm \sqrt{\frac{R_0(f) + 2 \sum_{h \geq 1} R_h(f)}{N}}, \quad (2.31)$$

where $R_h(f) = \frac{1}{N-h} \sum_{i=1}^{N-h} (f(X_i) - \langle f \rangle)(f(X_{i+h}) - \langle f \rangle)$.

A simple stochastic process commonly used for Monte Carlo integrations is a Markov chain. Markov chains are defined by the property that the conditional probability for next event depends only on the current event, i.e., $P(X_t|X_0, \dots, X_{t-1}) = P(X_t|X_{t-1})$. Ergodic Markov chains possess the

¹The samples are separated in Monte Carlo time. This is completely distinct from the dynamical time of the models we will consider.

remarkable property that irrespective of the initial transition probabilities (conditional probability to go from one state to the next) when the chain is started, the transition probability converges to a unique probability distribution as the chain approaches equilibrium. Combined with the property that ergodic Markov chains always tend towards stationarity, this can be exploited to develop an algorithm to sample a Markov chain whose unique stationary distribution is the target distribution we are interested in. The process of bringing a Markov chain into equilibrium is known as thermalization. Further details about Markov processes can be found in the review [74].

2.4.2 Metropolis - Hastings algorithm

Given a PDF $G(x)$ that we are interested in sampling, the above discussion instructs us to construct a Markov chain whose limiting stationary distribution is $G(X)$. The Metropolis - Hastings algorithm is a simple method for constructing such a Markov chain [54]. Moreover, it has the advantage that the normalization of the PDF is not required for the calculation. This is particularly useful when the normalization for a function $g(x)$ cannot be calculated explicitly. The algorithm proceeds as follows:

1. Given an event X , propose a new event \tilde{X} using a normalized proposal density $P(\tilde{X} \leftarrow X)$

2. Accept the new event with probability

$$A(\tilde{X} \leftarrow X) = \min \left(1, \frac{P(X \leftarrow \tilde{X})G(\tilde{X})}{P(\tilde{X} \leftarrow X)G(X)} \right)$$

3. If the proposed event is rejected, retain the old event X .

The Metropolis-Hastings algorithm exploits detailed balance² at each step to construct an ergodic Markov Chain with the stationary distribution $G(X)$. A disadvantage of the method is the high autocorrelation between successive events. Usually the autocorrelation decreases as the number of steps between events in the chain is increased. Therefore, the autocorrelation between sampled random variates can be reduced by increasing the number of steps between sampled events. Generally, the Markov chain generated using Metropolis - Hastings algorithm is not stationary to begin with. Therefore, we discard several events in the chain and only start sampling after the chain is thermalized.

²Detailed balance implies that the probability of going from one event s_i to another event s_j is the same as the probability of going from s_j to s_i . Formally, let w_i be the probability of finding the Markov chain at event s_i in equilibrium and let w_{ij} be the transition probability to go from s_i to s_j , then detailed balance implies $w_i p_{ij} = w_j p_{ji}$.

2.4.3 Evaluating Path Integrals

The Metropolis-Hastings algorithm allows us to sample a probability distribution in order to generate samples to calculate Monte Carlo averages. Path Integral Monte Carlo employs an importance sampling algorithm, like Metropolis-Hastings, to calculate path integrals. In order to make path integrals amenable to Monte Carlo integration we need to work in the imaginary time formalism. Let us consider a single particle system with action $S(x, \dot{x})$. The path integral for this system is defined as

$$Z = \int \mathcal{D}x e^{iS}, \quad (2.32)$$

with

$$\mathcal{D}x = \lim_{N \rightarrow \infty} \prod_{i=1}^N x_i. \quad (2.33)$$

Expectation values of observables are calculated as

$$\langle \hat{O} \rangle = \int \mathcal{D}x O e^{iS}. \quad (2.34)$$

The integral in Eq. (2.32) & (2.34) is an N dimensional integral and highly oscillatory. To alleviate this issue we can turn to the imaginary time formalism using a Wick rotation. Under a Wick rotation $t \rightarrow it$, the path integral transforms as

$$Z \rightarrow \int \mathcal{D}x e^{-S_E(x, \dot{x})}, \quad (2.35)$$

where the overdot denotes a derivative with respect to Euclidean time. The path integral after Wick rotation involves the factor $e^{-S_E(x,\dot{x})}$, which is a normalisable function when S_E is bounded below. Thus, we can apply Monte Carlo integration to calculate integrals like Eq. (2.34) by generating samples (paths) from the PDF

$$\frac{e^{-S_E}}{\int \mathcal{D}\phi e^{-S_E}}. \quad (2.36)$$

Since the normalization factor is not generally calculable, we apply the Metropolis-Hastings algorithm for sampling this distribution. This calculation yields expectation values for the Euclidean sector of the theory and these numerical results can usually not be rotated to the Lorentzian sector. However, from quantum mechanics we know that the ground state of the system can be obtained from the Euclidean propagator in the limit of infinite Euclidean time (τ), i.e.

$$\lim_{\tau \rightarrow \infty} \int_{x_i}^{x_f} \mathcal{D}x e^{-S_E(x,\dot{x})} = |\psi_0(x_i, x_f)|^2. \quad (2.37)$$

Moreover, correlation functions can also be obtained from the Euclidean path integral as

$$\langle x(t_2)x(t_1) \rangle = \frac{\int_{x_i}^{x_f} \mathcal{D}x x(t_2)x(t_1) \exp \left\{ - \int_{-\infty}^{\infty} d\tau L(x, \dot{x}) \right\}}{\int \mathcal{D}x \exp \left\{ - \int_{-\infty}^{\infty} d\tau L(x, \dot{x}) \right\}}. \quad (2.38)$$

Analogously for the gravitational path integral we can define the ground state wavefunction as

$$|\psi_0[q]\|^2 = \lim_{\tau \rightarrow \infty} \int \mathcal{D}[q] \mathcal{D}N^a \exp\{-S_E^{GF}\} \quad (2.39)$$

where S_E^{GF} is the Euclidean analog of the gauge fixed action defined in Eq. (2.13).

Let us consider the PIMC technique applied to a gravity model. In [6] we studied a closed FLRW model with dust and a cosmological constant using PIMC. The ADM variables for a closed homogeneous and isotropic cosmology are

$$q_{ab} = \frac{3}{8} A^{4/3}(t) h_{ab}, \quad \pi^{ab} = 2A^{-1/3}(t) p_A(t) \sqrt{h} h^{ab}, \quad (2.40)$$

where $h_{ab} = \frac{1}{f^2(r)} e_{ab}$ with $f(r) = 1 + \kappa r^2/4$, $e_{ab} = \text{diag}\{1, 1, 1\}$, and $\text{sgn}(\kappa) = 1$.

The gauge fixed action for this model is

$$S = \int dt \left(\frac{\dot{A}^2}{2} + \frac{\Lambda}{2} A^2 - \kappa A^{2/3} \right). \quad (2.41)$$

After the Wick rotation $t \rightarrow -it$, the Euclidean path integral is

$$G(A_f, A_i) = \int_{A_i}^{A_f} \mathcal{D}A \exp(-S_E), \quad (2.42)$$

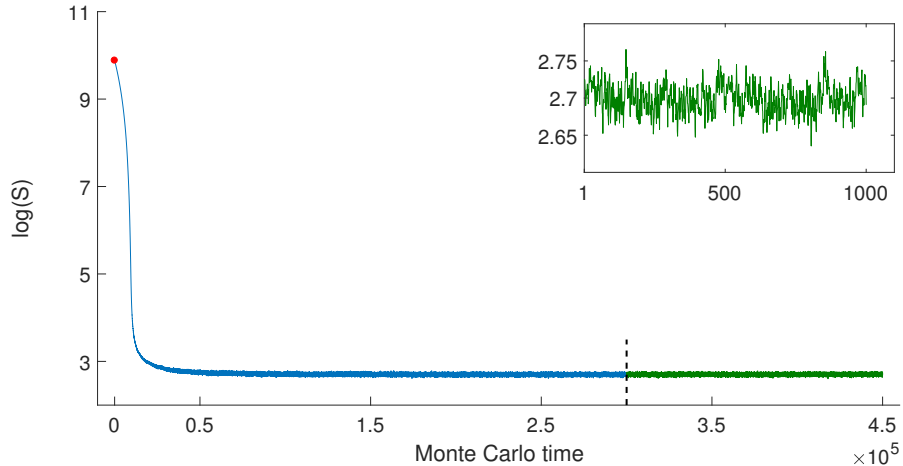


Figure 2.1: Log of the action S vs Monte Carlo time ($\#$ of MC sweeps) from one representative run. The red dot shows the starting value of the action (for a random initial path), the blue curve shows the action during thermalization, the dashed black line marks the point where measurements are started, and the green curve shows the action values during measurement. It is clear that the action achieves thermalization after around 100,000 thermalization steps. In the inset, the last thousand samples taken during measurement are plotted, to show the variations in the action around its mean value.

where

$$S_E = \int_0^T d\tau \left(\frac{\dot{A}^2}{2} - \frac{\Lambda}{2} A^2 + \kappa A^{2/3} \right). \quad (2.43)$$

As is well known, in classical theory there is a unique on-shell path once the initial conditions are specified, whereas in quantum theory an infinite number of paths contribute to the Feynman path integral, each with a phase $\exp(iS)$. After Wick rotation, the amplitude $\exp(-S_E)$ may be treated as a probability distribution on the space of paths. The PIMC technique generates a Markov chain of paths from an initial seed path, such that the stationary distribution for the Markov chain is given by the amplitude $\exp(-S_E) / \int \mathcal{D}A \exp(-S_E)$. In order to probe the space of paths effectively we use the Metropolis algorithm for importance sampling.

We start by discretizing the Euclidean action for the model. The time

interval from 0 to T is divided into N steps; $A(t) \rightarrow A_i, i = 1..N$. For the time-derivative, we use a forward step, $\dot{A}(t) \rightarrow (A_{i+1} - A_i)/\epsilon$. The corresponding discrete action is

$$S_E = \sum_{i=1}^{N-1} \epsilon \left[\frac{(A_{i+1} - A_i)^2}{2\epsilon^2} - \Lambda A_i^2 + \kappa A_i^{2/3} \right]. \quad (2.44)$$

With this discretization, the PIMC method we use proceeds as follows. After fixing an initial path $A_{\{i\}}^{start}$, (which could be selected by a deterministic or random rule),

1. Change a random element of the array: $A_i \rightarrow A_i^{new} = A_i + \delta$, where $\delta \in [-\Delta, \Delta]$ is a random number chosen from a uniform distribution, with Δ a fixed parameter;
2. Calculate the change in the Euclidean action: $\Delta S = S_{new} - S_{old}$;
3. Accept or reject this change. If $\Delta S \leq 0$, the change is accepted, otherwise it is accepted with a probability $\exp(-\Delta S)$; if accepted, the selected element is updated: $A_i := A_i^{new}$;
4. Repeat steps 1–3, N times. This defines one Monte Carlo (MC) sweep.

As discussed earlier, the Markov chain must be allowed to settle into a stationary state via the process of thermalization. We perform M_{therm} MC sweeps to thermalize the chain and our criteria for thermalization is that the value of the action stabilizes to some equilibrium value. Fig. 2.1 shows the

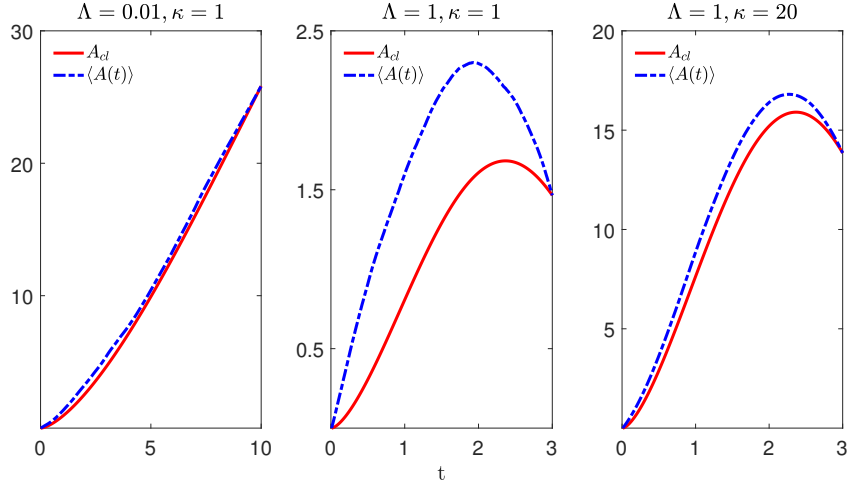


Figure 2.2: The average quantum path $\langle A(t) \rangle$ and the classical solution $A_{cl}(t)$ for various values of Λ and κ . The quantum path is close to, but distinct from the classical path.

thermalization of the action for a representative run for a given set of MC parameters, for a specific $A_{\{i\}}^{start}$. After the Markov chain is thermalized the paths are sampled. We generate a set of M_{samp} paths by sampling a path after every M_{skip} MC sweeps. The number M_{skip} is chosen to reduce the autocorrelation among paths. Once the set of sample paths are collected, expectation values of observables are calculated by averaging over the set of samples.

By seeding the Markov chain with a classical solution we can study quantum fluctuations around fixed classical solutions. The end points of the path are fixed to classical values throughout the thermalization and sampling process. Using the sampled paths we can compute the expectation value of the scale factor $A(t)$ and the fluctuations in the spatial volume $\Delta V(t)/\langle V(t) \rangle \equiv \sqrt{\langle V(t)^2 \rangle - \langle V(t) \rangle^2} / \langle V(t) \rangle$. Figures 2.2 & 2.3 show the results of these computations for three sets of values of Λ and κ .

For the $\Lambda \leq 0$ case the Euclidean action for this model is bounded below and we can calculate two-point correlation functions (Figure 2.4) as well as

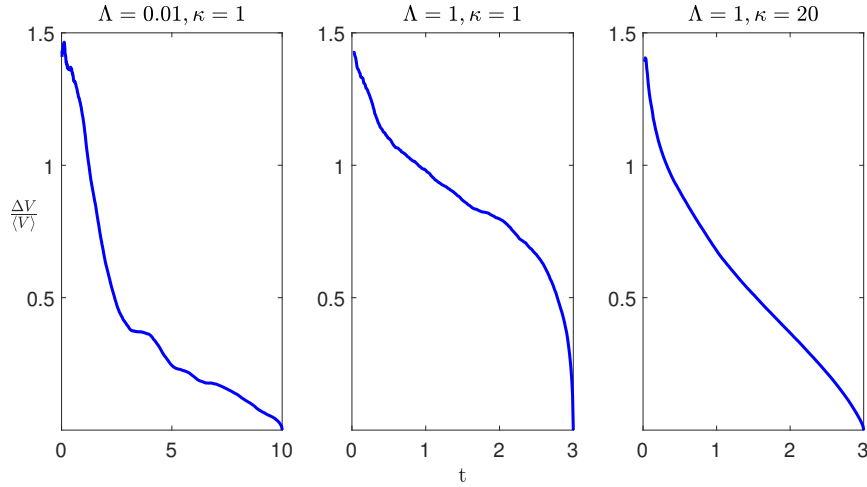


Figure 2.3: Fluctuations in the volume $\Delta V/\langle V \rangle$ for the same paths as in Figure 2.2. It is apparent that at early times and small Universes, fluctuations

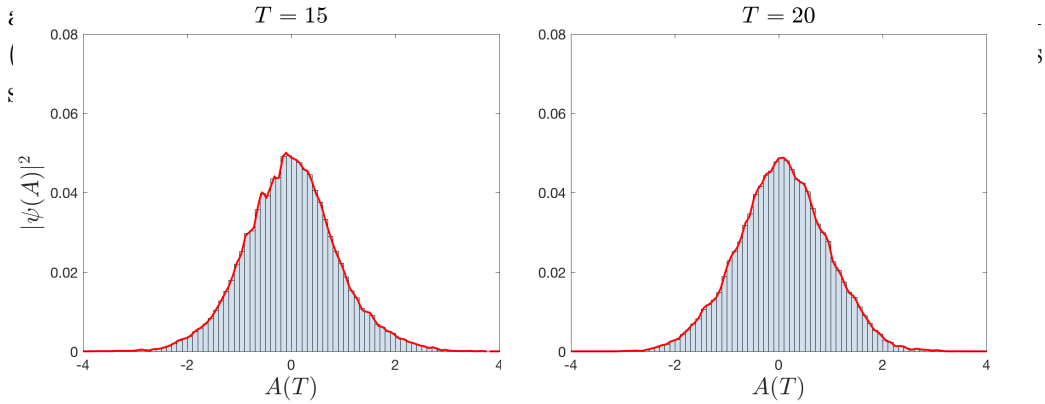


Figure 2.4: The unique ground state wavefunction for the case $\Lambda = -1$. The minor variations in the wave function are due to sample size and bin size.

the unique ground state of the model (Figure 2.5).

For $\Lambda > 0$, the Euclidean action is not bounded below and no unique ground state exists. However, we can still use the PIMC technique to calculate wavefunctions of the universe. In particular, we calculate the no-boundary wavefunction. In this model, the no-boundary proposal corresponds to calculating the amplitude of a finite spatial volume 3-geometry to emerge from a zero volume one. That is, we integrate over sets of paths with $A(0) = 0$ with the

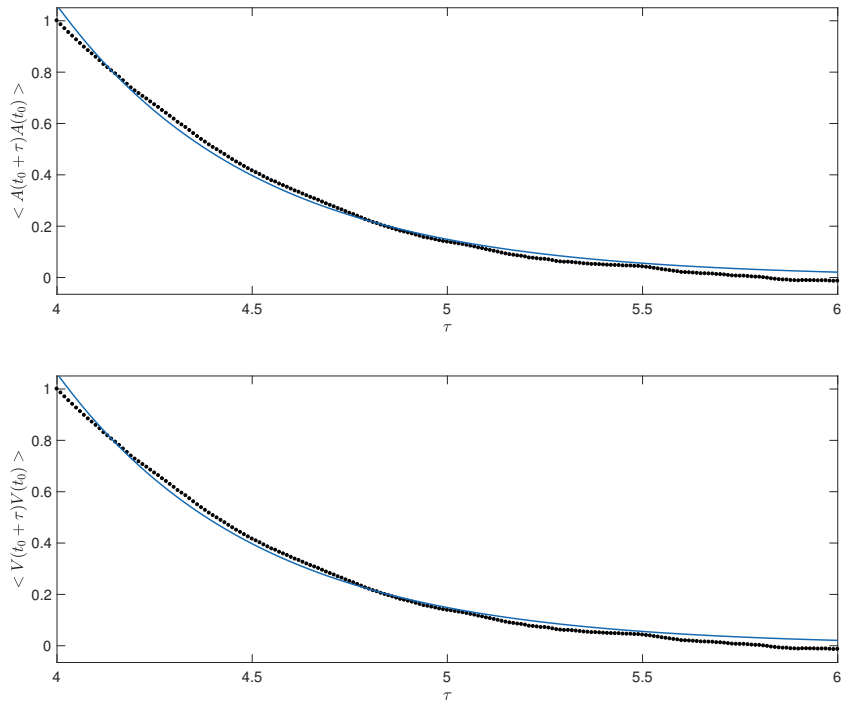


Figure 2.5: Plots of the correlation function for $A(t)$ and the volume $V(t)$. The black dots indicate the actual data points while the solid blue lines indicate exponential curves fitted to the data. Both functions show an exponential decay.

final value $A(T) \equiv q$ left unspecified; the wavefunction we calculate is

$$\psi(q, T) = \prod_{i=1}^{N-1} \int dA_i \exp \left\{ - \sum_{i=1}^{N-1} \frac{(A_{i+1} - A_i)^2}{2\epsilon} - \frac{\Lambda}{2} A_i^2 + \kappa A_i^{2/3} \right\}, \quad (2.45)$$

where the sample paths include only those with $A_0 = 0$ and $A_N = q$ left free. The wavefunctions $\psi(q, T)$ for both $\Lambda \leq 0$ and $\Lambda > 0$ are determined by binning the values of q at the last time step T . Figure 2.6 displays the no-boundary wavefunction for $\Lambda = 1$.

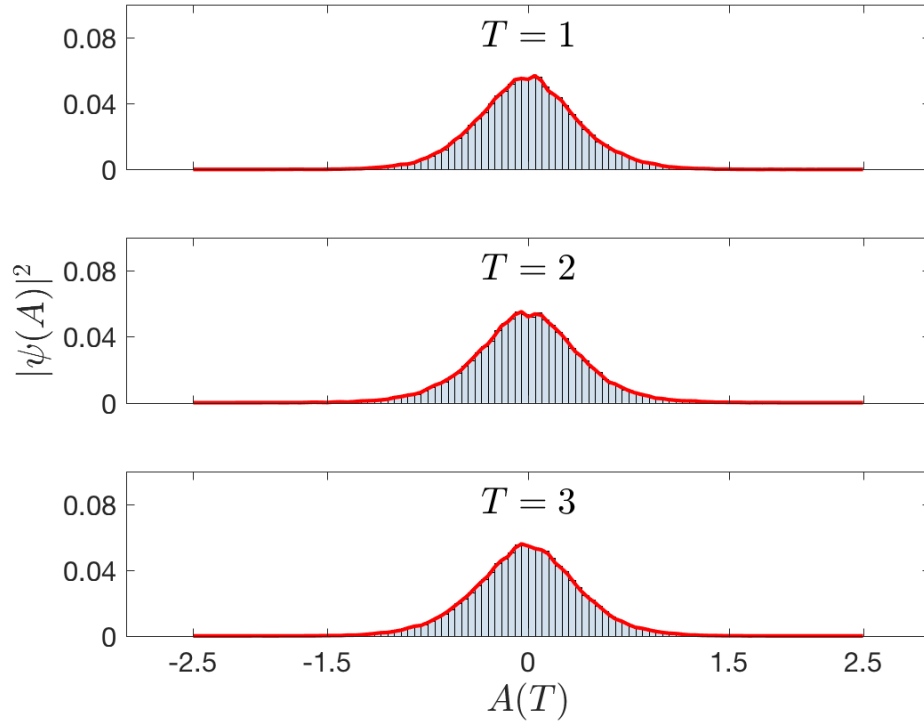


Figure 2.6: The no boundary wavefunction for $\Lambda = 1$, $\kappa = 20$. The plot was generated using 50,000 sample paths for each value of T . The MC runs were started with a random path with $A(t) \in [-500, 500]$ and $A(0) = 0$. We used $\epsilon = 0.01$, $\Delta = 0.1$ and $M_{therm} = 10^6$. The histogram was computed using a bin size of 0.05.

In Chapter 6 we present similar calculations for the Bianchi I model. We will adapt the algorithm detailed here for a single scale factor to three independent variables. Interestingly, for the Bianchi I model, a natural regularization scheme results in a Euclidean action that is bounded below.

Chapter 3

Linearized theory with dust

The transverse-traceless (TT) gauge is common to both the covariant and ADM analysis of vacuum linearized theory and in both analyses yields the two unconstrained graviton degrees of freedom. The ADM analysis starts with the expansion of the constraints of general relativity (GR) around the flat spacetime solution, followed by the imposition of TT gauge conditions [13], which are four conditions that fix four coordinates. These are conditions on the gravitational phase space variables alone, even when matter perturbations are considered [65].

In a Hamiltonian setting with general relativity coupled to matter, it is clearly possible to use matter degrees of freedom in making coordinate gauge choices. This is not usually done because the interpretation of gravitational waves as spin 2 fields on a background spacetime is lost. Furthermore, it is apparent that if matter degrees of freedom (“matter reference systems”) are

used to fix spacetime diffeomorphism freedom, then the gauge fixed theory has additional local degrees of freedom in the geometry sector, which makes it harder to interpret physically.

In [8] we considered this possibility in the setting of general relativity coupled to dust and any other matter field. The analysis used the dust time gauge detailed in Chapter 2. This chapter details the analysis and results of [8]. The main result of this chapter is that after a complete gauge fixing the dust degree of freedom is manifest as an ultralocal scalar mode in the spatial metric, and the interpretation of gravitational waves as spin 2 fields on the background is preserved.

In the next section we present the linearized theory of general relativity coupled to a dust field in the dust time gauge. Section 3.2 comments on the extension of the model by including a potential for the dust field. In Section 3.3 we explore the deformation of the physical Hamiltonian to include the Hořava-Lifshitz parameter and consider its impact on the linearized theory. Section 3.4 provides some concluding remarks for this chapter.

3.1 The Linearized Theory

Let us consider the action (2.16) without matter, i.e. $\chi = p_\chi = \mathcal{H}^M = \mathcal{C}_a^M = 0$. It is easy to check that Minkowski spacetime, $q_{ab} = \delta_{ab}$, $\pi^{ab} = 0 = N^a$, is a solution to the equations of motion in the dust time gauge¹. We linearize

¹It might seem strange that Minkowski spacetime is a solution in the presence of a dust field. But it is important to note that for a Minkowski spacetime $H_p = 0$ implying

the theory on this background by writing

$$q_{ab}(x, t) = \delta_{ab} + h_{ab}(x, t), \quad \pi^{ab} = 0 + p^{ab}(x, t), \quad N^a = 0 + \xi^a(x, t). \quad (3.1)$$

It is convenient to work in 3-momentum space by expanding the perturbations h_{ab}, p^{ab}, ξ^a in modes of the flat space Laplacian (plane waves) as

$$\begin{aligned} h_{ab}(x, t) &= \frac{1}{(2\pi)^3} \int d^3k e^{ikx} \bar{h}_{ab}(k, t), \\ p^{ab}(x, t) &= \frac{1}{(2\pi)^3} \int d^3k e^{ikx} \bar{p}^{ab}(k, t) \\ \xi^a(x, t) &= \frac{1}{(2\pi)^3} \int d^3k e^{ikx} \bar{\xi}^a(k, t). \end{aligned} \quad (3.2)$$

This allows us to write the Hamiltonian and equations of motion in Fourier space. The background solution δ_{ab} and k^a may be used to define an orthonormal basis of symmetric 3×3 matrices M^I so that the perturbations can be decomposed as

$$\bar{h}_{ab} = h_I(k, t) M_{ab}^I, \quad \bar{p}^{ab} = p^I(k, t) M_I^{ab}, \quad I = 1, 2 \dots 6. \quad (3.3)$$

As we see below, the coefficients (h_I, p^I) provide a natural separation of the perturbations into scalar, vector and tensor modes. Furthermore, if the chosen basis is static and orthonormal in the inner product

$$\text{Tr}(M^I M^J) = \delta^{IJ}, \quad (3.4)$$

that the energy density of dust field (M) vanishes for this solution.

the symplectic form decomposes as

$$\int d^3k \bar{p}^{ab} \dot{h}_{ab} = \int d^3k p^I \dot{h}_I. \quad (3.5)$$

This identifies the six canonically conjugate degrees of freedom $(h_I(k, t), p^I(k, t))$.

A basis that fulfils these requirements is obtained by using an orthonormal basis of vectors

$$\hat{k}^a = k^a/|k|, \quad e_1^a, \quad e_2^a, \quad (3.6)$$

where the latter pair span the plane orthogonal to k^a . By considering rotations J_σ by angle σ about the k^a -axis, one obtains a definition of ‘helicity’ for the eigenvectors of these rotations; see e.g., appendix A.2.1 in [15]). The eigenvectors of J_σ are the linear combinations $e_\pm^a = (e_1^a \pm ie_2^a)/\sqrt{2}$. These satisfy $J_\sigma e_\pm^a = e^{\pm i\sigma} e_\pm^a$, $\delta_{ab} e_\pm^a e_\pm^b = 0$ and $\delta_{ab} e_+^a e_-^b = 1$. The matrices

$$\delta_{ab}, \quad \hat{k}^a \hat{k}^b, \quad e_\pm^{(a} \hat{k}^{b)}, \quad e_\pm^a e_\pm^b. \quad (3.7)$$

are the eigentensors of J_σ : the first two are rotationally invariant and so are (helicity 0) scalars, the next pair are (helicity ± 1) vectors, and the last pair are (helicity ± 2) tensors.

A basis M^I with the above properties may be made as a linear combinations of these elements. We choose the scalar, tensor, and vector bases

respectively as

$$M_1^{ab} = \frac{1}{\sqrt{3}} \delta^{ab}, \quad M_2^{ab} = \sqrt{\frac{3}{2}} \left(\hat{k}^a \hat{k}^b - \frac{1}{3} \delta^{ab} \right), \quad (3.8)$$

$$M_3^{ab} = \frac{i}{\sqrt{2}} (e_-^a e_-^b - e_+^a e_+^b), \quad M_4^{ab} = \frac{1}{\sqrt{2}} (e_-^a e_-^b + e_+^a e_+^b), \quad (3.9)$$

$$M_5^{ab} = i \left(e_-^{(a} \hat{k}^{b)} - e_+^{(a} \hat{k}^{b)} \right), \quad M_6^{ab} = \left(e_-^{(a} \hat{k}^{b)} + e_+^{(a} \hat{k}^{b)} \right). \quad (3.10)$$

The subset $M_I, I = 2 \cdots 6$ are trace free, $M_I^{ab} \delta_{ab} = 0$, and satisfy the transversality conditions $k_a M_3^{ab} = k_a M_4^{ab} = 0$ and $k_a k_b M_5^{ab} = k_a k_b M_6^{ab} = 0$. We note that the tensors of definite helicity in (3.7) have zero norm in the inner product (3.4) and lead to a degenerate reduction of the symplectic form. For this reason the above linear combinations of helicity tensors are necessary as basis elements in order to derive canonical equations of motion.

Our goal now is to write the linearized canonical Einstein equations in the dust time gauge in k -space, fix three phase space gauge conditions and solve the spatial diffeomorphism constraint. This will identify the three local physical degrees of freedom. As we will see, two of these turn out to be the usual polarizations of the graviton, and the third is the manifestation in the metric of the dust degree of freedom. The details of these steps follow.

3.1.1 Linearized equations of motion

The linearized equations about the flat background solution are

$$\begin{aligned}\dot{h}_{ab} &= 2 \left(p_{ab} - \frac{1}{2} \delta_{ab} p \right) + \mathcal{L}_\xi \delta_{ab} \\ \dot{p}^{ab} &= -\partial^c \partial^{(b} h_c^{a)} + \frac{1}{2} \partial^c \partial_c h^{ab} + \frac{1}{2} \partial^a \partial^b h + \frac{1}{2} \delta^{ab} (\partial^c \partial^d h_{cd} - \partial^c \partial_c h)\end{aligned}\quad (3.11)$$

which in k -space are

$$\begin{aligned}\dot{\bar{h}}_{ab} &= 2 \left(\bar{p}_{ab} - \frac{1}{2} \delta_{ab} \bar{p} \right) + 2i k_{(a} \bar{\xi}_{b)} \\ \dot{\bar{p}}^{ab} &= k^c k^{(b} \bar{h}_c^{a)} - \frac{1}{2} k^c k_c \bar{h}^{ab} - \frac{1}{2} k^a k^b \bar{h} - \frac{1}{2} \delta^{ab} (k^c k^d \bar{h}_{cd} - k^c k_c \bar{h})\end{aligned}\quad (3.12)$$

From these, the equations for the phase space pairs (h_I, p^I) are obtained by projecting onto each basis element M^I . The shift vector can be decomposed as

$$\bar{\xi}^a = \xi_{\parallel} \hat{k}^a + \xi_1 e_1^a + \xi_2 e_2^a. \quad (3.13)$$

The scalar mode equations are

$$\dot{h}_1 = -p_1 + \frac{2i}{\sqrt{3}}|k|\xi_{\parallel}, \quad (3.14)$$

$$\dot{h}_2 = 2p_2 + 2i\sqrt{\frac{2}{3}}|k|\xi_{\parallel}, \quad (3.15)$$

$$\dot{p}_1 = \frac{1}{3}|k|^2 h_1 - \frac{1}{3\sqrt{2}}|k|^2 h_2, \quad (3.16)$$

$$\dot{p}_2 = -\frac{1}{3\sqrt{2}}|k|^2 h_1 + \frac{1}{6}|k|^2 h_2. \quad (3.17)$$

The tensor mode equations are

$$\dot{h}_3 = 2p_3, \quad \dot{p}_3 = -\frac{1}{2}|k|^2 h_3, \quad (3.18)$$

$$\dot{h}_4 = 2p_4, \quad \dot{p}_4 = -\frac{1}{2}|k|^2 h_4, \quad (3.19)$$

and the vector mode equations are

$$\dot{h}_5 = 2p_5 + i\sqrt{2}|k|\xi_2, \quad \dot{p}_5 = 0, \quad (3.20)$$

$$\dot{h}_6 = 2p_6 + i\sqrt{2}|k|\xi_1, \quad \dot{p}_6 = 0. \quad (3.21)$$

These equations are supplemented by the linearized diffeomorphism constraint which we discuss next.

3.1.2 Diffeomorphism constraint

The position space diffeomorphism constraint $D_a \tilde{\pi}^{ab} = 0$ linearizes about the flat background to $\partial_a p^{ab} = 0$. In k -space this is

$$\begin{aligned} k_a \bar{p}^{ab} &= k_a p^I(k, t) M_I^{ab} = 0 \\ \implies \left(\frac{1}{\sqrt{3}} p_1 + \sqrt{\frac{2}{3}} p_2 \right) k^b + \frac{|k|}{\sqrt{2}} (p_5 e_2^b + p_6 e_1^b) &= 0. \end{aligned} \quad (3.22)$$

It is evident that this constraint has transverse and longitudinal components, and furthermore, that a partial solution of this constraint must come from setting $p_5 = p_6 = 0$, since these are the only coefficients in the transverse directions e_1^a and e_2^a .

More systematically, the vector modes are eliminated in three steps: (i) imposing the gauge conditions

$$h_5 = 0, \quad h_6 = 0, \quad (3.23)$$

which are second class with the linearized diffeomorphism constraint, (ii) solving the transverse component of the diffeomorphism constraint by setting $p_5 = p_6 = 0$, and (iii) using the conditions that the gauge be dynamically preserved to fix the transverse components of the shift perturbation (3.13),

$$\dot{h}_5 = i\sqrt{2}|k|\xi_2 = 0, \quad (3.24)$$

$$\dot{h}_6 = i\sqrt{2}|k|\xi_1 = 0. \quad (3.25)$$

This fixes $\xi_1 = \xi_2 = 0$. The longitudinal component of the shift $\bar{\xi}^a = \xi_{\parallel} \hat{k}^a$ remains undetermined at this stage.

This leaves the scalar and tensor mode equations for $(h_I, p_I), I = 1 \cdots 4$, and the longitudinal part of the diffeomorphism constraint

$$\left(\frac{1}{\sqrt{3}} p_1 + \sqrt{\frac{2}{3}} p_2 \right) = 0. \quad (3.26)$$

This remaining constraint is on the two scalar degrees of freedom. After one more gauge fixing, the last of the three necessary to fully gauge fix the theory, only one scalar mode and the transverse traceless graviton modes (h_3, p_3) and (h_4, p_4) remain. The former may be chosen as either the canonical pair (h_1, p_1) or (h_2, p_2) .

Let us consider the gauge $h_2 = 0$, and solve the remaining diffeomorphism constraint, giving $p_2 = -p_1/\sqrt{2}$. The corresponding evolution equation gives

$$\dot{h}_2 = 2p_2 + 2|k|i\sqrt{\frac{2}{3}}\xi_{\parallel} = 0 \implies \xi_{\parallel} = -i\frac{\sqrt{3}}{2|k|} p_1, \quad (3.27)$$

and the \dot{p}_1 and \dot{p}_2 equations become identical. The remaining scalar mode equations reduce, using the above expression for ξ_{\parallel} , to

$$\dot{h}_1 = 0, \quad \dot{p}_1 = \frac{1}{3}|k|^2 h_1,^2 \quad (3.28)$$

²Though the growth in p_1 is linear it does not pose a problem for perturbation theory as h_1 is an infinitesimal perturbation (by assumption) which remains constant

or equivalently,

$$\ddot{h}_1 = 0. \tag{3.29}$$

Thus the scalar mode induced by the dust degree of freedom is ultralocal: there are no spatial derivatives in the equation, so h_1 evolves independently at each space point. In fact it is a constant at linear order. Had we chosen the gauge $h_1 = 0$ (instead of $h_2 = 0$), a similar analysis would reveal the same equation of motion for the scalar mode h_2 .

Lastly we note that the graviton (TT) modes (3.18)-(3.19) satisfy the expected light speed wave equation

$$\ddot{h}_I = -|k|^2 h_I, \quad I = 3, 4, \tag{3.30}$$

despite the dust time gauge fixing, which remarkably does not affect Lorentz invariance in the linearized theory. This demonstrates that “solving the problem of time” by adding a dust field is compatible with Lorentz invariance, and that the dust time gauge leads to no pathologies.

3.2 Dust potential

We note in passing that it is possible to include a potential for the dust field in the starting theory [66]. This modifies the dust Lagrangian to

$$S^D = \int d^4x \sqrt{-g} [m(g^{\mu\nu} \partial_\mu \phi \partial_\nu \phi + 1) - V(\phi)], \quad (3.31)$$

and the dust contribution to the Hamiltonian constraint becomes

$$\mathcal{H}^D = \frac{1}{2} \left(\frac{p_\phi^2}{m\sqrt{q}} + m\sqrt{q}(q^{ab} \partial_a \phi \partial_b \phi + 1) \right) + \sqrt{q} V(\phi). \quad (3.32)$$

Now the dust time gauge canonical action (2.16) becomes

$$\begin{aligned} S = & \frac{1}{2\pi} \int dt d^3x [\pi^{ab} \dot{q}_{ab} + p_\chi \dot{\chi} \\ & - (\mathcal{H}^G + \sqrt{q} V(t) + \mathcal{H}^M) - N^a (\mathcal{C}_a^G + \mathcal{C}_a^M)]. \end{aligned} \quad (3.33)$$

This shows that the dust potential acts as a time dependent cosmological constant in the dust time gauge. It has been studied in explicit cosmological solutions in the context of mimetic gravity models and their extensions [33, 75].

The consequences of $V(t)$ for constructing a linearized theory are interesting. The first question is selecting a background solution on which to linearize the theory. Minkowski space is no longer a solution due to the change in the equation for the ADM momentum π^{ab} . Rather the simplest equations are

cosmological for given $V(t)$, and the analysis differs significantly from the flat space linearized theory due to non-zero ADM momentum in the background solution. We leave this for future work, but note in particular that the time dependent potential would drastically affect the graviton mode equation by introducing into it an explicit time dependence. This would obviously violate Lorentz covariance, which may be recoverable in epochs where $V(t)$ is chosen to be very slowly varying with t .

3.3 Deformation of the Hamiltonian

So far we have described the linearized theory of canonical general relativity in a matter time gauge, which results in the action (2.16). Taking the latter as a starting point for defining the theory, we introduce a deformation of the gravitational Hamiltonian

$$\mathcal{H}_\alpha^G := -\sqrt{q}R^{(3)} + \frac{1}{\sqrt{q}} (\pi^{ab}\pi_{ab} - \alpha\pi^2), \quad (3.34)$$

motivated by the Hořava-Lifshitz (HL) models. In their original formulation, these models are also constructed from a first order action made from the spatial metric and extrinsic curvature; there is no covariant second order action as the starting point. These models also have higher derivative 3-metric self-interactions through terms such as $R_{ab}R^{ab}$, as well as a deformation of the ADM kinetic term. The generalization we consider however only introduces

the latter through a parameter α :

$$S_\alpha = \frac{1}{2\pi} \int dt d^3x [\pi^{ab} \dot{q}_{ab} + p_\chi \dot{\chi} - (\mathcal{H}_\alpha^G + \mathcal{H}^M) - N^a (\mathcal{C}_a^G + \mathcal{C}_a^M)]. \quad (3.35)$$

Although this generalization is motivated by HL theory, we emphasize that it is a different theory in a key aspect. There is no Hamiltonian constraint. Rather there is a physical Hamiltonian which now has an additional coupling constant α . The only constraint algebra is that of the spatial diffeomorphism constraints, which closes in the usual manner, and the physical Hamiltonian density transforms via the bracket

$$\{\mathcal{C}^G(N), \mathcal{H}_\alpha^G(x), \} = \mathcal{L}_N \mathcal{H}_\alpha^G(x), \quad (3.36)$$

where \mathcal{L}_N denotes the Lie derivative with respect to the vector field N^a .

After linearization, we find the following equations of motion:

$$\begin{aligned} \dot{h}_{ab} &= 2(p_{ab} - \alpha \delta_{ab} p) + \mathcal{L}_\xi \delta_{ab} \\ \dot{p}^{ab} &= -\partial^c \partial^{(b} h_c^{a)} + \frac{1}{2} \partial^c \partial_c h^{ab} + \frac{1}{2} \partial^a \partial^b h \\ &\quad + \frac{1}{2} \delta^{ab} (\partial^c \partial^d h_{cd} - \partial^c \partial_c h). \end{aligned} \quad (3.37)$$

The deformation parameter α only appears in the equation of motion for h_{ab} . Repeating the analysis above, we find after gauge fixing that the only α

dependent equation of motion is:

$$\dot{h}_1 = 3(1 - 2\alpha)p_1. \quad (3.38)$$

Along with the equation $\dot{p}_1 = \frac{1}{3}|k|^2 h_1$, we have

$$\ddot{h}_1 = (1 - 2\alpha)|k|^2 h_1. \quad (3.39)$$

These are equivalent to the position space wave equation

$$\ddot{h}_1 = (2\alpha - 1) \delta^{ab} \partial_a \partial_b h_1, \quad (3.40)$$

so the propagation speed is $v = \sqrt{2\alpha - 1}$. It is therefore evident that for the GR value $\alpha = 1/2$, this scalar mode is ultralocal: there are no spatial derivatives in the equation, so h_1 evolves independently at each space point. For $\alpha > 1/2$ the propagation speed varies from e.g., to superluminal (at $\alpha = 1$), whereas for $\alpha < 1/2$ the equation becomes a $4d$ Laplacian!

3.4 Discussion

In a Hamiltonian setting with general relativity (GR) coupled to matter fields, the matter fields are not usually used in fixing coordinate gauges. This is because the interpretation of gravitational waves as spin 2 fields on a background spacetime is lost with such a gauge choice. Moreover, the

matter degrees of freedom used for gauge fixing appear as degrees of freedom in the geometry sector and their physical interpretation is very difficult. We showed that it is possible to use a dust field as time (dust time gauge) and still preserve the conventional interpretation of gravitational waves in 3+1 dimensions. Moreover, the additional degree of freedom that appears in the metric due to this gauge fixing is ultra-local (non-propagating) and thus causes no difficulties in physical interpretation. This chapter also demonstrates that the choice of dust as time is compatible with standard Lorentz covariant field theory on Minkowski (flat) spacetime and can still solve the “problem of time“ in quantum gravity.

Chapter 4

Mixmaster dynamics in the dust time gauge

For the remainder of this thesis we will focus on using the dust time gauge for classical and quantum investigations of homogeneous models. The central aim of this thesis is an exploration of Hamiltonian cosmology in the context of the physical time-independent Hamiltonian obtained in the dust time gauge. Homogenous models provide a simple use case for developing intuition about new techniques as well as for testing new ideas. We view this to be a potentially useful step towards studying the classical and quantum dynamics of more complex models such as the Gowdy cosmologies using a physical time-independent Hamiltonian. These models have so far only been studied to some extent in a volume time gauge, which introduces explicit time dependence in the Hamiltonian and equations of motion.

For classical general relativity, homogeneous models are specially important due to the Belinskii-Khalatnikov-Lifschitz (BKL) conjecture which states that the approach to space-like singularities is homogeneous and vacuum dominated i.e., the time derivatives in the Einstein Field Equations dominate and the dynamics at each spacetime point can be described by a suitable vacuum homogeneous model. BKL in a series of seminal works [16, 17, 18] argued that the Bianchi IX spacetime provides a sufficiently general model to investigate this approach to a space-like singularity. Since then several analytical and numerical works have validated this conjecture [27, 21, 47, 10, 11]. For a review of recent work on Bianchi IX cosmologies see [56, 48, 26].

The BKL conjecture introduces the possibility that the approach to the singularity in the quantum theory, may be particularly simple if the classical equations are indeed vacuum dominated and homogenous.¹ For then the classical singularity to be resolved is the one provided by a homogeneous cosmology. Along this direction, we will explore some quantum aspects of Bianchi I models in a later chapter.

The vacuum Bianchi I model is considered the “free theory” of anisotropic cosmology, where dynamics is governed only by the gravitational kinetic term in the Hamiltonian constraint. Its solution is the Kasner metric

$$ds^2 = -dt^2 + t^{2p_1} dx^2 + t^{2p_2} dy^2 + t^{2p_3} dz^2, \quad (4.1)$$

¹D. Garfinkle, personal communication.

where the (real) parameters p_1, p_2 and p_3 are integration constants satisfying the two sum rules

$$p_1 + p_2 + p_3 = 1, \quad p_1^2 + p_2^2 + p_3^2 = 1. \quad (4.2)$$

The solution is thus characterized by one free parameter on the so-called Kasner circle at the intersection of this plane and unit sphere.

More complicated Bianchi models have interactions between the three scale factors arising from the Ricci curvature term in the Hamiltonian constraint. This is clear in the Hamiltonian formulation of Bianchi IX (or Mixmaster) Universe first studied by Misner [72, 73]. The Bianchi IX potential is an equilateral triangular box in configuration space with exponentially high sides. The potential vanishes in the region near the origin, so the solution there is the (vacuum) Kasner metric. Bianchi IX dynamics is thus equivalent to a particle in this box that undergoes collisions at the walls, and after each collision enters a new Kasner phase:

$$(p_1, p_2, p_3) \rightarrow (p'_1, p'_2, p'_3). \quad (4.3)$$

BKL derived a precise transition law for these exponents in the vacuum case, which was subsequently re-derived by Misner in a Hamiltonian formulation cited above. In the non-vacuum case it is clear that solutions are also labelled by matter integration constants, and so it is natural to expect that these additional constants should also participate in a generalized transition

law and drop out in the asymptotic limit to the singularity.

In this chapter we will detail the following results from [7]:

- Bianchi IX dynamics in the dust time gauge can be formulated in terms of a generalized transition law, akin to the BKL-Misner law, using the matter and geometry integrations constants for dust-Bianchi I solutions.
- This generalized transition law reduces to the BKL-Misner law in the near singularity limit, thus recovering the “matter does not matter result.”

In the next section we discuss the general formulation of spatially homogeneous spacetimes in the dust time gauge. In Section 4.2 we detail a new Hamiltonian derivation of the dust-Bianchi I or Heckmann-Schücking solution. In Sections 4.3 and 4.4 an analysis of dust-Bianchi IX dynamics is given. We show that the dynamics is characterized by transitions between dust-Bianchi I solutions and derive the corresponding transition law which reduces to the vacuum BKL map sufficiently close to the singularity. In Section 4.5 we add a scalar field to the model and analyze the dynamics using the method of consistent potentials. We conclude the chapter with Section 4.6 with a summary of our results and some remarks.

4.1 The spatially homogeneous sector

In the dust time gauge we equate the surfaces of homogeneity with level surfaces of the dust field. The general four dimensional spatially homogeneous metric can then be written as:

$$ds^2 = -dt^2 + q_{ij}(t)\omega^i\omega^j \quad (4.4)$$

where ω^i are invariant 1-forms corresponding to the three dimensional isometry group of the manifold and $N^i = 0$. In the absence of matter fields besides the dust, the physical Hamiltonian in the dust time gauge for a spatially homogeneous background is

$$H_p = -\frac{1}{2\pi} \int d^3x \mathcal{H}^G. \quad (4.5)$$

When $q_{ij}(t)$ is diagonal, a parametrization of the ADM canonical variables is

$$\begin{aligned} q_{ij} &= \text{diag}[e^{2\alpha_1(t)}, e^{2\alpha_2(t)}, e^{2\alpha_3(t)}], \\ \pi^{ij} &= \frac{1}{2} \text{diag}[\pi_1(t)e^{-2\alpha_1(t)}, \pi_2(t)e^{-2\alpha_2(t)}, \pi_3(t)e^{-2\alpha_3(t)}], \end{aligned} \quad (4.6)$$

so the canonically conjugate pairs are (α_i, π_i) , $i = 1, 2, 3$. The physical Hamiltonian then takes the form

$$\begin{aligned} H_p &= v_0 \left[-\frac{1}{4\sqrt{q}} \left(\frac{1}{2} \sum_i \pi_i^2 - \sum_{i<j} \pi_i \pi_j \right) + V(\alpha) \right] \\ &\equiv H_K + V, \end{aligned} \quad (4.7)$$

where $V(\alpha)$ is derived from the scalar curvature of the spatial slice, $\sqrt{q} = \exp(\sum_{i=1}^3 \alpha_i)$, and v_0 is a fiducial volume we set to unity.

An alternative set of phase space variables, obtained from the above by canonical transformation, are the Misner variables $(\Omega, \beta_+, \beta_-)$, and their conjugate momenta. The physical Hamiltonian in these variables is

$$H_p = \left[-\frac{e^{3\Omega}}{24} (p_+^2 + p_-^2 - p_\Omega^2) + V(\Omega, \beta_+, \beta_-) \right]. \quad (4.8)$$

We consider here the diagonal Bianchi I and IX spacetimes, for which the potentials $V(\Omega, \beta_+, \beta_-)$ are

$$V_I = 0 \quad (4.9)$$

$$\begin{aligned} V_{IX} &= -6e^{-\Omega} \left[\frac{2}{3} e^{4\beta_+} (\cosh(4\sqrt{3}\beta_-) - 1) - \frac{4}{3} e^{-2\beta_+} \cosh(2\sqrt{3}\beta_-) + \frac{1}{3} e^{-8\beta_+} \right], \\ &\equiv -6e^{-\Omega} v(\beta_+, \beta_-). \end{aligned} \quad (4.10)$$

We make use of both sets of variables, the first to give a derivation of the dust-Bianchi I solution, and the second to study Bianchi IX dynamics.

In either parametrization, since H_p is a constant of the motion, the energy density of the dust $m = H_p/\sqrt{q}$ diverges as the metric determinant goes to zero. Thus, $\sqrt{q} \rightarrow 0$ corresponds to a physical singularity.

4.2 Dust-Bianchi I spacetime

The isometry group of the Bianchi I model is the three parameter group of translations in three dimensional Euclidean space. In the synchronous basis the metric is

$$ds^2 = -dt^2 + e^{2\alpha_1(t)} dx^2 + e^{2\alpha_2(t)} dy^2 + e^{2\alpha_3(t)} dz^2. \quad (4.11)$$

The Kasner metric is the vacuum solution of this form. We now derive a metric of the same form with dust, in the dust time gauge. As we will see, this will turn out to be the Heckmann and Schücking solution [55].

The physical Hamiltonian for this model is given by (4.7) with $V(\alpha) = 0$. The Hamilton equations of motion are

$$\begin{aligned} \dot{\alpha}_1 &= -\frac{1}{\sqrt{q}} (\pi_1 - \pi_2 - \pi_3), \quad \{\text{with cyclic perm. on } \pi_i \text{ for } \dot{\alpha}_2 \text{ and } \dot{\alpha}_3\} \\ \dot{\pi}_i &= H_K. \end{aligned} \quad (4.12)$$

The second equation gives

$$\pi_i(t) = H_K t + \lambda_i \quad (4.13)$$

with integration constants λ_i .

4.2.1 Kasner solution: $H_K = 0$

In this case the above evolution equations imply

$$(\sqrt{q})' = \frac{1}{4}(\pi_1 + \pi_2 + \pi_3) = \frac{\Lambda}{4}. \quad (4.14)$$

and

$$\dot{\alpha}_i = \frac{\Lambda - 2\lambda_i}{\Lambda t + 4\delta}, \quad \Lambda = \sum_i \lambda_i. \quad (4.15)$$

Here, $\Lambda = \sum_{i=1}^3 \lambda_i$ and $\delta \geq 0$ is an integration constant. This gives the following solution for the scale factors $a_i = e^{\alpha_i}$:

$$a_i = \xi_i \left(t + \frac{4\delta}{\Lambda} \right)^{1 - \frac{2\lambda_i}{\Lambda}}, \quad (4.16)$$

where ξ_i are constants of integration. The scale factors are not all independent, since they satisfy

$$\sqrt{q} = a_1 a_2 a_3 = \frac{\Lambda t}{4} + \delta, \quad (4.17)$$

which is derived from (4.14), and $\delta = \sqrt{q}(0)$.

Defining the exponents

$$p_i \equiv 1 - \frac{2\lambda_i}{\Lambda}, \quad (4.18)$$

we see that $p_1 + p_2 + p_3 = 1$, as for the Kasner solution. Furthermore, sub-

stituting the solution (4.13) into the physical Hamiltonian H_K , and setting $H_K = 0$, yields

$$\begin{aligned}\lambda_1^2 + \lambda_2^2 + \lambda_3^2 &= 2(\lambda_1\lambda_2 + \lambda_1\lambda_3 + \lambda_2\lambda_3), \\ \implies p_1^2 + p_2^2 + p_3^2 &= 1,\end{aligned}\tag{4.19}$$

using the definition (4.18). Lastly, we can absorb the integration constants ξ_i in the coordinates, and redefine $t \rightarrow t + 4\delta/\Lambda$ to recover the Kasner solution. Therefore, the dust time gauge, with initial data chosen such that $H_K = 0$, gives the vacuum Kasner solution – an unsurprising result since the dust energy density m vanishes for this case. We now turn to the $H_K = \text{constant} \neq 0$ cases.

4.2.2 Dust-Kasner solution: $H_K > 0$

For $H_K \neq 0$ we can invert the expression for the Hamiltonian to obtain an expression for \sqrt{q} ,

$$\sqrt{q} = \frac{1}{8} (3H_K t^2 + 2\Lambda t + 8\delta).\tag{4.20}$$

This gives

$$\dot{\alpha}_i = \frac{6H_K (H_K t + \Lambda - 2\lambda_i)}{(3H_K t + \Lambda)^2 + 24H_K \delta - \Lambda^2}\tag{4.21}$$

$H_K > 0$ requires

$$\frac{\Lambda^2}{2} > \lambda_1^2 + \lambda_2^2 + \lambda_3^2,\tag{4.22}$$

while the term $24H_K\delta - \Lambda^2$ is proportional to

$$\frac{\Lambda^2}{3} - (\lambda_1^2 + \lambda_2^2 + \lambda_3^2). \quad (4.23)$$

Therefore, for $H_K > 0$, there are two classes of solutions, with initial data satisfying either

$$\frac{\Lambda^2}{2} > \lambda_1^2 + \lambda_2^2 + \lambda_3^2 > \frac{\Lambda^2}{3}, \quad (4.24)$$

or

$$\frac{\Lambda^2}{3} > \lambda_1^2 + \lambda_2^2 + \lambda_3^2. \quad (4.25)$$

At the end of this section we'll show that the second class of solutions is not physically viable.

If (4.24) is satisfied, then (4.21) can be integrated to give

$$a_i = \xi_i (y - \Gamma)^{\frac{1}{3} + \beta_i} (y + \Gamma)^{\frac{1}{3} - \beta_i}, \quad (4.26)$$

where $y = 3H_K t + \Lambda$,

$$\Gamma^2 = -24H_K\delta + \Lambda^2, \quad \beta_i = \frac{2}{3\Gamma} (\Lambda - 3\lambda_i) \quad (4.27)$$

and ξ_i are integration constants satisfying $\xi_1\xi_2\xi_3 = -1/(24H_K)$. This is the Heckmann-Schücking solution

$$a_i = \xi_i \tau^{p_i} (\tau + 2\Gamma)^{\frac{2}{3} - p_i}, \quad (4.28)$$

as can be seen by defining

$$p_i = \frac{1}{3} + \beta_i, \quad \tau = 3H_K t + \Lambda - \Gamma, \quad (4.29)$$

Interestingly, even for $H_K \neq 0$, the exponents p_i again satisfy

$$p_1 + p_2 + p_3 = 1, \quad p_1^2 + p_2^2 + p_3^2 = 1. \quad (4.30)$$

Addressing now the second set of data (4.25), it is convenient to define $\Gamma^2 \equiv 24H_K\delta - \Lambda^2$. Then the solution of (4.21)

$$a_i = \xi_i (y^2 + \Gamma^2)^{\frac{2}{3}} \exp \left[4B_i \arctan \left(\frac{y}{\Gamma} \right) \right], \quad (4.31)$$

where $B_i = (\Lambda/3 - \lambda_i)/\Gamma$. Now $\sum_i B_i^2 < 0$, implying that at least one of the B_i is imaginary and the solutions are not physical.

4.2.3 Dust-Kasner solution for $H_K < 0$

For completeness, we also present solutions with $H_K < 0$. These solutions are not physically relevant since they correspond to a negative energy density for the dust. When $H_K < 0$ we have

$$\frac{\Lambda^2}{3} < \frac{\Lambda^2}{2} < \lambda_1^2 + \lambda^2 + \lambda_3^2. \quad (4.32)$$

This implies that $24H_K\delta - \Lambda^2 < 0$. Up to this change, the solution solution has the same form

$$a_i = \xi_i \tau^{p_i} (\tau + 2\Gamma)^{\frac{2}{3}-p_i} \quad (4.33)$$

where τ and the exponents p_i are defined as before.

4.2.4 Dust-Bianchi I spacetime with scalar field

In the presence of a free scalar field χ the physical Hamiltonian in the dust time gauge is

$$H_p = H_K - \frac{p_\chi^2}{2\sqrt{q}}. \quad (4.34)$$

The equations of motion for the scale factor remain the same as in (4.12).

However equations for the momenta are now

$$\pi_i = H_p, \quad (4.35)$$

and those for the scalar field are

$$\dot{\chi} = -e^{-\sum_i \alpha_i} p_\chi, \quad \dot{p}_\chi = 0 \quad (4.36)$$

Consequently

$$\pi_i = H_p t + \lambda_i. \quad (4.37)$$

The solution for π_i substituted into the expression for the physical Hamiltonian H_p gives

$$\sqrt{q} = \frac{1}{8} (3H_p t^2 + 2\Lambda t + 8\delta), \quad (4.38)$$

where now

$$\delta \equiv \sqrt{q(0)} = -\frac{1}{4H_p} \left(\frac{1}{2} \sum_i \lambda_i^2 - \sum_{i<j} \lambda_i \lambda_j + 2p_\chi^2 \right). \quad (4.39)$$

The solution for the scale factors is

$$a_i = \eta_i (\tau)^{\frac{1}{3} + \beta_i} (\tau + 2\Gamma)^{\frac{1}{3} - \beta_i} \quad (4.40)$$

where

$$\tau \equiv 3H_p t + \lambda - \Gamma, \quad \Gamma^2 = -24H_p \delta + \Lambda^2, \quad \beta_i = \frac{2}{3\Gamma} (\Lambda - 3\lambda_i). \quad (4.41)$$

(The definition of Γ now uses H_p rather than H_K for the pure dust case).

Defining the exponents

$$p_i \equiv \frac{1}{3} + \beta_i, \quad (4.42)$$

now gives

$$\sum_{i=1}^3 p_i = 1, \quad \sum_{i=1}^3 p_i^2 = 1 - \frac{8p_\chi^2}{\Gamma^2}. \quad (4.43)$$

The second sum rule depends on the value of the conserved scalar field momentum and the integrations constants λ_i . This has the correct limits for

$p_\chi = 0$ (dust only), and for $H_p = 0$ (vacuum).

Substituting for the scale factors in the equation of motion for χ we have

$$\dot{\chi} = \frac{8p_\chi}{\tau(\tau + 2\Gamma)}, \quad (4.44)$$

Since $p_\chi = \text{const}$, this can be integrated to give

$$\chi = \frac{8p_\chi}{2\Gamma} \ln \left[\frac{\tau}{\tau + 2\Gamma} \right]. \quad (4.45)$$

4.3 Dust-Bianchi IX spacetime

The Bianchi IX dynamics is most easily studied from the Hamiltonian perspective using Misner variables. The physical Hamiltonian is (4.8) with the non-zero potential in (4.9). The metric is

$$ds^2 = -dt^2 + e^{-2\Omega} (e^{2\beta})_{ij} \omega^i \omega^j \quad (4.46)$$

where ω_i are $\text{SO}(3)$ covariant 1-forms and

$$\beta_{ij} = \text{diag}(\beta_+ + \sqrt{3}\beta_-, \beta_+ - \sqrt{3}\beta_-, -2\beta_+). \quad (4.47)$$

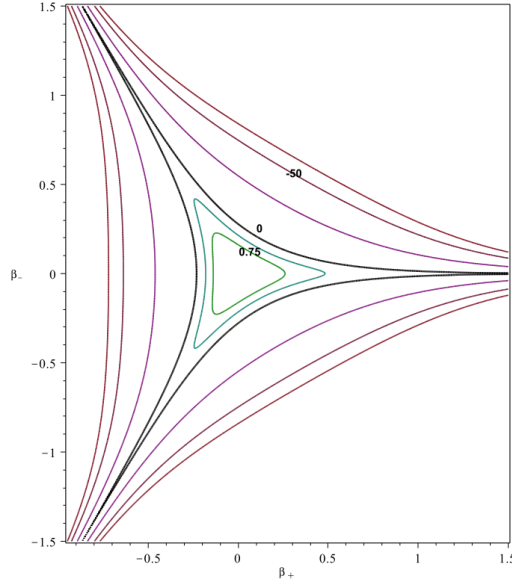


Figure 4.1: Contours of $v(\beta_+, \beta_-)$ for the potential $V_{IX} = e^{-\Omega}v(\beta_+, \beta_-)$. v is bounded above by +1, the bold line is the $v = 0$ contour, the innermost contour is $v = 0.75$ and the outermost contour is $v = -100$.

The canonical equations of motion are

$$\dot{\Omega} = \frac{\exp(3\Omega)}{12} p_{\Omega}, \quad \dot{p}_{\Omega} = -3H_p - 24e^{-\Omega}v(\beta_+, \beta_-) \quad (4.48)$$

$$\dot{\beta}_{\pm} = -\frac{\exp(3\Omega)}{12} p_{\pm}, \quad \dot{p}_{\pm} = 6e^{-\Omega} \frac{\partial v}{\partial \beta_{\pm}}. \quad (4.49)$$

The difference between these equations and the vacuum case studied by Misner is that with the dust there are three physical configuration degrees of freedom. Since the dust is used to fix the time gauge, all three degrees of freedom are manifested in the spatial metric, and the potential is a function of all three. Moreover, even though Ω appears only in the overall factor, it still has non-trivial dynamics in dust time.

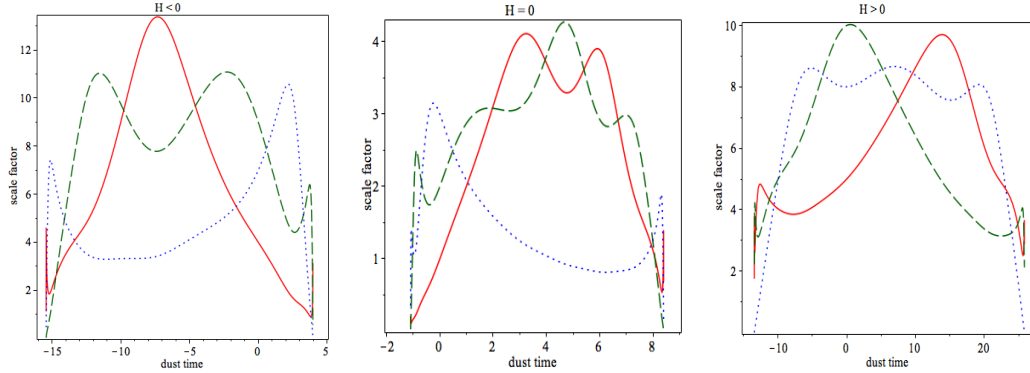


Figure 4.2: Numerical integration of the equations of motion for different values of H_p show that oscillatory behaviour of the scale factors $a(t)$ (solid red line), $b(t)$ (dashed green line) and $c(t)$ (dotted blue line).

The volume of the universe scales as $e^{-3\Omega}$, therefore the singularity is approached as Ω tends to infinity. Thus near the singularity the potential V_{IX} (4.9) only plays a role when $|v(\beta_+, \beta_-)|$ is sufficiently large. When the potential term is not dominant, the universe behaves like the dust-Bianchi I system studied in the last section. Therefore, Misner's picture of a particle in a time dependent triangular box can be interchanged with the particle inside a pyramidal well in configuration space depicted in Fig. 4.1.

Projected on the (β_+, β_-) plane, the contours of $v(\beta_+, \beta_-)$ scale linearly with Ω . As Ω increases, the contours move outwards. This can be seen by considering one section of the potential, say $V = -2e^{-\Omega-8\beta_+}$ for $\beta_+ < 0$: setting $-2e^{-\Omega-8\beta_+} = -C$ corresponds to contour section given by $-8\beta_+ = \ln\left(\frac{C}{2}\right) + \Omega$. The particle velocity in the (β_+, β_-) plane, $\vec{v} = (\dot{\beta}_+, \dot{\beta}_-)$, scales as $e^{3\Omega}$ (from the above equations), while the contours have a linear dependence on Ω . It is therefore reasonable to assume that the particle bounces off the

exponential walls of the pyramidal potential, and that these bounces are interspersed by durations in which the dynamics is kinetic term dominated and described by the dust-Bianchi I solution. A key difference between the dust time dynamics in the present case, and Ω time in the standard (no dust) case, is that the singularity is reached in finite dust time. Indeed for $H_p > 0$ i.e., the energy density of the dust is positive, the dust filled Bianchi IX universe has two physical singularities as shown in Fig. 4.2; this is an example of a more general result [67]. Fig. 4.2 also demonstrates that Bianchi IX dynamics in dust time gives oscillatory dynamics, just as for volume time in the vacuum case.

We note that as the universe expands, Ω and $|\vec{v}| = |(\dot{\beta}_+, \dot{\beta}_-)| \approx e^{3\Omega}$ decrease, and the potential walls move inwards. Therefore the dust-Bianchi I phases last for shorter periods of dust-time. However, since Ω is bounded below (the point of maximum expansion), when the universe begins to recontract, the potential walls start to move outwards again, and the frequency of collisions decreases. This observation, which holds for all dust-time, will be important in interpreting the generalized transition law we derive below.

4.3.1 Method of Consistent Potentials

One way to establish that the Universe particle undergoes bounces at the moving walls of the potential (as the singularity is approached) is a self-consistent analysis called the Method of Consistent Potentials (MCP) [51]. The basic idea is to obtain a solution by neglecting the potential terms in

the Hamiltonian, ie. a Bianchi I solution, and substitute this solution into the full Hamiltonian, ie. with the potential terms included. If the dynamics is asymptotically velocity dominated, the neglected potential terms remain exponentially suppressed i.e., the Bianchi I phase dominates. On the other hand, if one or more of the potential terms grow as the singularity is approached, the Universe may undergo a bounce to a new Bianchi I phase.

To apply MCP in our case we observe that the physical Hamiltonian for a dust-Bianchi IX spacetime is the sum of two terms H_K and H_V where

$$\begin{aligned} H_K &= -\frac{e^{3\Omega}}{24} (p_+^2 + p_-^2 - p_\Omega^2) & (4.50) \\ H_V &= -6e^{-\Omega} \left(\frac{2}{3} e^{4\beta_+} (\cosh(4\sqrt{3}\beta_-)) \right. \\ &\quad \left. - \frac{4}{3} e^{-2\beta_+} \cosh(2\sqrt{3}\beta_-) + \frac{1}{3} e^{-8\beta_+} \right). \end{aligned}$$

Near the singularity, $\Omega \rightarrow \infty$, so we use the dust-Kasner equations to find $\beta_\pm(\Omega)$ and substitute these into the potential. For large Ω the Hamilton equations give

$$\frac{\partial \beta_\pm}{\partial \Omega} = \mp \frac{p_\pm^0}{|\Gamma|} \left(1 - \frac{24He^{-3\Omega}}{\Gamma^2} \right)^{-1/2} \approx \mp \frac{p_\pm^0}{|\Gamma|} \left(1 + \frac{12He^{-3\Omega}}{\Gamma^2} \right), \quad (4.52)$$

where H is the value of the dust-Kasner hamiltonian and Γ, p_\pm^0 are integration constants related by $p_+^0 = \Gamma \cos \theta$, $p_-^0 = \Gamma \sin \theta$, a result which follows from

the p_Ω equation. Thus to linear order we have

$$\beta_\pm = -\mp \frac{p_\pm^0}{\Gamma} \Omega + \beta_\pm^0. \quad (4.53)$$

Near the singularity the dominant terms in H_V are

$$H_V \approx 2e^{-\Omega} \left(e^{-8\beta_+} + e^{4\beta_+ + 4\sqrt{3}\beta_-} + e^{4\beta_+ - 4\sqrt{3}\beta_-} \right), \quad (4.54)$$

which for later convenience we label V_1 , V_2 and V_3 respectively. Substituting the asymptotic form of β_\pm gives

$$H_V \approx 2 \left(e^{\Omega(\pm 4 \sin \theta \pm 4\sqrt{3} \cos \theta - 1)} + e^{\Omega(\pm 4 \sin \theta \mp 4\sqrt{3} \cos \theta - 1)} + e^{\Omega(\mp 8 \sin \theta - 1)} \right). \quad (4.55)$$

If all the terms above are to be negligible, we require the following equations to be satisfied simultaneously

$$\begin{aligned} 4 \sin \theta + 4\sqrt{3} \cos \theta - 1 &< 0 \\ 4 \sin \theta - 4\sqrt{3} \cos \theta - 1 &< 0 \\ -8 \sin \theta - 1 &< 0. \end{aligned} \quad (4.56)$$

It is clear from Fig.4.3 that these three conditions cannot be satisfied simultaneously and at least one of the terms is growing at any given time. Thus the particle is approaching one section of the walls of the pyramidal box at any given time. Therefore the dynamics of the dust-Bianchi IX near the

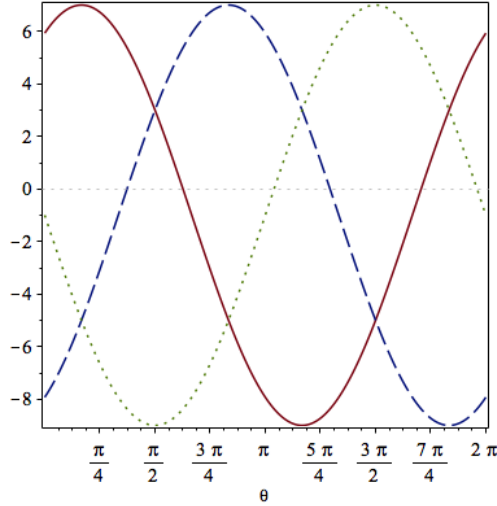


Figure 4.3: This is a plot of the expressions on the left hand side of (4.56) with respect to θ . The solid line indicates the first condition, the dashed line indicates the second condition and the dotted line indicates the last condition. It is clear from the plot above that the inequalities in (4.56) cannot be simultaneously satisfied. Moreover, for any value of θ only one of the terms in the potential is dominant.

singularity is characterized by periods in which H_V is negligible compared to H_K , and the dynamics resembles that of the dust-Bianchi I model (dust-Kasner phase). These periods are punctuated by periods in which one of the terms in (4.55) is large enough that H_V cannot be neglected causing a “bounce” from one dust-Bianchi I solution to another.

Thus, unlike vacuum Bianchi IX, the dust-Bianchi IX universe bounces between Bianchi I solutions that are not vacuum Kasner. In BKL’s language, the dynamics of dust-Bianchi IX is characterised by oscillations between dust-Bianchi I regimes. This gives a new physical picture of the approach to the singularity in the dust time gauge.

4.4 Transitions between dust-Bianchi I epochs

We have established that dust doesn't change the oscillatory nature of the Bianchi IX dynamics near the singularity. The dynamics can still be viewed as that of a particle bouncing in a steep triangular potential well, with dust-Kasner regimes between bounces. We would now like to quantify this oscillatory behaviour.

The cornerstone of BKL's analysis of Bianchi IX dynamics is the transition rule governing transitions between various Kasner epochs. In the same spirit we derive a rule that relates the pre- and post-bounce dust-Bianchi I solutions, when these bounces occur away from the corners of the potential. The method of consistent potentials shows that the three dominant terms in the potential peak at different times. Let us consider first the potential term

$$V_1 = -2e^{-\Omega-8\beta_+} \tag{4.57}$$

which is (a section of) one of the walls of the triangular potential. The truncated Hamiltonian for this wall is then

$$H_1 \equiv H_K + V_1. \tag{4.58}$$

It is evident that p_- is conserved since the poisson bracket $\{p_-, H_1\} = 0$.

Therefore its change at this potential wall is zero:

$$\Delta p_- = 0. \quad (4.59)$$

However the momentum p_+ (which is conserved for dust-Bianchi I) undergoes a change upon collision. To find this change let us consider the equations of motion in dust-time:

$$\dot{p}_\Omega = -3H_1 + 4 V_1 (\Omega, \beta_+, \beta_-) \quad (4.60)$$

$$\dot{p}_+ = 8 V_1 (\Omega, \beta_+, \beta_-). \quad (4.61)$$

These imply

$$p_\Omega - \frac{1}{2}p_+ = -3H_1 t + \alpha, \quad (4.62)$$

where α is an integration constant for the Bianchi IX universe near the section of the potential characterized by V_1 . Now recalling that p_+ and p_- are (approximate) conserved quantities away from the potential wall (where $H_K \gg V_1$), the Universe returns to this region with a different value of p_+ after a bounce at the wall. Therefore the dust-Bianchi I regimes before and after collision at the wall $V_{IX} \approx V_1$ are all characterized by the following condition on the integration constants (ie. the last equation evaluated at $t = 0$):

$$p_\Omega^0 - \frac{1}{2}p_+^0 = \alpha. \quad (4.63)$$

Now since α is a dust-Bianchi IX integration constant for this wall, we have

the relation

$$\Delta p_\Omega^0 - \frac{1}{2}\Delta p_+^0 = 0, \quad (4.64)$$

which gives the initial data change for the dust-Kasner phase after collision with V_1 . *This equation is central to our analysis below.*

4.4.1 Transition Law: $H_p = 0$

This is the vacuum case. The following steps give an elegant derivation of the BKL law, which demonstrates the utility of the dust time gauge. Away from the potential wall we have $H_p \approx H_K = 0$, therefore

$$p_+^2 + p_-^2 - p_\Omega^2 = 0. \quad (4.65)$$

This suggests the parameterization $\cos \theta \equiv p_+/p_\Omega$ and $\sin \theta \equiv p_-/p_\Omega$. Since θ undergoes a change at a wall, let us denote its values before and after the bounce respectively as $(p_+/p_\Omega)^{(i)} = \cos \theta_i$, $(p_-/p_\Omega)^{(i)} = \sin \theta_i$, and $(p_+/p_\Omega)^{(f)} = -\cos \theta_f$, $(p_-/p_\Omega)^{(f)} = \sin \theta_f$. (θ provides an abstract parametrization and in general we cannot interpret it as the angle of incidence or deflection in the (β_+, β_-) plane.)

The conservation of p_- at the wall V_1 gives

$$p_\Omega^{(i)} \sin \theta_i = p_\Omega^{(f)} \sin \theta_f, \quad (4.66)$$

and (4.64) gives

$$p_{\Omega}^{(i)} \left(1 - \frac{1}{2} \cos \theta_i \right) = p_{\Omega}^{(f)} \left(1 + \frac{1}{2} \cos \theta_f \right). \quad (4.67)$$

Combining these equations gives

$$\sin \theta_f - \sin \theta_i = \frac{1}{2} \sin(\theta_i + \theta_f). \quad (4.68)$$

This rule can be cast in terms of one parameter u . Since p_{Ω} is a constant when $H_p \approx H_K = 0$, following Misner [73] we choose the parametrization

$$\frac{p_+}{p_{\Omega}} = \cos \theta = \frac{u^2 + u - 1/2}{u^2 + u + 1}, \quad \frac{p_-}{p_{\Omega}} = \sin \theta = \frac{\sqrt{3}(u + 1/2)}{u^2 + u + 1}. \quad (4.69)$$

Then the transition law (4.68) becomes $u_f = (u_i - 1)/3$.

4.4.2 Transition Law: $H_p \neq 0$

This is the case that gives one of our new results. It differs from the previous ($H_p = 0$) case in two respects. First, in contrast to (4.65), the dust-Kasner physical Hamiltonian (4.50) now gives

$$p_+^2 + p_-^2 = (p_{\Omega}^0)^2 - 24H_p\delta = \Gamma^2, \quad (4.70)$$

where $\delta = e^{-3\Omega(0)}$ is the initial volume of the dust-Bianchi I solution and Γ is defined in Section 4.2.2. It is important to remember that though the dust-

Kasner solution involves six integration constants, the dust-Kasner phase is completely characterized by three integration constants as three constants can be absorbed in redefinitions of the spatial coordinates. Thus a collision with Bianchi IX wall V_1 induces the shift:

$$(p_\Omega^0, p_+, \delta) \longrightarrow (p_\Omega^{0'}, p_+', \delta'). \quad (4.71)$$

Importantly, the shift in δ is now relevant since $H_p \neq 0$. Its role is critical for extracting the matter independence of the near singularity transition law we derive below.

Secondly, in the kinetic term dominated region (i.e., $H_1 \approx H_K$), p_Ω is not a constant but depends linearly on t . Thus $\frac{1}{2}p_+ - p_\Omega \neq \text{const}$. Nevertheless from (4.63) we still have (4.64) as the relation between the integration constants for dust-Bianchi I before and after the bounce at V_1 , since this condition was derived from the full Bianchi IX equations at wall V_1 .

Given (4.70), we define the modified parametrization, before (i) and after (f) the collision, by

$$\begin{aligned} \left(\frac{p_+}{\Gamma}\right)^{(i)} &= \cos \theta_i, & \left(\frac{p_-}{\Gamma}\right)^{(i)} &= \sin \theta_i, \\ \left(\frac{p_+}{\Gamma}\right)^{(f)} &= -\cos \theta_f, & \left(\frac{p_-}{\Gamma}\right)^{(f)} &= \sin \theta_f \end{aligned} \quad (4.72)$$

Then the conservation of p_- at the bounce gives, as before,

$$\Gamma^{(i)} \sin \theta_i = \Gamma^{(f)} \sin \theta_f. \quad (4.73)$$

Note, θ is a redundant parameter introduced for convenience and the shift in θ is determined by the shift in Γ which in turn is governed by the shift in p_Ω^0 and δ . Now the condition $\frac{1}{2}\Delta p_+^0 = \Delta p_\Omega^0$, combined with the last equation, gives

$$\left(\frac{p_\Omega^0}{\Gamma}\right)^{(i)} \sin \theta_f - \left(\frac{p_\Omega^0}{\Gamma}\right)^{(f)} \sin \theta_i = \frac{1}{2} \sin(\theta_i + \theta_f). \quad (4.74)$$

We note that if $H_p = 0$ (ie. no dust) this reduces to the BKL-Misner rule. However, as it stands the transition rule is not complete since we have so far not given a prescription for how δ changes. The shift in δ can be obtained by using the dust-Kasner energy conservation, which for the wall V_1 gives

$$-\Delta(p_+^2) + \Delta(p_\Omega^2) = 24H_p\Delta\delta. \quad (4.75)$$

Equation (4.74) supplemented by (4.75) is one of our main results.

We contend that the transition rule derived above, (4.74) and (4.75), also applies away from the singularity. This is because the only input in its derivation is collision at this wall, regardless of the size of the Universe. Indeed, the universe undergoes bounces between dust-Kasner regimes for all dust-time (unlike volume time which is not monotonic), though the bounce frequency decreases as the singularity is approached; in the latter regime, the universe spends longer periods of dust-time in each dust-Kasner phase, but still bounces to a different phase when the potential term in the Hamiltonian becomes dominant. This fact is evident in numerical simulations in dust-time.

We now show how these equations yield the vacuum BKL-Misner rule.

Matter does not matter: δ transition law

As it stands (4.74) raises the question of compatibility with results from other approaches which establish that the transition rule is matter independent. We now show that sufficiently close to a singularity, the transition rule is such that $\delta \rightarrow 0$. Therefore $\Gamma \rightarrow p_\Omega$, and our new law reduces to BKL-Misner rule. We demonstrate this for both the initial and final singularity. As a byproduct, we see that our law is the first generalization to include matter, via a matter time gauge, in the intermediate region where “matter begins to matter.”

To establish this let us note the following: the transition law (dust-Kasner)⁽ⁱ⁾ \rightarrow (dust-Kasner)^(f) at any wall is governed by the dust-Kasner energy conservation equation

$$-\Delta(p_+^2) - \Delta(p_-^2) + \Delta(p_\Omega^2) = 24H_p\Delta\delta, \quad (4.76)$$

since the total energy H_p of the Bianchi IX solution does not change. Now the change in p_+ and p_- is bounded since \dot{p}_\pm can be positive or negative at different walls. Therefore close to a singularity, the sign of $\Delta\delta$ is completely determined by $\Delta(p_\Omega^2)$.

We now establish that $\Delta\delta > 0$ during the expansion phase and $\Delta\delta < 0$ during the contraction phase. This is sufficient to show that (4.74) reduces

to the vacuum rule sufficiently close to a singularity. We do this by showing that $\Delta(p_\Omega^2)$ accumulates in one direction.

Let us first note that the dust-Kasner evolution implies

$$\dot{\Omega}^I < 0, \quad \ddot{p}_\Omega^I = 0. \quad (4.77)$$

Since the sign of $\dot{\Omega}$ is determined by the sign of p_Ω , we have $p_\Omega < 0$ for dust-Kasner evolution. During the expansion phase $\dot{\Omega}^I$ and $\dot{\Omega}^{IX}$ have the same sign (–ve), and near the singularity in regions where the potential is significant, (4.49) gives

$$\dot{p}_\Omega^{IX} \ll \dot{p}_\Omega^I < 0. \quad (4.78)$$

Thus, after a bounce from the wall V_1 , \dot{p}_Ω^{IX} decreases more than it would due to dust-Kasner evolution alone. This extra decrease implies that the shift in the dust-Kasner parameter p_Ω^0 is negative i.e., $\Delta p_\Omega^0 < 0$. Moreover, as the singularity is approached, the inequality in (4.78) grows and so does the magnitude of the shift. Since the inequality in (4.77) always holds, if the initial conditions for the initial dust-Kasner phase are set such that $\delta^i = 0$, then $p_\Omega^0{}^i < 0$. (This choice of initial conditions is always possible by shifting the dust time origin by $t_0 = (\Gamma^i - \Lambda^i)/3H_p$.)

Thus, $\Delta(p_\Omega^0)^2 > 0$ and increases with each successive bounce, while Δp_\pm^2 remains bounded. Therefore, $\Delta\delta > 0$ in the expanding phase. A similar argument leads to the conclusion that $\Delta\delta < 0$ in the contracting phase. Coupled with the fact that the inequality (4.78) grows as the singularity is

approached this implies that the change in δ is not only negative but also accelerating in the negative direction. Therefore, as either the past or future singularity is approached in dust times, δ (which is ≥ 0) asymptotes to 0 and we have

$$\Gamma \rightarrow p_\Omega. \quad (4.79)$$

Thus, our transition law (4.74) reduces to the matter-independent BKL-Misner rule.

We note that in Misner variables the transition rules at the other walls (V_2 & V_3) will in general be different from the law derived above. This is because though the quantity conserved at these walls can be obtained by suitably rotating (4.59), it is not possible to obtain the analog of (4.64) in a similar fashion. Therefore, the transition law at the other walls cannot be easily transformed into the law derived above. However, since the kinetic and potential terms in the Hamiltonian are invariant under rotations of $\frac{2\pi}{3}$, these transformations exist and are obvious in the terms of the scale factor variables.

Lastly, we can recover the dust-Kasner scale factors before and after a bounce by noting that the integration constants appearing in the transition rule are related to dust-Kasner exponents by

$$p_1 = \frac{1}{3}(1 - \cos \theta - \sqrt{3} \sin \theta), \quad p_2 = \frac{1}{3}(1 - \cos \theta + \sqrt{3} \sin \theta), \quad p_3 = \frac{1}{3}(1 + 2 \cos \theta). \quad (4.80)$$

4.5 Bianchi IX dynamics with dust and scalar field

It is known that a scalar field suppresses the oscillations between Kasner regimes that characterize the mixmaster dynamics of a generic approach to a singularity. Berger [25] first used MCP to clarify the role of the scalar field. In this section we apply this technique to investigate the near singularity dynamics of a Bianchi IX universe filled with dust and a homogeneous scalar field. In the dust time gauge, the physical Hamiltonian for a Bianchi IX spacetime with dust and a homogeneous scalar field χ is

$$H_p = -\frac{e^{3\Omega}}{24} (p_+^2 + p_-^2 - p_\Omega^2 + 12p_\chi^2) + V_{IX}(\Omega, \beta_+, \beta_-) - e^{-3\Omega}V_\chi(\chi), \quad (4.81)$$

where p_χ denotes the momentum conjugate to the scalar field and $V_\chi(\chi)$ is the scalar field potential. As in the last section, we can again view the Hamiltonian as a sum of two terms H_K and H_V where

$$H_K = -\frac{e^{3\Omega}}{24} (p_+^2 + p_-^2 - p_\Omega^2 + 12p_\chi^2) \quad (4.82)$$

$$H_V = V_{IX}(\Omega, \beta_+, \beta_-) - e^{-3\Omega}V_\chi(\chi). \quad (4.83)$$

To apply MCP we are interested in the solutions with the free Hamiltonian H_K . The equations of motion are the set (4.49) with $v = 0$. We note also

that from (4.82)

$$p_+^2 + p_-^2 + 12p_\chi^2 = \text{constant} \equiv L. \quad (4.84)$$

Therefore, we can parameterize p_\pm as

$$p_+ = k\sqrt{L} \sin \theta, \quad p_- = k\sqrt{L} \cos \theta, \quad (4.85)$$

with

$$k = \sqrt{1 - \frac{12p_\chi^2}{c}}. \quad (4.86)$$

Using the asymptotic expansions for β_\pm in H_V , near the singularity we have

$$H_V \approx 2 \left(e^{\Omega(\pm 4k \sin \theta \pm 4\sqrt{3}k \cos \theta - 1)} + e^{\Omega(\pm 4k \sin \theta \mp 4\sqrt{3}k \cos \theta - 1)} + e^{\Omega(\mp 8k \sin \theta - 1)} \right). \quad (4.87)$$

None of the terms in H_V are significant if the following inequalities are satisfied simultaneously

$$\begin{aligned} \pm 4k \sin \theta \pm 4\sqrt{3}k \cos \theta - 1 &< 0 \\ \pm 4k \sin \theta \mp 4\sqrt{3}k \cos \theta - 1 &< 0 \\ \mp 8k \sin \theta - 1 &< 0. \end{aligned} \quad (4.88)$$

All three inequalities are satisfied for $k < 1/4$. Thus, in the presence of a scalar field the oscillatory dynamics of the dust filled Bianchi IX model is

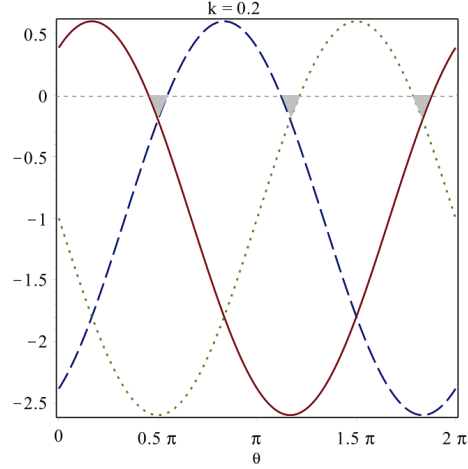


Figure 4.4: This is a plot of the expressions on the left hand side of (4.88) with respect to θ for a value of $k < 0.25$. The solid line indicates the first condition, the dashed line indicates the second condition and the dotted line indicates the last condition. The gray regions indicate θ values for which all the terms in the potential are decaying. As the value of k decreases this region grows larger.

suppressed when the scalar field momentum satisfies

$$\frac{4}{5}p_x^2 > p_+^2 + p_-^2. \quad (4.89)$$

Given the dynamics for the anisotropy momenta, the above equation will necessarily be satisfied in the asymptotic limit.

4.6 Discussion

This chapter presented the Bianchi I and IX cosmologies with dust in the Hamiltonian theory in the dust time gauge. We first gave a new derivation of the Heckmann-Schücking solution (dust-Kasner) in the dust time gauge, and used this to study the Bianchi IX dynamics. We showed this approach gives a new physical picture of Bianchi IX evolution, as a series of dust-Kasner epochs between bounces from the anisotropy potential walls. We then derived the transition law for these dust-Kasner epochs. This law differs significantly in detail from the vacuum case derived by BKL and Misner, and its form is different at each of the potential walls.

In the dust time gauge it is not possible to separate the dust degrees of freedom from the gravitational degrees of freedom, since the extra degree of freedom is manifested in the metric, and matter is “locked in” with time. Therefore it is not surprising that the transition between different dust-Kasner regimes is governed by more than one parameter.

This leads to a puzzle: how does the “matter does not matter” result arise in a context where evolution is defined with respect to matter time (dust in our case)? To answer this we showed that the transition rule we derived reduces to the vacuum BKL-Misner law sufficiently close to a singularity.

We emphasize that our analysis in deriving the generalized transition law makes no assumption about the size of the Universe. Rather, it relies only on the fact that collisions with walls occur throughout evolution in dust time.

As such it may be interpreted as simply a “wall collision law.”

In the following chapters we will explore the quantum dynamics of the FLRW and Bianchi I models in the dust time gauge.

Chapter 5

The Universe as an Oscillator

In this chapter we will explore the reduced phase space quantization of a spatially flat Friedmann-Lemaître-Robertson-Walker (FLRW) model with dust and a cosmological constant. This remains the typical model to consider since current observations suggest that our Universe is modelled by an FLRW cosmology with nearly zero spatial curvature and a very small positive cosmological constant ($\Lambda \sim 3 \times 10^{-22} t_p^{-2}$). In the reduced phase space quantization approach with the dust time gauge, the quantum theory is completely solvable and the model exhibits the key feature of singularity avoidance that is expected from more complex quantum gravity models [6].

A surprising consequence of using the dust time gauge is that in the Arnowitt-Deser-Misner (ADM) formalism the physical Hamiltonian, after a canonical transformation, is exactly that of the simple harmonic oscillator with the oscillator frequency determined by $\sqrt{\Lambda}$. The quantum theory is

therefore immediate.

For $\Lambda < 0$ the potential is that of the usual oscillator, whereas for $\Lambda > 0$ it is the inverted oscillator. The former case describes Universes either as stationary states, or as wave packets that expand and contract ad-infinitum. The latter case has only scattering solutions that give Universes with a single bounce. Depending on the choice of canonical parametrization, the oscillator is either on the half or the full line. All cases gives singularity avoidance, and for all choices of self-adjoint extensions of the Hamiltonian. This model also exhibits one of the situations where Dirac and reduced phase space quantization give similar results for a particular choice of operator ordering in the Wheeler-DeWitt equation.

Section 5.1 details the model and the canonical transformation that maps its dynamics on to an oscillator. In Section 5.2 we discuss the quantum theory of the model and in Section 5.3 we provide a summary of our results and discuss their relevance.

5.1 The Homogeneous and Isotropic Sector

Let us consider the reduction of the dust-time gauge theory to the homogeneous and isotropic cosmology. The general homogeneous and isotropic metric in the dust time gauge can be written as:

$$ds^2 = -dt^2 + q_{ij}w^i w^j, \tag{5.1}$$

where w^i are invariant 1-forms corresponding to the isometry group of the spatial 3-manifold and the spatial metric is given by

$$q_{ij} = a^2(t)e_{ij}$$

with $e_{ij} = \text{diag}(1, 1, 1)$ the fiducial flat metric. The momentum conjugate to this spatial metric is

$$\pi^{ij} = \frac{p_a(t)}{6a(t)}e^{ij}, \quad (5.2)$$

The reduced phase space coordinates are (a, p_a) , and we take $a \in (0, \infty)$ and $p_a \in \mathbb{R}$ as the definition of this parametrization (since we must have $\det(q_{ij}) = a^3 > 0$).

The physical Hamiltonian in the dust time gauge for the case of flat spatial hypersurfaces then becomes

$$\mathcal{H}_p = \frac{p_a^2}{24a} - \Lambda a^3. \quad (5.3)$$

To briefly recap, this FRW model started with a four-dimensional phase space, that of the dust field and the scale factor. After fixing the time gauge and solving the Hamiltonian constraint, the reduced phase space becomes two-dimensional, with canonical coordinates (a, p_a) . This is unlike the vacuum deSitter model (see e.g.[52]), which actually has no physical degrees of freedom; the physical meaning of “wave functions of the Universe” without additional degrees of freedom is therefore unclear.

The canonical transformation

$$p = \frac{p_a}{\sqrt{12a}}, \quad x = \frac{4}{\sqrt{3}}a^{3/2} \quad (5.4)$$

and the rescaling $\Lambda \rightarrow 4\Lambda/\sqrt{3}$ transforms the Hamiltonian to

$$\mathcal{H}_p = \frac{1}{2}(p^2 - \Lambda x^2). \quad (5.5)$$

There are thus three cases of interest: $\Lambda = 0$ is a free particle, $\Lambda < 0$ is the oscillator and $\Lambda > 0$ is the inverted oscillator.

5.2 Quantization and wave functions of the Universe

This section consists of two parts where we describe quantization in the dust time gauge for two choices of the configuration space. These lead to quantum theories on either the half-line or the full line. In the former case there is a one parameter family of self-adjoint extensions of the physical Hamiltonian.

5.2.1 Quantization on the half-line

The classical theory is on the half-line, $x \in (0, \infty)$, so the obvious choice for the Hilbert space is $L^2(\mathbb{R}^+, dx)$. In this space it is known that Hamiltonians of the form $p^2 + V(x)$ have self-adjoint extensions. Specifically, it is readily

checked that the physical Hamiltonian (5.5) is symmetric in the usual representation $\hat{p} \rightarrow -i\partial_x$, i.e. that $(\psi, \widehat{\mathcal{H}}_p\phi) = (\widehat{\mathcal{H}}_p\psi, \phi)$, provided $\lim_{x \rightarrow \infty} \phi = 0$ and

$$\lim_{x \rightarrow 0} [\psi^* \phi' - \phi \psi'^*] = 0. \quad (5.6)$$

This gives the boundary condition $\phi'(0) = \alpha\phi(0)$, $\alpha \in \mathbb{R}$. Thus there is a one-parameter (α) family of self-adjoint extensions of $\widehat{\mathcal{H}}_p$ on the half-line, so the Hilbert space is the subspace specified by

$$\mathbb{H}_\alpha = \left\{ \phi \in \mathcal{L}^2(\mathbb{R}^+, dx) \mid \lim_{x \rightarrow 0} (\ln \phi)' = \alpha \in \mathbb{R} \right\}. \quad (5.7)$$

We are interested in solving the time-dependent Schrödinger equation,

$$i \frac{\partial}{\partial t} \phi(x, t) = -\frac{1}{2} \frac{\partial^2}{\partial x^2} \phi(x, t) - \frac{1}{2} \Lambda x^2 \phi(x, t), \quad (5.8)$$

with the boundary condition mentioned above. (In this equation all variables are dimensionless, or equivalently, written in Planck units.)

$\Lambda = 0$: There are two types of elementary solutions. The first are the ingoing and outgoing waves of fixed energy (in the dust time gauge), and satisfying the above boundary condition,

$$\phi_{\alpha k}(x, t) = e^{-ik^2 t/2} \left[e^{ikx} - \left(\frac{\alpha - ik}{\alpha + ik} \right) e^{-ikx} \right] \quad (5.9)$$

Normalizable wave functions are constructed in the usual manner as

$$\psi_\alpha(x, t) = \int_{-\infty}^{\infty} dk f(k) \phi_{\alpha k}(x, t) \quad (5.10)$$

All such solutions describe Universes with singularity avoidance and a bounce at the origin with a phase shift given by α . Here singularity avoidance refers to the fact that the quantum equations of motion remain well defined even when $x = 0$. This does not imply that the curvature invariants remain bounded as $x \rightarrow 0$ as in LQC models where singularity avoidance is observed.

The second type of solution is a bound state,

$$\phi(x, t) = e^{i\kappa^2 t/2} e^{-\kappa x}, \quad \kappa > 0 \quad (5.11)$$

This corresponds to $\alpha = -\kappa$, a choice permitted by the boundary conditions. The Universe this describes is ruled out by experiment, since $\langle a^{3/2} \rangle \sim \langle x \rangle = (2\kappa)^{-1}$ which has the interpretation of an emergent flat spacetime from the expectation value of the metric.

$\Lambda < 0$: This is the oscillator on the half-line with the boundary condition, $\psi'(0) - \alpha\psi(0) = 0$. With $\Lambda = -1/l^2$ and $\zeta = t/l$, the propagator on \mathbb{R} is a

basic result,

$$K(x, \zeta; x', 0) = \sqrt{\frac{1}{2\pi i l \sin \zeta}} \times \exp \left\{ \frac{i[(x^2 + x'^2) \cos \zeta - 2xx']}{2l \sin \zeta} \right\}. \quad (5.12)$$

For the half-line problem at hand, given initial data $\psi(x, 0) = f(x)$ for $x > 0$, the solution with the required boundary condition at $x = 0$ may be obtained by extending the given initial data $f(x)$ on \mathbb{R}^+ to the region $x < 0$, such that

$$f'(x) - \alpha f(x) = -(f'(-x) - \alpha f(-x)), \quad x < 0, \quad (5.13)$$

i.e. imposing antisymmetry on the boundary condition function. Solving this equation gives the required extension

$$f_L(x) \equiv e^{\alpha x} \int_x^0 du e^{-\alpha u} [f'(-u) - \alpha f(-u)] + e^{\alpha x} f(0), \quad x < 0, \quad (5.14)$$

where the integration constant is chosen such that $f_L(0) = f(0)$.

Convoluting the data so extended with the full-line propagator (5.12) then gives the solution

$$\psi(x, \zeta) = \int_{-\infty}^0 dx' K(x, \zeta; x', 0) f_L(x') + \int_0^{\infty} dx' K(x, \zeta; x', 0) f(x'), \quad x > 0. \quad (5.15)$$

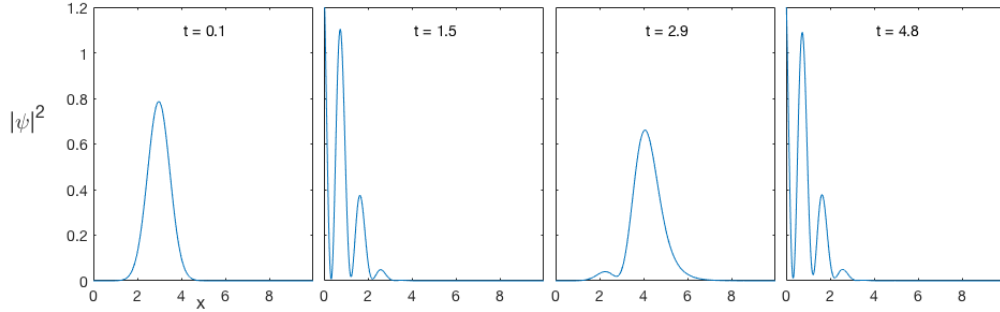


Figure 5.1: Snapshots of $|\psi(x,t)|^2$ with the initial data $f(x) = \frac{e^{-(x-3)^2}}{\sqrt[4]{\pi/2}}$, and parameters $\Lambda = -1$ and $\alpha = 1.0$. The Universe moves toward the origin ($t = 0.1 - 1.5$), expands asymmetrically ($t = 2.9$), and contracts again ($t = 4.8$). The profiles at $t = 1.5$ and $t = 4.8$ are nearly identical.

It is straightforward to construct explicit examples of such solutions; all describe Universes that expand out to a maximum size, re-collapse, and bounce again. This is of course expected since wave packets are confined in the half-oscillator potential. Figure (5.1) shows the dynamics of a representative Gaussian wave function with $\Lambda = -1$, and $\alpha = 1$. The asymmetric bounce is evident, and the second and fourth frames demonstrate the multiple bounce feature.

$\Lambda > 0$: The Hamiltonian is not bounded below. However the unitary evolution operator is still well defined since the Hamiltonian has self-adjoint extensions. The propagator on \mathbb{R} is obtained by the replacement $l \rightarrow il$ to

give

$$\begin{aligned} \bar{K}(x, \zeta; x', 0) = & \sqrt{\frac{1}{2\pi i l \sinh \zeta}} \\ & \times \exp \left\{ \frac{i[(x^2 + x'^2) \cosh \zeta - 2xx']}{2l \sinh \zeta} \right\}. \end{aligned} \quad (5.16)$$

Solutions of the time-dependent Schrödinger equation with the boundary condition $\phi'(0) - \alpha\phi(0) = 0$ are found in the same way as above by extending the initial data function to $x < 0$. It is evident that the propagator is damped for large times ζ due to the prefactor. However for the very small Λ that is experimentally observed, the decay time would be very large. (It is useful to note that the issue of convergence of the Euclidean functional integral for the inverted oscillator was studied in [32], where it is shown that the integral for the propagator converges if the propagation time is bounded by a factor of the oscillator frequency.) Fig. 2 shows the propagation of the same initial Gaussian wave packet as that in Fig. 1, but now for positive Λ . The wave packet moves outward and spreads rapidly.

5.2.2 Quantization on \mathbb{R}

In the above we started with the standard canonical parametrization for the FLRW cosmology which led to the oscillator on the half-line. There is an alternative parametrization that directly gives the oscillator on the real line

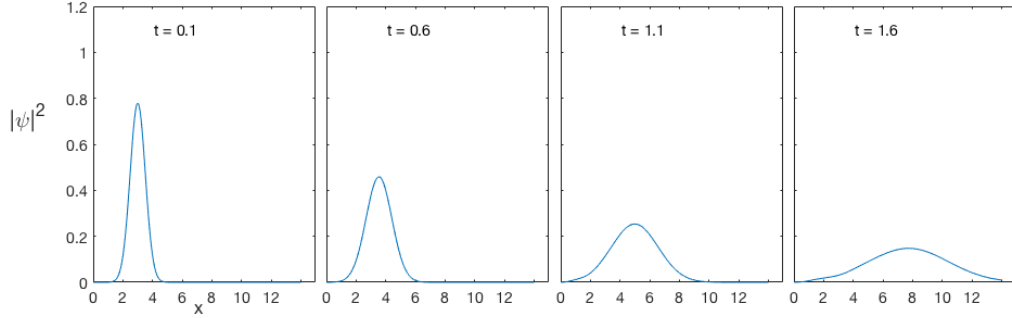


Figure 5.2: Snapshots of $|\psi(x, t)|^2$ with the initial data $f(x) = \frac{e^{-(x-3)^2}}{\sqrt[4]{\pi/2}}$, and parameters $\Lambda = 1$ and $\alpha = 1.0$. The initial wave packet travels outwards and spreads.

after a rescaling of variables. This is

$$\begin{aligned} q_{ab} &= A^{4/3}(t)e_{ab} \\ \pi^{ab} &= \frac{1}{4A^{1/3}(t)} P_A(t)e^{ab}, \end{aligned} \quad (5.17)$$

where the phase space (A, P_A) is now \mathbb{R}^2 .

In this parametrization there is an exact Lorentzian ‘‘Hartle-Hawking’’ wave function, which is the ‘‘amplitude for a three-geometry given by a path integral over all compact positive-definite four-geometries which have the three-geometry as a boundary’’ [53]:

$$\psi[q] = \int D[g]D[\phi] \exp(-S[g, \phi]), \quad (5.18)$$

where the S is the Euclidean action for matter and gravity, and the gravity measure is designed to reflect the definition above.

In our case, we deploy the boundary condition obtained by setting $x' = 0$ in (5.16); this is the closest to the HH condition in Lorenzian theory:

$$\Psi_{HH} \equiv \bar{K}(A, \zeta; 0, 0) = \sqrt{\frac{1}{2\pi i l \sinh \zeta}} \exp\left(-\frac{iA^2}{2l \tanh \zeta}\right), \quad (5.19)$$

where $A^4 = \det(q_{ab}) \equiv q$, and since we are now on the full line, $A \in \mathbb{R}$. This expression is just the oscillator propagator on the real line for $\Lambda = 1/l^2$ with $A_0 = \zeta_0 = 0$. For large times $\zeta = t/l$ this is

$$\bar{K}(q, \zeta; 0, 0) \longrightarrow \frac{1}{\sqrt{\pi i l}} \exp\left(-\frac{i\sqrt{q} + t}{2l}\right). \quad (5.20)$$

This is oscillatory in 3-volume, and decays exponentially in time t .

5.3 Discussion

The main result detailed in this chapter is that in general relativity coupled to pressureless dust in the dust time gauge, the FLRW model with a cosmological constant has a physical Hamiltonian that is exactly that of a harmonic oscillator with frequency determined by $\sqrt{\Lambda}$. The Hamiltonian has a one-parameter(α) set of self-adjoint extensions, and explicit solutions of the time-dependent Schrödinger equation are readily constructed. All cases give singularity avoidance, which here means that wave functions describing the Universe bounce at small spatial volume for any value of α , regardless of whether the configuration space is the half line or the full line.

It is interesting to compare these results with those obtained in LQC [3] using the connection-triad variables. There the $\Lambda = 0$ case was studied with scalar field time, where the form of the Hamiltonian is such that wave function dynamics requires numerical study. It was subsequently studied in dust time in [60]. In both these cases the Hamiltonian is essentially self-adjoint. In our case the bounce occurs for all self-adjoint extensions, and can be asymmetric in the sense that there is a phase shift at the bounce determined by α . Only the $\alpha = 0$ case gives a symmetric bounce.

For comparison with Dirac quantization, the corresponding quantum theory also resembles the oscillator, but only for the Laplace-Beltrami operator ordering in the kinetic term in the Wheeler-DeWitt operator [68]. However, in [68] only the $\Lambda = 1$ case is considered and the most general self-adjoint extension with Robin boundary conditions is not addressed. Nevertheless, it is one of the few cases where it seems possible to rigorously establish equivalence between Dirac and reduced phase space quantizations. It would be interesting to study this issue for full quantum gravity with dust time [61].

Our consideration and results are entirely in the Lorentzian theory, and as such may be compared with similar models that invoke the Hartle-Hawking prescription in Lorentzian time, in particular the recent debate concerning integration contours for the propagator [45, 38]. The latter work reports a suppression factor $\exp(-\Lambda l_p^2)$ in the propagator for the no boundary wave function of the Universe in the semiclassical approximation. We find a similar result, but our state is *exact*, (i.e. not just a semiclassical approximation),

and also has explicit (dust) time dependence: eqn. (5.20) has the factor $\exp(-t/2l)$, which for fixed $t = t_0$ exhibits an exponential decay. From the currently observed value of Λ , $l \sim 10^{60}l_p$, therefore the characteristic decay time is $\sim 10^{60}$ Planck times, which is close to the age of the Universe.

The model with spatial curvature $k \neq 0$ and additional matter fields such as the minimally coupled scalar field is not exactly solvable. The physical Hamiltonian for this case in the dust time gauge (after the canonical transformation (5.4)) is

$$\mathcal{H}_p^k = \frac{1}{2} (p^2 - \Lambda x^2) + kx^{2/3} + \frac{p_\phi^2}{2x^2} + x^2V(\phi). \quad (5.21)$$

Models such as this demonstrate that it is useful to consider matter time gauges in the cosmological setting. Gravitational perturbations can be added to the physical Hamiltonian in a similar way, while retaining the oscillator form of the homogeneous part of the kinetic term. This may provide a useful starting point for studying singularity avoidance in dust time gauge in the inhomogeneous setting.

We note that it is an important consideration to extend the model we have studied in two ways – to include anisotropy, and beyond that, inhomogeneity. The former is a larger minisuperspace model with a few more phase space degrees of freedom. A classical analysis in dust time gauge appears in [7] and was detailed in Chapter 4. Inclusion of general inhomogeneities is of course more difficult in that it involves studying field theoretic models such as the

Gowdy cosmologies [44]. The importance of such extensions is of current interest due to the issue of whether the no-boundary wave function is stable to perturbations: there are claims for [39] and against [37]. These works do not use the dust time gauge and physical Hamiltonian that we study here, so an extension of our approach beyond FLRW to include a gravitational perturbation of fixed wavenumber along the lines studied in these papers would be potentially useful.

Lastly the $\Lambda < 0$ case may be of interest in the context of the AdS/CFT conjecture and holography. Specifically the idea of using matter (or other) time gauge in the bulk might provide a useful mechanism to probe bulk dynamics and the holographic signatures of resolved singularities in such settings [29], something which appears so far to be largely unexplored.

Chapter 6

Quantum dynamics of Bianchi I spacetimes

In this chapter we will explore the quantum dynamics of Bianchi I spacetimes using the dust time gauge. In the canonical setting, several aspects of the quantum Bianchi I model with and without a scalar field have been studied analytically within the context of Loop Quantum Cosmology (LQC) [70, 69]. Recently, this model was also studied numerically using effective dynamics techniques in LQC [40]. In these studies the scalar field or some geometrical quantity like volume provides a relational time. Another approach to quantizing the Bianchi I model is using the Feynman path integral. This was first discussed in [22, 19] using Misner variables for both vacuum and fluid-filled Bianchi I models using Ω as a time variable. The time gauge is implemented as a delta function in the path integral measure. In contrast, the approach

detailed in this chapter involves fixing the time gauge at the classical level and solving the Hamiltonian constraint to determine the physical Hamiltonian. This partial deparameterization of the theory is detailed in Chapter 2. We then determine the Lagrangian for the physical degrees of freedom via a Legendre transform of the physical Hamiltonian and define the path integral using this Lagrangian.

It is important to note that the model is symmetry reduced before quantization and the classically absent inhomogeneous degrees of freedom are neglected during quantization. It is not clear how such quantum cosmology models are related to full quantum gravity models, however as with LQC we expect several qualitative aspects to survive in the full quantum gravity models. Furthermore, classically there is ample evidence that near a cosmological singularity the dynamics is “velocity” dominated and the inhomogeneities can be neglected. If this conjecture also holds in the quantum regime then the symmetry reduced quantum dynamics of the Bianchi models will be of particular interest.

In the next section we define the Bianchi I path integral and detail the regularization and discretization of this path integral. Section 6.2 discusses the semiclassical analysis of the path integral using PIMC techniques and in Section 6.3 we calculate the no-boundary wavefunction for dust filled Bianchi I cosmologies.

6.1 Bianchi I Path Integral

The Hamiltonian for a Bianchi I spacetime in the dust time gauge ($N = -1$) is given by:

$$H_p = \frac{1}{4 \exp\{\sum_i \alpha_i\}} \left[-\frac{1}{2} \sum_i \pi_i^2 + \prod_{i<j} \pi_i \pi_j \right]. \quad (6.1)$$

The action for the system is:

$$S = 2 \int \exp\left\{ \left(\sum_i \alpha_i \right) \right\} \left[\prod_{i<j} \dot{\alpha}_i \dot{\alpha}_j \right] dt. \quad (6.2)$$

Transforming to a new set of variables (this is a canonical transformation):

$$x = \frac{4}{\sqrt{3}} \prod_{i=1}^3 \sqrt{\alpha_i}, \quad \beta_+ = \frac{1}{6} (\alpha_1 + \alpha_2 - 2\alpha_3), \quad \beta_- = \frac{1}{\sqrt{3}} (\alpha_1 - \alpha_2), \quad (6.3)$$

the action takes the form

$$S = \int d\tau \left[\frac{1}{2} \dot{x}^2 - \frac{9}{8} x^2 (\dot{\beta}_+^2 + \dot{\beta}_-^2) \right]. \quad (6.4)$$

We then define the Lorentzian path integral as:

$$Z = \int \mathcal{D}x \mathcal{D}\beta_+ \mathcal{D}\beta_- e^{-iS}. \quad (6.5)$$

Wick rotating $t \rightarrow -it$ in the lower half plane, we obtain the Euclidean action:

$$S_E = \int d\tau \frac{9}{8} x^2 (\dot{\beta}_+^2 + \dot{\beta}_-^2) - \frac{1}{2} \dot{x}^2, \quad (6.6)$$

where the overdots now indicate derivatives with respect to Euclidean time. The Euclidean path integral takes the form

$$Z = \int \mathcal{D}x \mathcal{D}\beta_+ \mathcal{D}\beta_- e^{-S_E}. \quad (6.7)$$

Physically reasonable matter fields have positive energy density. Requiring positive energy density for the dust field imposes $H_p > 0$. After Wick rotation, this leads to the condition $L_E > 0$ and thus the Euclidean action is positive definite yielding a convergent Euclidean path integral. Positivity of energy density is a classical expectation for reasonable sources of matter. However, there is no guarantee that this weak energy condition survives in the quantum regime. It is plausible that some form of an averaged weak energy condition survives in the quantum regime, even though the weak energy condition does not hold locally [58, 46, 71]. In the following sections we will discuss results of PIMC calculations that implement $L_E > 0$ locally at each time step as well as calculations which only implement $S_E \geq 0$ allowing $L_E < 0$ locally.

We numerically compute the path integral in Eq.(6.7) using the PIMC algorithm detailed in Chapter 2. We start by discretizing the time parameter into N time steps. Throughout this chapter we use a stepsize of $\epsilon = 0.01$ ¹. We

¹Smaller step sizes give similar results.

use a forward difference scheme to discretize the derivatives and a midpoint scheme for the configuration variables². The discretized Euclidean action is

$$\begin{aligned}
S_E &= \sum_{n=1}^{N-1} \frac{9}{8\epsilon} \left[\frac{(x(n+1) + x(n))^2}{4} \right] ((\beta_+(n+1) - \beta_+(n))^2 + (\beta_-(n+1) - \beta_-(n))^2) \\
&\quad - \frac{1}{2\epsilon} (x(n+1) - x(n))^2,
\end{aligned} \tag{6.8}$$

The discrete path integral is given by

$$Z = \prod_{n=1}^N \int dx_n \int d\beta_{+n} \int d\beta_{-n} e^{-S_E}. \tag{6.9}$$

Thus the PIMC amounts to carrying out $3N$ Monte Carlo integrations.

6.1.1 Classical Euclidean solutions

Before we investigate the quantum dynamics let us discuss the classical trajectories of the Euclidean time system³. We are interested in finding solutions to the Euler-Lagrange equations derived from S_E . In our old variables

$$S_E = -2 \int \exp \left\{ \left(\sum_i \alpha_i \right) \right\} \left[\prod_{i < j} \dot{\alpha}_i \dot{\alpha}_j \right] dt \tag{6.10}$$

²A midpoint scheme is commonly implemented for finite time path integrals in quantum mechanics to avoid large boundary effects. Furthermore, for quantum mechanical sigma models only the midpoint scheme yields the correct covariant continuum integrals [36]. Here this is one of the ingredients in our definition of the discrete path integral.

³From here on t denotes Euclidean time unless otherwise stated.

yields the equations of motion:

$$\ddot{\alpha}_i - \exp\left\{\left(\sum_i \alpha_i\right)\right\} \left[\prod_{i < j} \dot{\alpha}_i \dot{\alpha}_j\right] = 0. \quad (6.11)$$

These equations are more amenable in the Hamiltonian setting:

$$\dot{\alpha}_i = \frac{1}{4e^{\sum_i \alpha_i}} (\pi_i - \pi_j - \pi_k), \quad \dot{\pi}_i = H_E, \quad (6.12)$$

where the π_i are momenta conjugate to α_i and the Euclidean Hamiltonian, H_E , is a constant of motion. The solutions to the Euclidean equations of motion for ($L_E > 0$) are:

$$\alpha_i = p_i \ln \tau + \left(\frac{2}{3} - p_i\right) \ln (2\Gamma - \tau) + \ln \xi_i, \quad (6.13)$$

with $\tau = 3H_E t + \Lambda + \Gamma$ where Λ , Γ and ξ_i are integration constants with $\prod_i \xi_i = \frac{1}{24H_E}$. The exponents p_i satisfy

$$\sum_i p_i = 1, \quad \sum_i p_i^2 = 1. \quad (6.14)$$

In terms of the new variables (x, β_{\pm}) these solutions take the form:

$$\begin{aligned}
x &= \frac{4}{\sqrt{3}} \sqrt{\frac{\tau(2\Gamma - \tau)}{24H_E}} \\
\beta_+ &= \frac{1}{6} \left[(p_1 + p_2 - 2p_3) \ln \tau + (2/3 - p_1 - p_2 + 2p_3) \ln(2\Gamma - \tau) + \ln \left(\frac{\xi_1 \xi_2}{\xi_3} \right) \right] \\
\beta_- &= \frac{1}{2\sqrt{3}} (p_1 - p_2) \left[\ln \tau - \ln(2\Gamma - \tau) + \ln \left(\frac{\xi_1}{\xi_2} \right) \right].
\end{aligned} \tag{6.15}$$

The solutions have two cosmological singularities i.e., the universe expands and then contracts for $-\frac{\Gamma+\Lambda}{3H_E} \leq t \leq \frac{\Gamma-\Lambda}{3H_E}$.

6.2 Semiclassical PIMC Analysis

Though the Path Integral Monte Carlo (PIMC) technique detailed in the Chapter 2 can be used to perform fully non-perturbative calculations, a semiclassical analysis is useful to determine if our intuitions are borne out. Using the minisuperspace path integral detailed above we can explore homogeneous quantum fluctuations around classical dust-filled Bianchi I universes. In order to do this, we seed our Monte Carlo algorithm with a classical path i.e., classical trajectories for x, β_+, β_- for some initial data. We then explore the neighbourhood of this classical path by tuning the exploration parameter Δ .

The algorithm we use is detailed in Chapter 2 with the change that instead of one variable we now have three independent variables. At each Monte Carlo step we randomly select one of the three variables to change and then apply the single variable algorithm detailed in Chapter 2. We do not change

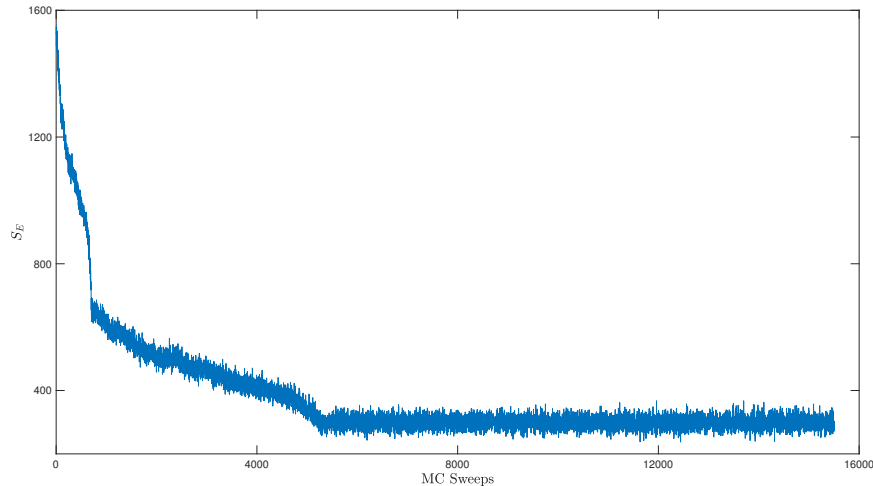


Figure 6.1: A plot of the action versus Monte Carlo sweeps($\times 100$) from a representative thermalization run. The run was seeded with a random path and the Markov chain allowed to thermalize for 1.6 million sweeps. It is clear that the action stabilizes after 500,000 sweeps. We assume the Markov chain has thermalized once the action stabilizes.

all three variables at once as this usually results in large changes in the action leading to lower acceptance rates. As always, sample paths are collected after the Markov Chain thermalizes, which is determined by observing the action (see Figure 6.1).

From the initial classical seed path we generate and thermalize five different Markov chains in order to better explore the path space. For these thermalization runs the parameter Δ is tuned such that the acceptance rate is between 15 – 30%. Interestingly this results in $\Delta \sim 0.01 - 0.03$. However, this is not surprising since we do expect the classical path to be a local minimum of the action. After the five chains are thermalized, we can collect sample paths to perform measurements. In order to calculate expectation values, samples from all five chains are merged and averages are computed

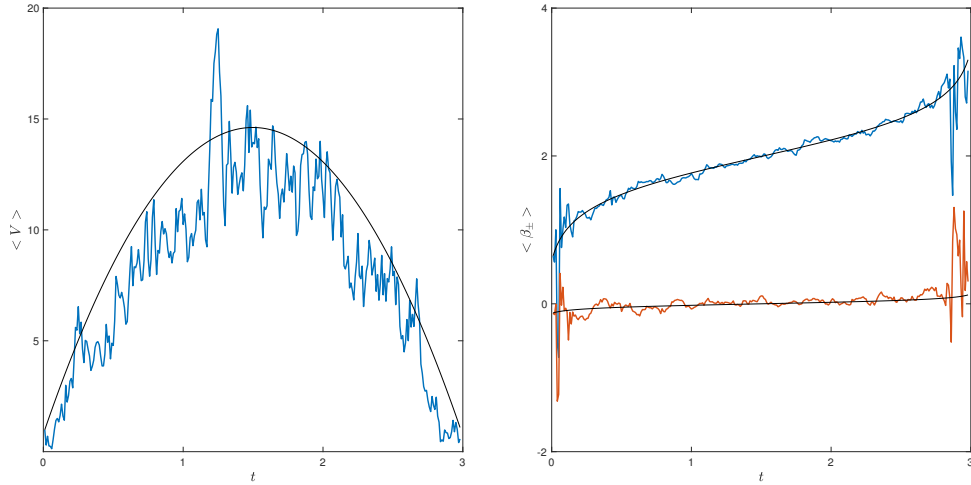


Figure 6.2: The average volume and anisotropies. The solid black lines indicate the classical trajectories. In the second plot the red curve denotes $\langle \beta_{-} \rangle$ and the blue curve denotes $\langle \beta_{+} \rangle$.

over this merged set of paths. The plots in Figure 6.2 show the average volume and anisotropies for the collected samples. In order to quantify the difference between quantum (semiclassical) paths and classical trajectories of the dust-filled Bianchi I universe, we define the relative deviation of the quantum path (X) from the classical one (X_{cl}) as

$$\sigma_X = \frac{\sqrt{\langle (X - X_{cl})^2 \rangle}}{X_{cl}} \quad (6.16)$$

The semiclassical expectation is that this fluctuation (σ_X) is large for small universe and decreases as the universe grows larger. The classical path used to seed the PIMC algorithm and the evolution time were chosen such that the universe starts out expanding from very small volumes ($0.8l_p^3$) to a maximum ($15l_p^3$) and then re-collapses to $0.8l_p^3$.

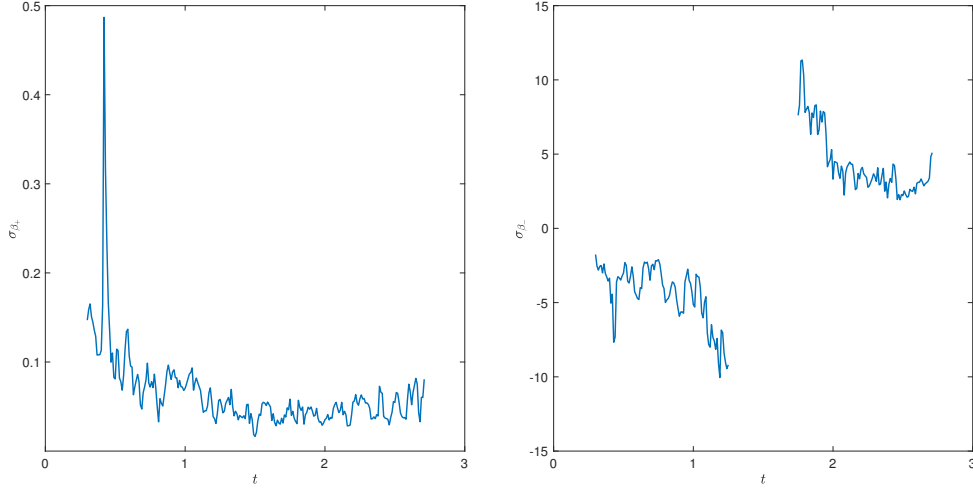


Figure 6.3: Fluctuations in the anisotropies with respect to time. Since $\sigma_X \rightarrow \infty$ as $X_{cl} \rightarrow 0$, we do not plot σ_X when the classical solution for X is less than 0.01. This is the reason for the gap in the second plot.

Figure 6.3 and Figure 6.4 display this deviation versus time for the variables x, β_+, β_- and the volume of the spatial slices. As expected we find that the quantum fluctuations are damped for large universes.

The Bianchi I exponents p_i satisfy

$$\sum_i p_i = 1, \quad \sum_i p_i^2 = 1. \quad (6.17)$$

In the semiclassical approximation the expectation values of the scale factors are expected to be close to the classical values and we may expect the exponents to approximately satisfy these conditions. In order to verify this consider the scale factors $a(t), b(t)$ and $c(t)$ which are related to our variables

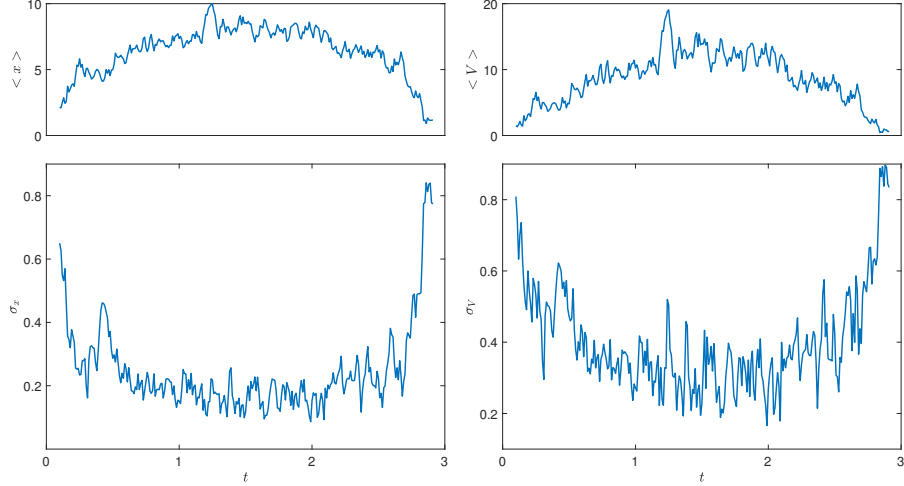


Figure 6.4: Fluctuations of x and spatial volume with respect to time. In the plots on top we plot $\langle x \rangle$ and $\langle V \rangle$ for comparison.

as

$$a = \left(\frac{3x^2}{16}\right)^{1/3} e^{\beta_+ + \sqrt{3}\beta_-}, \quad b(t) = \left(\frac{3x^2}{16}\right)^{1/3} e^{\beta_+ - \sqrt{3}\beta_-}, \quad c(t) = \left(\frac{3x^2}{16}\right)^{1/3} e^{-2\beta_+}. \quad (6.18)$$

We can calculate the expectation values $\langle a \rangle$, $\langle b \rangle$ and $\langle c \rangle$ by averaging the functions given above over all sample paths generated by the PIMC algorithm. We then fit a model to these averages of the form

$$f(t) = c_1(c_2 + 3Ht + \Lambda)^{c_3}(c_2 - 3Ht - \Lambda)^{2/3 - c_3}, \quad (6.19)$$

where the values of H and Λ are the same as for the classical paths with which the Markov chain is seeded and c_1 , c_2 and c_3 are the parameters to be

	Classical	Model	R^2
p_1	0.7180	0.709	0.94
p_2	0.6126	0.5699	0.91
p_3	-0.3305	-0.2595	0.99
$\sum_i p_i$	1	1.0194	—
$\sum_i p_i^2$	1	0.8948	—

Table 6.1: Values of the Kasner exponents extracted from fitting curves to the expectation values of the scale factors. The first Kasner sum rule is approximately satisfied by the quantum exponents but there is a discrepancy with the second sum rule.

fit. Figure 6.5 shows the results of this curve fitting and Table 6.1 provides the details. The semiclassical values of the exponents are close to the classical exponents but do not exactly satisfy Eq. (6.17). Only the first Kasner sum rule is approximately satisfied by the quantum exponents in the semiclassical regime. This is an indication that the Kasner transition law for a Bianchi IX spacetime may not be applicable in the semiclassical regime. However, a full simulation of the semiclassical dynamics of the Bianchi IX spacetime is needed to conclusively answer this question.

6.3 Wavefunction of the universe

As in the FLRW case we are interested in calculating the “no-boundary” wavefunction for this model. As usual, this corresponds to calculating the amplitude of a finite volume spatial geometry to emerge from a zero volume one. In this model, this corresponds to integration over paths with $x(0) = 0$ with $x(T)$ left unspecified. We explore two boundary conditions for the

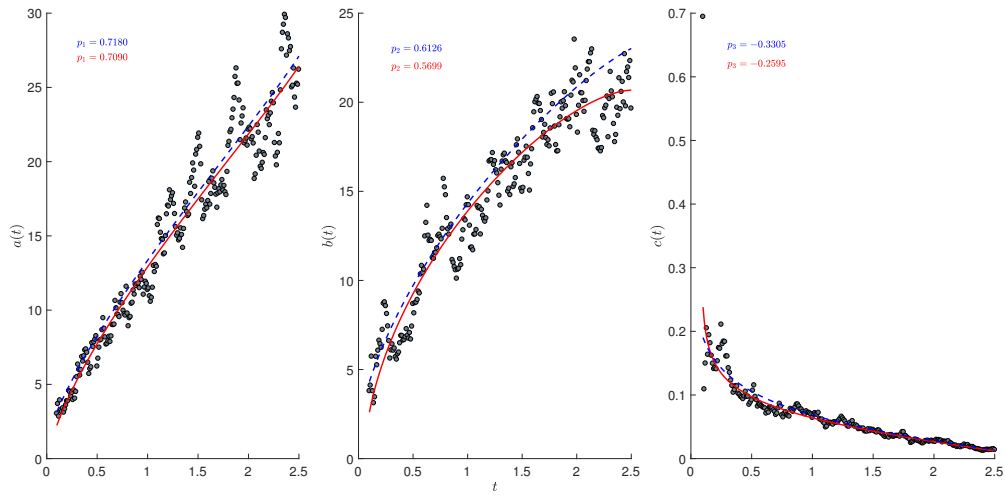


Figure 6.5: The scatter plot denotes the expectation values of the scale factor, the dashed blue line is the classical solution and the solid red line are the fits to the scatter plots. We see that the fitted values (in red) for all three Kasner exponents are close to the classical values (in blue). The fits are of high fidelity with $R^2 > 0.9$ for each of the fits.

anisotropies:

1. Fixed initial values for the anisotropies and unspecified final values.
2. Unspecified initial and final values (free boundaries)

For the PIMC algorithm we start with random arrays for x, β_+, β_- and fix $x = 0$. We then apply the algorithm detailed in the previous section with the following modifications:

- We always sample the last element of the arrays and always keep the first element of the x array fixed.
- After every Monte Carlo sweep we apply an overrelaxation step.⁴

6.3.1 $L_E > 0$

The Bianchi I path integral can be naturally regularized by only summing over paths which yield positive Lorentzian dust energy density. As detailed in Section 6.1 this implies that the Euclidean Lagrangian is positive definite. This is a local condition which couples consecutive array elements. We implement it in the PIMC algorithm by rejecting all proposals which result in paths which violate $L_E > 0$ at any timestep.

⁴Overrelaxation is a technique used to allow the algorithm to explore the configuration space more efficiently. The basic idea is to pick a proposal for a given variable that is as far as possible from the previous path without producing a large change in the action [35]. In our model the action is invariant under the parity transformation for any of the variables. Thus, in every overrelaxation step we apply the transformation $(x, \beta_+, \beta_-) \mapsto (-x, -\beta_+, -\beta_-)$ for all the variables.

The two different types of boundary conditions for the anisotropies described above (first elements fixed and sampled) result in different wavefunctions. However, these wavefunctions are qualitatively similar. In both cases we find that large spatial volumes are suppressed for all times, while large anisotropies dominate. Furthermore, the spread in the wavefunction with respect to the anisotropies is significantly larger than the spread in the volume component. For the first type of boundary conditions in which we fix $x(0) = 0$ and $\beta_{\pm}(0)$ to some initial value the wavefunction with respect to x is more sharply peaked (see Fig. 6.6). On the other hand the second set of boundary conditions with $\beta_{\pm}(0)$ kept free results in longer tails for x (see Fig. 6.7). Thus with these boundary conditions there is a small probability of larger universes emerging. These results are robust for different ranges of the random initial seed paths. We tested ranges from 1 – 200. Higher ranges resulted in longer thermalization times and it was not possible to go beyond the range $[-200, 200]$ for any of the variables using our implementation of the PIMC algorithm.

The numerical complexity of this model is rooted in the issue of thermalization of the Markov Chain. Even with acceptance rates of 30 – 50%, the thermalization is extremely slow. The acceptance rates decrease drastically as we increase the range of the initial random configurations, especially with large ranges for x . Thus, thermalization time seems to increase exponentially for such initial data. This dependence on the initial seed for the Markov chain

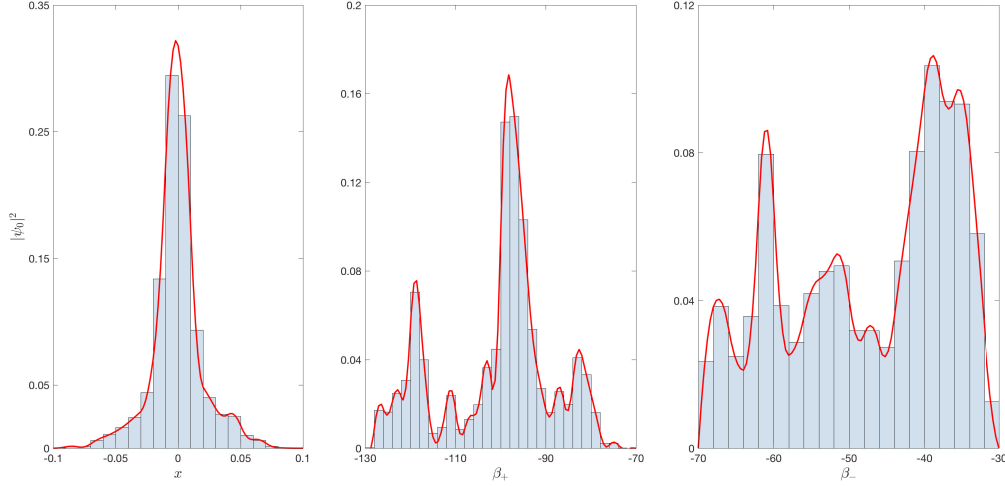


Figure 6.6: Plots of the no boundary wavefunction (squared) with respect to the variables (x, β_+, β_-) with $\beta_{\pm}(0)$ held fixed. The action stabilized after 60 million thermalization sweeps to a value of 158.05. We used an adaptive Δ in the range $0.05 - 0.5$ to maintain an acceptance rate of $30\% - 50\%$.

is also seen in simple systems like the Ising model ⁵. However, in the current model the effect is quite dramatic.

6.3.2 $S_E \geq 0$

Another regularization for the path integral is to only sum over paths with positive definite Euclidean action. We implement this by rejecting paths for which the Euclidean action is less than zero. As was observed for the closed FLRW model in [5] the Euclidean action rapidly approaches zero during thermalization and the path integral is dominated by paths with $S_E = 0$. In

⁵starting from a fully ordered configuration results in longer thermalization times for the Ising Model

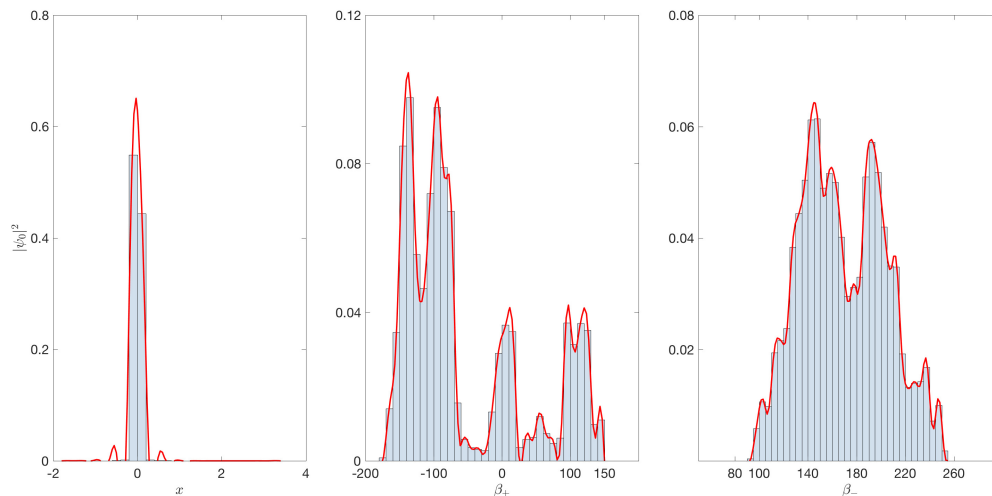


Figure 6.7: Plots of the no boundary wavefunction (squared) with respect to the variables (x, β_+, β_-) . The action stabilized after 60 million thermalization sweeps to a value of 185.62. We used an adaptive Δ in the range $0.05 - 0.5$ to maintain an acceptance rate of $30\% - 50\%$.

general the paths yielding $S_E \sim 0$ is uncountably infinite and diverse. We essentially have a continuum of vacua characterized by the surface $S_E = 0$. In a single PIMC run we can only explore a small subset of these paths. The size and characteristics of this subset are determined by the initial path used to seed the Markov chain and the parameter Δ . In each run the PIMC run converges to the subset of $S_E \sim 0$ paths closest to the initial path in path space. This implies that different runs result in different no-boundary wavefunctions. Figure 6.8 shows the no-boundary wavefunctions obtained from two different PIMC runs seeded by different random initial paths with the same range of allowed values. The two wave functions are quite different even though the runs were seeded with random paths in the same range.

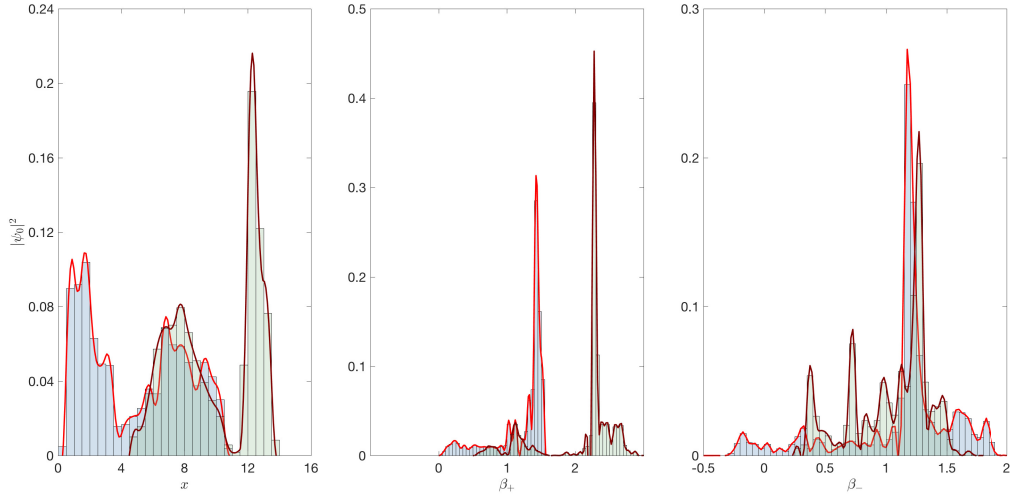


Figure 6.8: Plots of the no boundary wavefunction (squared) with respect to the variables (x, β_+, β_-) with the regularization $S_E \geq 0$.

The difference is particularly stark in the x variable where one wavefunction assigns significant probability to universes with spatial volume of the order of l_p^3 whereas the other assigns zero probability to such small universes.

6.4 Discussion

In this chapter we have investigated the quantum dynamics of a dust filled Bianchi I universe using PIMC techniques. We performed a semiclassical analysis by seeding the Markov Chain with a classical path. Given that we sample uniformly in the interval $[\Delta, \Delta]$ around the current path, this essentially restricts the set of paths allowed in the path integral to some neighborhood of the classical solution. Our results indicate that in this semi-

classical regime fluctuations in volume and anisotropy are large when the universe is small and decrease as the universe expands. Thus, as expected larger universes appear more classical.

We also checked if the Kasner sum rules remain valid in the semiclassical regime. We find mild violations of the sum rules indicating that the Kasner transition law derived using the sum rules may not be valid in the semiclassical regime. However, this does not rule out the possibility that quantum Bianchi IX dynamics can be quantified in terms of semiclassical Bianchi I dynamics.

Our semiclassical analysis did not attempt to rigorously define the neighborhood of a classical path but instead used the parameter Δ as a proxy for how far we explore from the classical path in path space in each Monte Carlo step. A more systematic exploration of the neighborhood of the classical path is possible by sampling the Lefschetz thimble containing the chosen classical path [4]. However, this is computationally much more intensive than the approach we have presented and is unlikely to provide a vast improvement over our approach given that the classical path dominates the path integral.

We also calculated no-boundary wavefunctions for this model. We define no-boundary conditions as the requirement that the spatial volume (and therefore x) at $t = 0$ vanishes. We considered two different boundary conditions for the anisotropies. The first set of conditions fixed the initial values of the anisotropies and left the final values free, while the second set corre-

sponds to free initial and final values for the anisotropies. Interestingly we find that both sets of boundary conditions result in wavefunctions that share some qualitative features. Our key result is that in this non-perturbative microsuperspace setting we find that with the no boundary condition large universes are suppressed and large anisotropies dominate. Furthermore, in-line with our semiclassical analysis multiple Monte Carlo runs with random initial configurations indicate that larger anisotropies are more probable for smaller universes and the spread in the distribution of the anisotropies is also larger for smaller universes.

The non-perturbative results for the Bianchi I spacetime detailed here provide a stark contrast to results obtained for the biaxial Bianchi IX spacetime in the semiclassical setting. These results suggest that for the Bianchi IX spacetime large anisotropies are suppressed in the path integral [63]. If the quantum dynamics for the Bianchi IX spacetime can be treated via transitions between quantum Bianchi I spacetimes, then our results would indicate that large anisotropies dominate in the Bianchi IX path integral. However, a proper PIMC calculation of the no-boundary wavefunction for a Bianchi IX model needs to be performed in order to draw useful comparisons with the results in [63]. We expect thermalization times for the Bianchi IX model to be significantly longer than for the Bianchi I model which maybe considered the free particle version of the problem. Therefore, the algorithm used here will need to be suitably modified to improve performance times.

One such direction for modification involves parallel rejection. Parallel

rejection utilizes several CPU cores to calculate multiple proposals (paths) at the same time. Once one of these is accepted the current path is updated and the parallel rejection is restarted.

Another direction to explore would be to use a Hybrid Monte Carlo (HMC) algorithm [76] in place of a simple Metropolis-Hastings algorithm. HMC relies on a supplementary Hamiltonian composed of the fictitious momenta (one for each original variable) that form the kinetic term and the original Euclidean action which acts as the potential term. At each step in the HMC the momenta are updated randomly and a proposal for the configuration (original) variables is made by evolving the Hamiltonian system for a specified time. The proposal is accepted or rejected using a Metropolis algorithm with a target distribution dependent on the Hamiltonian. The central idea is that the Hamiltonian dynamics can be used to provide distant proposals, thus allowing for wider and quicker exploration of the path space. The major drawback of this algorithm is the difficulty in tuning the algorithm parameters. Even small changes in parameters can result in extreme deterioration in performance.

Lastly, we investigated an alternative regularization for the path integral by restricting the Euclidean action to be positive semi-definite. This regularization results in a continuum of vacua to which the algorithm can converge and finite number of samples do not result in consistent results. It is possible that the convergence of the Euclidean action is not a suitable observable to

determine the thermalization of the Markov chain. Finding a suitable set of observables would require further study. Perhaps with such a set of observables in hand this regularization can be used to study qualitative features that are common to paths that are expected to dominate the path integral.

Chapter 7

Summary and Future

Directions

This thesis was an exploration of the classical and quantum aspects of a dust + gravity system with the dust field used to fix the time gauge.

A fundamental issue in quantizing GR is presented by the “problem of time” [62] caused by the absence of a preferred time-like Killing vector field for arbitrary spacetimes and thus a lack of a preferred global time coordinate. Classically, this manifests in the fact that the Hamiltonian is constrained to vanish; while in the quantum domain, the Hamiltonian annihilates all physical states leading to non-evolving observables. This is in sharp contrast with standard quantum theory where a non-zero Hamiltonian generates unitary time evolution. One path out of this quandary is to partially de-parametrize the theory before quantization by choosing an internal time (gauge choice).

Following [61], in this thesis we use a dust field as time. This is motivated by the observation that a clock in our usual experience is made of matter, therefore it is natural to use a matter field as a clock. Furthermore, the greatest advantage of using dust time is that the physical Hamiltonian is the same functional of all other phase space variables besides the dust as the Hamiltonian constraint, whereas other matter time gauges usually yield square root Hamiltonians. This considerably simplifies analytical and numerical calculations. For homogeneous models this approach is exactly equivalent to reduced phase space quantization, since the gauge fixing picks out a unique point on every gauge orbit. Moreover, this approach allows us to employ powerful tools developed for standard quantum theory in studying the quantum effects of gravity. This is especially remarkable given the roadblock of determining the physical Hilbert space of the Dirac quantized theory in order to obtain (observationally and theoretically) testable predictions.

In general, quantizing after solving the constraints is not equivalent to quantizing the constrained system and imposing the constraints as operators. However, both schemes involve several choices in the quantization procedure and it may be possible to make a consistent set of choices in both approaches to yield equivalent quantum theories. An example is provided by the equivalence of Dirac quantization using the Laplace-Beltrami operator ordering and reduced phase space quantization in the dust time gauge for a spatially flat FLRW cosmology with dust and a positive cosmological constant detailed in Chapter 5. Moreover, though the gauge fixed theories

are equivalent classically the resultant quantum theories in different gauges are inequivalent. Thus the quantum dynamics of these theories may not be comparable. Recently some work has been done to develop a framework to relate quantum theories resulting from using different gauges to gauge fix the same underlying classical theory before quantization [57, 88]. The procedure relies on connecting these myriad quantum theories to the Dirac quantized theory. Though it has been successfully applied to toy models, the arguments for gravitational models are still formal.

It is important to keep in mind certain caveats when using the dust field as time. Though the dust field provides an extremely useful matter based clock, it is an idealization. We must bear in mind that the dust field is not a fundamental physical matter field i.e. it is not part of the standard model of particle physics. Moreover, the dust field provides a specific foliation of the spacetime namely the proper time foliation. Not all 4 geometries admit this type of foliation and are thus excluded from both the classical and quantum models with dust. This also means that the quantum theory is a theory of a restricted set of 3-geometries relative to those allowed for GR with arbitrary matter sources. Though these are valid caveats such concerns are bound to arise in any type of quantization scheme that follows after gauge fixing. Furthermore, in GR the allowed set of the geometries are determined by the matter sources in the model and this is also to be expected with models with dust.

Another criticism of the models discussed in this thesis is that symmetry

reduction of the theory is done before quantization. However, given the complexity of quantizing full GR, applying this reduced phase space approach to symmetry reduced models is relatively simple and can yield crucial insights into the full theory. Our expectation is that certain qualitative features of these symmetry reduced models will survive in the full theory.

There are several interesting consequences of a dust field as a choice of time. In Chapter 3 we showed that in a $3 + 1$ dimensional system with dust coupled to gravity the usual interpretation of gravitational waves as spin 2 modes is preserved in the dust time gauge. Moreover, GR+dust in the dust time gauge allows us to solve the "problem of time" while maintaining consistency with standard Lorentz covariant field theory on Minkowski spacetime.

Dust time is also useful in understanding how matter decouples from geometry on the approach to a space-like singularity. In Chapter 4 we derived a transition law governing the near singularity dynamics of a Bianchi IX spacetime with dust which includes the dust degree of freedom. We show how this degree of freedom drops out in the asymptotic limit allowing us to recover the original vacuum Kasner transition law proposed by Belinskii-Khalatnikov-Lifschitz [18].

In the quantum domain Chapter 5 shows that the dynamics of a spatially flat FLRW spacetime with dust and a cosmological constant can be mapped onto an oscillator on a half line using the dust field as time. This system is

easily quantized and we provide a clean derivation of singularity avoidance for this model for all values of the cosmological constant. For studying more complex homogeneous models like the closed and open FLRW spacetimes and anisotropic spacetimes, we have developed a framework for applying Monte Carlo techniques to homogeneous cosmological models in the dust time gauge. We define our quantum theory using the path integral approach where paths are weighed by the gauge fixed action. By Wick rotating to Euclidean time, the exponentiated action behaves as a probability distribution which can be sampled using Markov Chain Monte Carlo (MCMC) techniques. The advantage of the dust time gauge is that in some settings it is possible to define a positive definite Euclidean action guaranteeing the convergence of the Euclidean Path Integral. In other settings, requiring positivity of the dust density restricts the paths that can be included in the path integral, allowing us to extract useful results. In Chapter 6 we study a Bianchi I model with dust using these numerical techniques. For this model we investigate the semiclassical dynamics and also calculate the no-boundary wavefunction using two different regularization schemes.

Our study of the Bianchi I model indicates that in the semiclassical regime the Kasner sum rules are violated. This raises the question whether a description of the quantum Bianchi IX spacetime can be constructed in terms of the Bianchi I dynamics as in the classical setting. Results from the effective dynamics studies of the Bianchi IX spacetime in LQC show that the

effective dynamics of Bianchi IX spacetimes exhibit Bianchi I phases with Bianchi II transitions [34]. It would be interesting to compare the semiclassical dynamics obtained from the path integral for the Bianchi IX model in the dust time gauge with these results. In order to do this the PIMC algorithm we implemented for the Bianchi I model will need to be modified to keep the rejection rates within an acceptable range. We hope to explore alternative algorithms in future work.

The work presented here can also be extended to include other matter fields besides dust. The interplay of matter and gravitational degrees of freedom in the quantum regime is crucial to understanding the physics of the early universe. Scalar fields would be especially interesting in understanding the quantum underpinnings of inflation. Including other matter sources is remarkably straightforward when using the dust time gauge since the additional matter Hamiltonians can just be added to the physical Hamiltonian.

It is important for any quantum exploration of gravity to include inhomogeneities. Including inhomogeneities beyond the framework of perturbation theory requires studying field theoretic models such as Gowdy cosmologies in the dust time gauge. In these models symmetries dictate that all metric functions depend on (dust) time and one other coordinate. Thus, these models are two-dimensional field theories with infinite degrees of freedom. Classically, Gowdy models are relatively simple and well-studied. They provide insights into general relativity that homogeneous models cannot. We expect this to be the case in the quantum setting as well. Classically, per-

haps the most relevant question to investigate for these models in dust time is the domain of validity of the dust time gauge. That is, does the choice of dust time provide a global foliation of the spacetime?

For the quantum model, we must deal with the spatial diffeomorphism constraint which was absent in the homogeneous setting. This can be done either by choosing a diffeo-gauge and solving the constraint before constructing the path integral or by imposing the constraint via a delta function in the path integral. These models provide the perfect testbed for Monte Carlo (MC) techniques (and algorithms) that need to be developed for infinite dimensional GR models and are the natural next step.

Bibliography

- [1] B. P. Abbott et al., *Observation of gravitational waves from a binary black hole merger*, Phys. Rev. Lett. **116** (2016), no. 6, 061102.
- [2] R. Abuter et al., *Detection of the gravitational redshift in the orbit of the star S2 near the Galactic centre massive black hole*, Astron. Astrophys. **615** (2018), L15.
- [3] Ivan Agullo and Parampreet Singh, *Loop Quantum Cosmology*, Loop Quantum Gravity: The First 30 Years (Abhay Ashtekar and Jorge Pullin, eds.), WSP, 2017, pp. 183–240.
- [4] Andrei Alexandru, Gökçe Başar, Paulo F. Bedaque, Sohan Vartak, and Neill C. Warrington, *Monte Carlo Study of real time dynamics on the lattice*, Phys. Rev. Lett. **117** (2016), 081602.
- [5] Masooma Ali, Syed Moez Hassan, and Viqar Husain, *Monte Carlo simulation of cosmologies with dust*, arXiv e-prints (2018), arXiv:1811.05047.

- [6] ———, *Universe as an oscillator*, Phys. Rev. **D98** (2018), no. 8, 086002.
- [7] Masooma Ali and Viqar Husain, *Mixmaster dynamics in the dust time gauge*, Phys. Rev. **D96** (2017), no. 4, 044032.
- [8] Masooma Ali, Viqar Husain, Shohreh Rahmati, and Jonathan Ziprick, *Linearized gravity with matter time*, Class. Quant. Grav. **33** (2016), no. 10, 105012.
- [9] Edward Anderson, *The Problem of Time in Quantum Gravity*, arXiv **1009.2157** (2010).
- [10] Lars Andersson and Alan D Rendall, *Quiescent cosmological singularities*, Communications in Mathematical Physics **218** (2001), no. 3, 479–511.
- [11] Lars Andersson, Henk van Elst, Woei Chet Lim, and Claes Uggla, *Asymptotic silence of generic cosmological singularities*, Phys. Rev. Lett. **94** (2005), 051101.
- [12] Cristian Armendariz-Picon and Gizem Şengör, *BRST Quantization of Cosmological Perturbations*, JCAP **1611** (2016), no. 11, 016.
- [13] Richard L. Arnowitt, Stanley Deser, and Charles W. Misner, *The Dynamics of general relativity*, Gen. Rel. Grav. **40** (2008), 1997–2027.
- [14] Martin Adrian Barstow, Howard E. Bond, J. B. Holberg, M. R. Burleigh, I. Hubeny, and D. Koester, *Hubble Space Telescope spectroscopy of the*

- Balmer lines in Sirius B*, Mon. Not. Roy. Astron. Soc. **362** (2005), 1134–1142.
- [15] Daniel Baumann, *Tasi lectures on inflation*, (2012).
- [16] V. A. Belinski and I. M. Khalatnikov, *On the nature of the singularities in the general solution of gravitational equations*, Sov. Phys. JETP **29** (1969), 911.
- [17] ———, *General solution of the gravitational equations with a physical singularity*, Sov. Phys. JETP **30** (1970), 1174.
- [18] V A Belinskiĭ, E M Lifshitz, and I M Khalatnikov, *Oscillatory approach to the singular point in relativistic cosmology*, Soviet Physics Uspekhi **13** (1971), no. 6, 745.
- [19] B. K. Berger, *Path Integral Quantum Cosmology 2 - Bianchi Type I with volume dependent source*, Phys. Rev. **D32** (1985), 2485–2488.
- [20] ———, *Application of Monte Carlo simulation methods to quantum cosmology*, Phys. Rev. **D48** (1993), 513–529.
- [21] B. K. Berger, D. Garfinkle, J. Isenberg, V. Moncrief, and M. Weaver, *The Singularity in generic gravitational collapse is space-like, local, and oscillatory*, Mod. Phys. Lett. **A13** (1998), 1565–1574.
- [22] B. K. Berger and C. N. Vogeli, *Path Integral Quantum Cosmology 1 - Vacuum Bianchi Type I*, Phys. Rev. **D32** (1985), 2477–2484.

- [23] Beverly K. Berger, *Monte Carlo simulation of a quantized universe*, General Relativity and Gravitation **20** (1988), no. 8, 755–763.
- [24] ———, *Quantum chaos in the mixmaster universe*, Phys. Rev. D **39** (1989), 2426–2429.
- [25] ———, *Influence of scalar fields on the approach to a cosmological singularity*, Phys. Rev. D **61** (1999), 023508.
- [26] ———, *Singularities in Cosmological Spacetimes*, Handbook of Space-time (Abhay Ashtekar and Vesselin Petkov, eds.), Springer, Berlin-Heidelberg, 2014, pp. 437–460.
- [27] Beverly K. Berger, David Garfinkle, and Vincent Moncrief, *Numerical study of cosmological singularities*, arXiv e-prints (1997), arXiv:gr-qc/9709073, [Annals Israel Phys. Soc.13,441(1997)].
- [28] Abhijit Biswas and Krishnan R. S. Mani, *Relativistic Perihelion Precession of Orbits of Venus and the Earth*, Central Eur. J. Phys. **6** (2008), 754.
- [29] Norbert Bodendorfer, Fabio M. Mele, and Johannes Münch, *Holographic Signatures of Resolved Cosmological Singularities II: Numerical Investigations*, arXiv e-prints (2018), arXiv:1804.01387.
- [30] J. David Brown and Karel V. Kuchar, *Dust as a standard of space and time in canonical quantum gravity*, Phys.Rev. **D51** (1995), 5600–5629.

- [31] J. Carlson, S. Gandolfi, F. Pederiva, Steven C. Pieper, R. Schiavilla, K. E. Schmidt, and R. B. Wiringa, *Quantum Monte Carlo methods for nuclear physics*, Rev. Mod. Phys. **87** (2015), 1067–1118.
- [32] Michel Carreau, Edward Farhi, Sam Gutmann, and Paul F. Mende, *The Functional Integral for Quantum Systems With Hamiltonians Unbounded From Below*, Annals Phys. **204** (1990), 186–207.
- [33] Ali H. Chamseddine and Viatcheslav Mukhanov, *Mimetic Dark Matter*, JHEP **11** (2013), 135.
- [34] Alejandro Corichi and Edison Montoya, *Loop quantum cosmology of Bianchi IX: effective dynamics*, Classical and Quantum Gravity **34** (2017), no. 5, 054001.
- [35] Michael Creutz, *Overrelaxation and Monte Carlo simulation*, Phys. Rev. D **36** (1987), 515–519.
- [36] Jan de Boer, Bas Peeters, Kostas Skenderis, and Peter van Nieuwenhuizen, *Loop calculations in quantum mechanical nonlinear sigma models with fermions and applications to anomalies*, Nucl. Phys. **B459** (1996), 631–692.
- [37] Alice Di Tucci and Jean-Luc Lehners, *Unstable no-boundary fluctuations from sums over regular metrics*, arXiv e-prints (2018), arXiv:1806.07134.

- [38] Juan Diaz Dorronsoro, Jonathan J. Halliwell, James B. Hartle, Thomas Hertog, and Oliver Janssen, *Real no-boundary wave function in Lorentzian quantum cosmology*, Phys. Rev. **D96** (2017), no. 4, 043505.
- [39] Juan Diaz Dorronsoro, Jonathan J. Halliwell, James B. Hartle, Thomas Hertog, Oliver Janssen, and Yannick Vreys, *Damped perturbations in the no-boundary state*, Phys. Rev. Lett. **121** (2018), no. 8, 081302.
- [40] Peter Diener, Anton Joe, Miguel Megevand, and Parampreet Singh, *Numerical simulations of Loop Quantum Bianchi-I spacetimes*, Class. Quant. Grav. **34** (2017), no. 9, 094004.
- [41] B. Dittrich, *Partial and complete observables for canonical General Relativity*, Class. Quant. Grav. **23** (2006), 6155–6184.
- [42] ———, *Partial and complete observables for Hamiltonian constrained systems*, Gen. Rel. Grav. **39** (2007), 1891–1927.
- [43] Albert Einstein, *Die Grundlage der allgemeinen Relativitätstheorie*, Annalen der Physik **354** (2006), no. 7, 769–822.
- [44] Beatriz Elizaga Navascués, Mercedes Martín-Benito, and Guillermo A. Mena Marugán, *Modified FRW cosmologies arising from states of the hybrid quantum Gowdy model*, Phys. Rev. **D92** (2015), no. 2, 024007.
- [45] Job Feldbrugge, Jean-Luc Lehners, and Neil Turok, *Lorentzian Quantum Cosmology*, Phys. Rev. **D95** (2017), no. 10, 103508.

- [46] Christopher J. Fewster and Thomas A. Roman, *Null energy conditions in quantum field theory*, Phys. Rev. **D67** (2003), 044003, [Erratum: Phys. Rev. D80,069903(2009)].
- [47] David Garfinkle, *Numerical simulations of generic singularities*, Phys. Rev. Lett. **93** (2004), 161101.
- [48] ———, *The Nature of gravitational singularities*, Int. J. Mod. Phys. **D13** (2004), 2261–2266.
- [49] Mirah Gary and Steven B. Giddings, *Relational observables in 2-D Quantum Gravity*, Phys. Rev. **D75** (2007), 104007.
- [50] Christof Gattringer and Christian B. Lang, *Quantum chromodynamics on the lattice*, Lect. Notes Phys. **788** (2010), 1–343.
- [51] Boro Grubišić and Vincent Moncrief, *Asymptotic behavior of the $T^3 \times R$ Gowdy space-times*, Phys. Rev. D **47** (1993), 2371–2382.
- [52] Jonathan J. Halliwell and Jorma Louko, *Steepest Descent Contours in the Path Integral Approach to Quantum Cosmology. 1. The De Sitter Minisuperspace Model*, Phys. Rev. **D39** (1989), 2206.
- [53] J. B. Hartle and S. W. Hawking, *Wave Function of the Universe*, Phys. Rev. **D28** (1983), 2960–2975.
- [54] W. K. Hastings, *Monte Carlo sampling methods using Markov Chains and their applications*, Biometrika **57** (1970), no. 1, 97–109.

- [55] G. Heckmann and E. Schucking, *Relativistic Cosmology*, Gravitation: An Introduction to Current Research (L. Witten, ed.), Wiley, 1962.
- [56] David Hobill, Adrian Burd, and Alan Coley (eds.), *Deterministic chaos in General Relativity*, Springer, NY, 1994.
- [57] Philipp A. Hoehn, *Switching internal times and a new perspective on the 'wave function of the universe'*, Universe **5** (2019), no. 5, 116.
- [58] Golam Mortuza Hossain, *On energy conditions and stability in effective loop quantum cosmology*, Class. Quant. Grav. **22** (2005), 2653–2670.
- [59] Nick Huggett, Tiziana Vistarini, and Christian Wuthrich, *Time in Quantum Gravity*, A Companion to the Philosophy of Time (Adrian Bardon and Heather Dyke, eds.), John Wiley & Sons Inc., 2012, pp. 242–261.
- [60] Viqar Husain and Tomasz Pawłowski, *Dust reference frame in quantum cosmology*, Class.Quant.Grav. **28** (2011), 225014.
- [61] ———, *Time and a physical Hamiltonian for quantum gravity*, Phys.Rev.Lett. **108** (2012), 141301.
- [62] C. J. Isham, *Canonical quantum gravity and the problem of time*, arXiv e-prints (1992), no. arXiv:gr-qc/9210011, 0157–288, [NATO Sci. Ser. C409,157(1993)].

- [63] Oliver Janssen, Jonathan J. Halliwell, and Thomas Hertog, *The no-boundary proposal in biaxial Bianchi IX minisuperspace*, arXiv e-prints (2019), arXiv:1904.11602.
- [64] M. Kramer et al., *Tests of General Relativity from timing the double pulsar*, *Science* **314** (2006), 97–102.
- [65] David Langlois, *Hamiltonian formalism and gauge invariance for linear perturbations in inflation*, *Class.Quant.Grav.* **11** (1993), 389–407.
- [66] Eugene A. Lim, Ignacy Sawicki, and Alexander Vikman, *Dust of Dark Energy*, *JCAP* **1005** (2010), 012.
- [67] Xue-feng Lin and Robert M. Wald, *Proof of the closed-universe recollapse conjecture for general Bianchi type-IX cosmologies*, *Phys. Rev. D* **41** (1990), 2444–2448.
- [68] Hideki Maeda, *Unitary evolution of the quantum Universe with a Brown–Kuchař dust*, *Class. Quant. Grav.* **32** (2015), no. 23, 235023.
- [69] M. Martin-Benito, L. J. Garay, G. A. Mena Marugan, and E. Wilson-Ewing, *Loop Quantum Cosmology of the Bianchi I model: complete quantization*, *J. Phys. Conf. Ser.* **360** (2012), 012031.
- [70] M. Martin-Benito, G. A. Mena Marugan, and T. Pawłowski, *Loop Quantization of Vacuum Bianchi I Cosmology*, *Phys. Rev.* **D78** (2008), 064008.

- [71] Prado Martín-Moruno and Matt Visser, *Classical and quantum flux energy conditions for quantum vacuum states*, Phys. Rev. **D88** (2013), no. 6, 061701.
- [72] Charles W. Misner, *Mixmaster universe*, Phys. Rev. Lett. **22** (1969), 1071–1074.
- [73] ———, *Quantum cosmology. 1.*, Phys. Rev. **186** (1969), 1319–1327.
- [74] Colin Morningstar, *The Monte Carlo method in quantum field theory*, 21st Annual Hampton University Graduate Studies Program (HUGS 2006) Newport News, Virginia, June 5-23, 2006, 2007.
- [75] R. Myrzakulov, L. Sebastiani, and S. Vagnozzi, *Inflation in $f(R, \phi)$ - theories and mimetic gravity scenario*, Eur. Phys. J. **C75** (2015), 444.
- [76] Radford M. Neal, *MCMC using Hamiltonian dynamics*, arXiv e-prints (2012), arXiv:1206.1901.
- [77] Tao Pang, *An Introduction to Quantum Monte Carlo Methods*, 2053-2571, Morgan & Claypool Publishers, 2016.
- [78] Carlo Rovelli, *Time in Quantum Gravity: Physics beyond the Schrodinger regime*, Phys. Rev. **D43** (1991), 442–456.
- [79] ———, *What Is Observable in Classical and Quantum Gravity?*, Class. Quant. Grav. **8** (1991), 297–316.
- [80] ———, *Partial observables*, Phys. Rev. **D65** (2002), 124013.

- [81] K. Schleich, *Is reduced phase space quantization equivalent to Dirac quantization?*, *Class. Quant. Grav.* **7** (1990), 1529–1538.
- [82] Irwin I. Shapiro, Michael E. Ash, Richard P. Ingalls, William B. Smith, Donald B. Campbell, Rolf B. Dyce, Raymond F. Jurgens, and Gordon H. Pettengill, *Fourth test of general relativity: New radar result*, *Phys. Rev. Lett.* **26** (1971), 1132–1135.
- [83] Jędrzej Świeżewski, *On the properties of the irrotational dust model*, *Class. Quant. Grav.* **30** (2013), 237001.
- [84] Gerard 't Hooft and M. J. G. Veltman, *One loop divergencies in the theory of gravitation*, *Ann. Inst. H. Poincaré Phys. Théor.* **A20** (1974), 69–94.
- [85] Johannes Tambornino, *Relational Observables in Gravity: a Review*, *SIGMA* **8** (2012), 017.
- [86] Claudio Teitelboim, *The Proper Time Gauge in quantum theory of gravitation*, *Phys. Rev.* **D28** (1983), 297.
- [87] Haruhiko Terao, *Quantum analysis of Jackiw and Teitelboim's model for (1+1)-D gravity and topological gauge theory*, *Nucl. Phys.* **B395** (1993), 623–646.
- [88] Augustin Vanrietvelde, Philipp A. Hoehn, Flaminia Giacomini, and Esteban Castro-Ruiz, *A change of perspective: switching quantum refer-*

- ence frames via a perspective-neutral framework*, arXiv e-prints (2018), arXiv:1809.00556.
- [89] Joel M. Weisberg and Joseph H. Taylor, *Relativistic binary pulsar B1913+16: Thirty years of observations and analysis*, ASP Conf. Ser. **328** (2005), 25.
- [90] Norbert Wex, *Testing Relativistic Gravity with Radio Pulsars*, arXiv e-prints (2014), arXiv:1402.5594.
- [91] Clifford M. Will, *The Confrontation between General Relativity and experiment*, Living Rev. Rel. **17** (2014), 4.

Vita

Full name: Masooma Ali

Universities attended :

2014 – present, Ph.D in Physics, University of New Brunswick, Canada

2009 – 2011, M.Sc. in Astrophysics, University of Bonn, Germany

2006 – 2009, B.Sc. (Hons) Physics, Delhi University, India

Publications:

Ali, M., Hassan, S. M., and Husain, V. (2018) Monte Carlo simulations of cosmologies with dust. arXiv: 1811.05047.

Ali, M., Hassan, S. M., and Husain, V. (2018) Universe as an oscillator. Physical Review D 98, 086002.

Ali, M., Seahra, S. S. (2017) Natural Inflation from Polymer Quantization. Physical Review D 96, 103524.

Ali, M., Husain, V. (2017) Mixmaster Dynamics in the dust time gauge. Physical Review D 96, 044032.

Ali, M., Husain, V., Rahmati, S., Ziprick, J. (2016) Linearized gravity with

matter time. *Classical and Quantum Gravity*. 33, 105012.

Conference Presentations:

Bianchi IX Dynamics in Dust time. Oral presentation at CAP Congress (2018).

Bianchi IX Dynamics in Dust time. Oral presentation at Theory Canada 13 (2018).

The Universe as an Oscillator. Oral presentation at Atlantic General Relativity (2018).

Bianchi IX Dynamics in Dust Time, Poster presentation at Making Quantum Gravity Computable Workshop (2017).

Bianchi IX Dynamics in Dust Time, Oral presentation at Atlantic General Relativity (2017).

Linearized gravity with matter time. Oral presentation at Canadian Conference on General Relativity and Relativistic Astrophysics (2016).

Linearized gravity with matter time. Oral presentation at Atlantic General Relativity (2016).